Particle Trajectories in Long Wave Models

Olufemi Elijah Ige

Thesis for the degree of Philosophiae Doctor (PhD)
University of Bergen, Norway
2024

UNIVERSITY OF BERGEN

Particle Trajectories in Long Wave Models

Olufemi Elijah Ige

Thesis for the degree of Philosophiae Doctor (PhD)
at the University of Bergen

Date of defense: 05.04.2024

Year: 2024

Title: Particle Trajectories in Long Wave Models

Name: Olufemi Elijah Ige

Print: Skipnes Kommunikasjon / University of Bergen

Preface

This dissertation is submitted as a partial fulfillment of the requirements for the degree of Doctor of Philosophy (PhD) in Applied Mathematics at the Department of Mathematics, University of Bergen. The scientific works in the thesis have been conducted under the supervision of Professor Henrik Kalisch and Dr. Didier Pilod at the Department of Mathematics at the University of Bergen, Norway.

Acknowledgments

I am very grateful to Almighty God for the grace and privilege given to me to embark on and complete my PhD studies. To him alone be the glory forever. My gratitude goes to the faculty of Natural and Mathematical Sciences at the University of Bergen for the opportunity given to me to work as a research fellow at the Department of Mathematics. I would like to appreciate their exceptional support throughout my studies. My heartfelt appreciation also goes to my wonderful supervisor, Prof. Henrik Kalisch for the love, inspiration, and encouragement shown to me in the course of my PhD program. I appreciate all the productive discussions we have had during this period. His patience and his positive mind towards issues are second to none. His dedication to giving directions and ability to help at all times are immeasurable. My gratitude also goes to Prof. Samer Israwi (Lebanese University, Lebanon) for the expository discussion we had at the beginning of my PhD program.

I would like to thank all the co-authors for the productive collaborations and for the discussions that had a great impact. A big thanks to Zahra Khorsand for the knowledge we shared during our frequent meetings. My appreciation goes to all the members of the fluid mechanics research group for all the wonderful times and discussions we had together. It was really an awesome learning experience. I also express my gratitude to the community at the mathematics department, everyone in the administration, the professors, the cleaners who make our office and environment look beautiful, my fellow Ph.D. students, and all my friends, including master's and bachelor's students. You all contributed to the accomplishment of this work. In addition, I want to thank my colleagues Anders Marifjæren Norevik and Jakob Seierstad Stokke for their efforts in helping with the translation of the thesis abstract into the Norwegian language.

Furthermore, I would like to express my thanks to my friends outside the university in Norway, especially the Redeemed Christian Church of God family, Bergen, and my friends back home in Nigeria. Your love is highly appreciated. Special thanks to my family, my parents, and my siblings. Words cannot express how grateful I am. Thank you very much. Moreover, I'm grateful to my doctor and the medical team at the Haukeland Hospital for taking good care of my health throughout my studies. This page will be incomplete without acknowledging my friend Oluwatobi Omotola Amusan for his encouragement throughout this study. A big thanks to my virtuous wife, VICTORIA IGE, for the love, support, and encouragement. May Almighty

God bless you abundantly.

Abstract

The behavior and patterns of the particle trajectories in the wave motion in shallow water have been examined by many researchers for decades, especially the investigation of the properties of flows beneath the surface waves in shallow water have been studied out of curiosity to know more about the features of long waves using mathematical models. In this thesis, the focus is on particle trajectories beneath the surface wave profile in shallow water. A different mathematical model which represents different cases has been developed to describe some properties of the waves under consideration.

In paper A, the regularized version of the Korteweg-de Vries (KdV) equation called the Benjamin-Bona-Mahony (BBM) equation has been used as a model equation for long waves in shallow water. This model is used to study the behavior of the waves at the surface of the inviscid fluid. Here, the particle paths are computed numerically with the aid of the velocity fields found in connection with the exact solutions of the BBM equation. In line with this concept, we examine the solitary wave and the periodic traveling wave solutions. For comparison purposes, we compute the closed-form solutions of the particle trajectories analytically.

In paper B, the work is centered on the numerical examination of particle trajectories associated with the propagation of long water waves of small but finite amplitude on a background shear flow over a flat bottom. Taking into consideration the assumption that the nonlinear and dispersive effects are small and of the same magnitude, the Boussinesq-type equations for two-dimensional water waves on a background flow with constant vorticity are derived. Restricting attention to waves propagating in a single direction, we find a new version of the BBM equation which takes into account the effect of vorticity. To investigate the particle trajectories of the flow, an approximate velocity field associated with the derivation of the BBM equation over a shear flow is obtained. Several cases of particle paths under surface wave profiles such as solitary waves and periodic traveling waves are examined.

In paper C, the KdV equation is used to model the interfacial waves in the two-layer fluid of different densities. For the numerical computation, the three equations representing the Boussinesq-type system which is later reduced to the two equations were derived. The KdV equation is derived as a result of investigating the waves going in only one direction in the two-layer fluids. The study of the particle paths of the flow led to the derivation of the velocity field connected to the exact solutions of

the KdV equation. In this context, the particle trajectories of flows that correspond to the solitary waves were studied.

In paper D, we focus on the numerical evaluation of the particle trajectories associated with the solitary-wave solution of the Gardner equation as a model for water waves at the surface of an inviscid fluid. A secondary objective is to obtain the highest solitary wave which does not feature wave breaking. The Gardner equation is derived from a Boussinesq-type system for surface water waves. By focusing on the one-directional waves, the Gardner equation which is sometimes called the extended Korteweg-de Vries (eKdV) equation is obtained. The derivation also yield expressions for the horizontal and vertical velocity components which can be used to understand particle trajectories and wave-breaking properties in connection with the exact solitary-wave solution.

Abstrakt

Atferden og mønstrene til partikkelbaner i bølgebevegelser i grunt vann har blitt studert av forskere i flere tiår, spesielt har egenskapene til strømmer under overflatebølger i grunt vann blitt studert ved bruk av matematiske modeller ut fra et ønske om å lære mer om egenskapene til lange bølger.

I denne avhandlingen er fokuset på partikkelbaner under profilene til overflatebølger på grunt vann. En ny matematisk modell som representerer ulike scenarioer har blitt utviklet for å beskrive noen av egenskapene til bølgene vi studerer her.

I artikkel A brukte vi den regulariserte versjonen av Korteweg-de Vries (KdV)-ligningen, kalt Benjamin-Bona-Mahony (BBM)-ligningen, for å modellere lange bølger på grunt vann. Denne modellen ble brukt for å studere atferden til bølger på overflaten av et fluid uten viskositet. Her beregnet vi partikkelbanene numerisk ved hjelp av hastighetsfelt funnet under arbeid med eksakte løsninger for BBM-ligningen. I tråd med dette utgangspunktet beregnet vi løsninger på lukket form for partikkelbanene analytisk.

I artikkel B er arbeidet sentrert rundt numeriske undersøkelser av partikkelbaner assosiert med forflytningsbevegelsen til lange bølger i vann over en flat bunn, der amplituden er liten men avgrenset, og vi har en skjærstrøm i bakgrunnen. Ved å ta i betraktning antagelsen om at ikke-lineære og dispersive effekter er små og omtrent i samme størrelsesorden, utledet vi ligninger av Boussinesq-type for todimensjonale bølger i vann med en bakgrunnsstrøm der vortisiteten er konstant. Ved videre å avgrense fokuset til bølger som beveger seg kun i en bestemt retning, fant vi en ny versjon av BBM-ligningen som inkluderer vortisitet. For å undersøke partikkelbanene i strømningen utledet vi en approksimativ tilnærming til uttrykkene for fluidhastighetene som dukker opp i forbindelse med utledningen av BBM-ligningen når vortisitetseffekter inkluderes. Flere scenarioer for partikkelbaner under overflatebølger ble undersøkt, blant annet under solitærbølger og under periodiske bølger.

I artikkel C brukte vi KdV-ligningen til å modellere bølger i grensesnittet mellom to ulike lag med forskjellig tetthet i et todelt fluid. For den numeriske beregningen utledet vi de tre ligningene som representerer systemet av Boussinesq-type, og senere reduseres til to ligninger. KdV-ligningen ble utledet som et resultat av å studere bølgene, som beveger seg utelukkende i en retning i det todelte fluidet. Granskningen av partikkelbanene i strømningen førte til utledningen av ligninger

for fluidhastighetsfeltet for de eksakte løsningene til KdV-ligningen. I dette arbeidet studerte vi partikkelbanene i strømninger assosiert med solitærbølger.

I artikkel D konsentrerte vi oss om numeriske løsninger for partikkelbaner i sammenheng med solitærbølge-løsningen til Gardner-ligningen, der ligningen er en modell for overflatebølger i vann der vi ser vekk fra viskositet. Et sekundært mål var å finne den maksimale høyden en solitærbølge kan ha uten at bølgebryting oppstår. Gardner-ligningen utledes fra et ligningssystem av Boussinesq-type for overflatebølger. Ved å fokusere kun på bølger som beveger seg i en retning, finner man Gardner-ligningen. Denne ligningen kalles også noen ganger for den utvidede Korteweg-de Vries (eKdV)-ligningen. Utledningen resulterer også i uttrykk for de horisontale og vertikale hastighetskomponentene, som kan brukes for å forstå partikkelbaner og egenskaper ved bølgebryting i sammenheng med den analytiske solitærbølgeløsningen.

Outline

This thesis is organized into two parts. Part I contains general background information, an introduction, and preliminary concepts of fluid mechanics. Part II presents the papers contributing to this thesis.

In part I, chapter 1 contains the general introduction in which the background of the study is presented. The motivation as well as the preliminary concepts were also included. Chapter 2 presents the computations of linear and nonlinear wave theory. Chapter 3 features the methodology which comprises the particle trajectories in the BBM equation, particle trajectories in the nonlinear waves on a uniform shear flow, fluid transport induced by internal waves, and particle trajectories and wave breaking in the Gardner equation. Chapter 4 gives an overview of the included papers.

Part II contains the scientific research work. The contribution to the thesis consists of the following scientific papers:

List of papers

Paper A: **Ige, O. E.** and Khorsand, Z., Particle Trajectories in the BBM Approximation. *IAENG International Journal of Applied Mathematics*, (2020), **50** (3), 589–600.

Paper B: **Ige, O. E.** and Kalisch, H., Particle Trajectories in a Weakly Nonlinear Long-Wave Model on a Shear Flow. *Applied Numerical Mathematics*, (2023). (Article in press).

Paper C: **Ige, O. E.**, and Kalisch, H. Fluid Transport Induced by Internal Waves. (To be submitted).

Paper D: **Ige, O. E.**, Kalisch, H., Elgåen K., and Aase S. M. Particle Trajectories and Wave Breaking in the Gardner Equation. (To be submitted).

Contents

Part I

General Background

Chapter 1

Introduction

The study of particle paths beneath a surface wave can be traced to the late nineteenth century [43]. A standard first-order approximation proposed that all particle trajectories are closed in linear wave theory [19, 38, 49]. However, Stokes [50] proved that particle paths are not closed for periodic waves. In fact, the motion of a periodic surface wave is associated with particle trajectories that are not closed and lead to net mass transport in the direction of the wave. This discovery is known today as the Stokes drift. Stokes drift in channels of finite depth was reviewed by Ursell [54]. Constantin [15] gave a mathematical proof that the particle paths are not closed. Other effects, such as infragravity wave motion and inertia, may also affect the particle motion [2, 6]. Munk considered particle motion under waves in the surf zone and applied a backward current in order to describe nearly closed particle paths that were observed under some conditions [42]. Moreover, Borluk and Kalisch examined the behaviors of particle paths underneath the waves at the surface. Their study consists of numerical computation of solitary wave solution, periodic traveling waves solution, and the two-soliton solutions [8]. It is established that the particle paths are nearly closed for the cnoidal waves.

The incorporation of the vorticity to the shallow-water theory was first considered by Burns [11], who modified the shallow-water theory by including the effects of the vorticity and examined the range of wave speeds for general velocity profiles. Following the publication of [52], constant background shear has been used in many works (see for example, [1, 13, 29, 53, 55, 56]). In addition, the discovery of internal solitary waves has led to groundbreaking research in applied mathematics and physics. In [12], the authors performed experiments in the laboratory to study the internal solitary wave in the waters covered by ice. The study is based on the propagation of internal solitary waves within a stable stratified two-layer fluid. In the experiments, the upper boundary condition has changed to ice from open water, and the ice is moved horizontally by the internal solitary wave-induced current, and the speed of the movement of long ice floes depends linearly on the length of the floe in connection to the range of parameter used.

In addition, the construction of a Boussinesq system of interfacial waves, which targeted two-way propagation is studied in [44]. When the interfacial waves have rigid boundaries in the full Euler equations set-up, the configuration bounds the central core amplitude. When dealing with solitary waves, if the speed of the wave advances to a critical value, the maximum amplitude is attained by the solution while continuing to be wider indefinitely; such waves are referred to as 'table-top' waves. The wave becomes a front when the width of the central core reaches infinite [20]. An extended Korteweg-de Vries (eKdV) equation [24, 26] is usually used to model this action. It is important to know that the KdV-type models can only express the propagation of waves in one direction, while the Boussinesq-type systems can describe the propagation of the two-way wave.

However, Choi and Camassa [14] established the general models in the configuration of both shallow and deep water. The two-layer form of the Green-Naghdi model is used in the case of shallow water. Their equations have been extended to handle the configuration of free-surface [3]. In the two-layer flows, the numerical computation of solitary waves solutions to the full incompressible Euler equations, which feature an interface has been studied by many researchers (for example [37]). Moreover, Dias and Vanden-Broeck [20, 21] have computed fronts.

Moreover, we considered the eKdV equation, sometimes called the Gardner equation. This equation is able to describe larger amplitude waves than the KdV equation. For such models to be useful in practical situations in coastal engineering, certain wave effects such as wave breaking and fluid transport should be considered [8, 10].

Wave breaking is known in connection with stagnation at the free surface [5, 23]. At the free surface, this happens when the particle's horizontal velocity at the wave-crest approaches the same value as the phase velocity. The accuracy of the kinematic breaking criterion in the prediction of wave-breaking onset has been given much consideration. Several studies argue that in some practical circumstances that concern the onset of breaking, the kinematic criterion can be useful [27, 32, 34, 58] but if the kinematic criterion is to be used in a practical situation, estimates of phase or crest velocity have to be provided [45, 46] which may be difficult, especially in three-dimensional situations. Some works suggest that simpler criteria may be more expedient [28, 40]. In [47], a convective breaking criterion is used to find the inception of wave breaking in solitary and periodic traveling waves using the KdV equation on a flow with constant vorticity.

The investigation of particle trajectories in the long wave models has been the center of attraction in this thesis. The behavior of the particle paths at the surface of the fluid using the BBM equations was examined. The interesting results motivated the idea of extending the findings to other areas of interest. In this chapter, the general introduction, background of the study, motivation, aim and objectives, and the preliminary concepts are presented.

1.1 General Introduction

D.J. Korteweg and G. de Vries collaborated to derive the well-known Korteweg-de Vries (KdV) equation. The KdV equation is proposed as a description of the propagation of shallow water waves. The model formulated subsequently comes to the limelight to become a paradigm on which the nonlinear partial differential equations feature soliton solutions. The formulated KdV model is given as

$$\eta_t + \eta_x + \eta\eta_x + \eta_{xxx} = 0. \tag{1.1}$$

However, Benjamin, Bona, and Mahony developed another equation named the Benjamin-Bona-Mahony (BBM) equation, which is also known as the regularized long-wave model, and it is given in the form of the partial differential equation

$$\eta_t + \eta_x + \eta\eta_x - \eta_{xxt} = 0. \tag{1.2}$$

The equation (1.2) is studied as an improvement of the KdV equation (1.1). It is used for modeling long surface gravity waves of small amplitude propagating in only one direction in 1+1 dimensions. The establishment of the stability and uniqueness of solutions to the BBM equation is highlighted in [4]. This contradicts the theory of the KdV equation, which is unstable in its high wavenumber components.

1.2 Background of the study

The experiments conducted by John Scott Russell in 1834 led to the discovery of the KdV equation. The claims postulated by John Scott Russell were later investigated and introduced by Lord Rayleigh and Boussinesq in 1877 [9], and this was later rediscovered by D. J. Korteweg and G. de Vries in 1895 [18]. The KdV model was originally derived under the assumption of small wave amplitude and large wavelength for water waves, and it is justifiable as a model for long waves in many other physical systems [4]. Much attention was not given to the KdV equation after its discovery until 1986, when Zabusky and Kruskal's numerical discovery shows that its solutions appeared to decompose at large times into a collection of "solitons" [60]. Furthermore, the solitons seem to be almost unaffected in shape when passing through each other (though this could cause a change in their position).

In the field of applied mathematics and physics, the use of the KdV equation has great significance, especially its application in modeling waves on shallow water surfaces. However, it is indisputably that this model has some exceptional properties embedded in it [22], but not appropriate in some applications. This led to a need for improvement in order to cater for some of its limitations, for example, the non-physical unbounded dispersion relation, coupled with the previous aforementioned and other defects. Because of this, in 1972, Benjamin, Bona, and Mahony developed another model named the BBM equation, which is given in relation (1.2) as an alternative model to the KdV equation (1.1).

1.3 Motivation

In science and engineering, the common practice is to express real-life problems as nonlinear differential equations since most of the daily activities are nonlinear.

The previous results which are in accordance with the present study were obtained by Borluk and Kalisch [8], they found the velocity fields which are associated with the exact solutions of the KdV equation and constructed the particle paths beneath the surface. Solutions that include solitary waves and periodic traveling waves were considered. However, we are motivated to extend their findings using the KdV-type and BBM-type approximation to investigate how the particle trajectories behave in the fluid.

1.4 Aim and Objectives

1.4.1 Aim

The main aim of this thesis is to explore the various properties embedded in the KdV-type and BBM-type models, most especially the numerical computation of how the particle trajectories behave in the fluid flow.

1.4.2 Objectives

The specific objectives to achieve our aim are

- To derive the Boussinesq system associated with the given problem.
- To obtain the KdV-type and the BBM-type equation from the associated Boussinesq system.
- To derive the horizontal and vertical velocity components associated with the KdV and BBM model under consideration.
- To incorporate the horizontal and vertical velocity components into the given formula of the particle trajectory which are associated with the exact solutions of the model.

1.5 Preliminary Concepts

In this section, the background principle of the surface water waves will be presented. We are starting with the conservation of mass, followed by the conservation of momentum. The surface wave problem will be developed through various assumptions and boundary conditions. We will concentrate more on the principles and theories presented in [36] and [49].

1.5.1 Conservation of mass

Consider a fluid of density $\rho(\mathbf{x}, t)$ within a material control volume $V(t)$, the mass contained within it is defined as

$$\int_{V(t)} \rho \, dV,$$

where the position $\mathbf{x} = (x, y, z)$ at time t. An assumption that the mass of the material volume does not change with time yields the formula

$$\frac{d}{dt} \int_V \rho \, dV = 0.$$

In the control volume V, the rate of change of mass inside the volume is equal to the rate of mass flux crossing out of the boundary surface A. This is given as

$$\frac{d}{dt} \int_V \rho \, dV = - \int_A \rho \mathbf{u} \cdot \mathbf{n} \, dA,$$

where the outward normal vector to the surface A is denoted as $\mathbf{n}$. The representation of the velocities in the (x, y, z) directions are given as the fluid velocity vector in the components $\mathbf{u}(\mathbf{x}, t) = (u_1, u_2, u_3)$, respectively. Next, the differential form is obtained by changing the surface integral on the right-hand side to a volume integral. However, by applying the Leibniz rule and the divergence theorem, the resulting expression is given as

$$\int_V \left[\frac{\partial \rho}{\partial t} + \nabla \cdot (\rho \mathbf{u}) \right] \, dV = 0.$$

This expression is valid for any volume, it is possible only if the integrand vanishes at every point. Since the volume boundaries can be chosen arbitrarily, the above expression gives

$$\frac{\partial \rho}{\partial t} + \nabla \cdot (\rho \mathbf{u}) = 0.$$

This expression is called the continuity equation and represents the differential form of the conservation of mass principle.

Noting that $\nabla \cdot (\rho \mathbf{u}) = \rho \nabla \cdot \mathbf{u} + \mathbf{u} \cdot \nabla \rho$, and the material derivative $\dfrac{D}{Dt} = \dfrac{\partial}{\partial t} + \mathbf{u} \cdot \nabla$. Hence, the continuity equation gives

$$\frac{1}{\rho} \frac{D\rho}{Dt} + \nabla \cdot \mathbf{u} = 0.$$

In incompressible fluid, if the density remains constant, the material derivative of the density will become zero, and the above equation yields

$$\nabla \cdot \mathbf{u} = 0. \tag{1.3}$$

This is known as the continuity equation at constant density.

1.5.2 Conservation of momentum

Newton's second law is used to establish the law of conservation of momentum. The law states that in a control volume V, the rate of change of momentum is equal to the sum of the external forces acting on the volume, this is written in integral form as

$$\frac{D}{Dt}\int_V \rho\mathbf{u}\ dV = \int_V \rho\frac{D\mathbf{u}}{Dt}\ dV = \int_V \rho\mathbf{g}\ dV + \int_A \mathbf{F}\ dA.$$

This equation can be rewritten as

$$\int_V \frac{\partial}{\partial t}(\rho\mathbf{u})\ dV + \int_A \rho\mathbf{u}(\mathbf{u}\cdot\mathbf{n})\ dA = \int_V \rho\mathbf{g}\ dV + \int_A \mathbf{F}\ dA.$$

The rate of change of momentum in volume V and the momentum flux across the surface A are represented on the left-hand side, while on the right-hand side, the external forces are split into a surface force $\mathbf{F}$ per unit area acting on the volume boundary and a body force $\mathbf{g}$. Note that the vector force $\mathbf{F}$ is defined as $\mathbf{F} = n_i \cdot \sigma_{ij}$, where the stress tensor is denoted as σ_{ij} and the normal vector is given as n_i. Furthermore, the stress tensor σ_{ij} is divided into a normal stress $-p\delta_{ij}$ and shear stress τ_{ij}, where the fluid pressure and the identity matrix are represented as p and δ_{ij}, respectively. However, after using the Gauss theorem, the surface integral is transformed into a volume integral, then the equation for the conservation of momentum gives

$$\int_V \left[\frac{\partial}{\partial t}(\rho\mathbf{u}) + \nabla\cdot(\rho\mathbf{u}\mathbf{u})\right]\ dV = \int_V \left[\rho\mathbf{g} + \nabla\cdot(-p\delta_{ij} + \tau_{ij})\right]\ dV. \tag{1.4}$$

In the Newtonian fluid, the stress tensor τ_{ij} is a linear function of $\dfrac{\partial u_i}{\partial x_j}$. Therefore, $\tau_{ij} = 2\mu\left(\dfrac{\partial u_i}{\partial x_j} + \dfrac{\partial u_j}{\partial x_i}\right)$. The left hand is expressed as follows

$$\begin{aligned}\int_V \left[\frac{\partial}{\partial t}(\rho\mathbf{u}) + \nabla\cdot(\rho\mathbf{u}\mathbf{u})\right]\ dV &= \int_V \left[\rho\frac{\partial\mathbf{u}}{\partial t} + \mathbf{u}\left[\frac{\partial\rho}{\partial t} + \nabla\cdot(\rho\mathbf{u})\right] + (\rho\mathbf{u})\cdot\nabla\mathbf{u}\right]\ dV \\ &= \int_V \rho\frac{D\mathbf{u}}{Dt}\ dV.\end{aligned}$$

Using these relations, (1.4) becomes

$$\int_V \rho\frac{D\mathbf{u}}{Dt}\ dV = \int_V \left[\rho\mathbf{g} - \nabla p + +\mu\nabla^2\mathbf{u}\right]\ dV.$$

Thus, the integrand must vanish at every point $(\mathbf{x}, t)$ since it holds for any volume to obtain

$$\rho\frac{D\mathbf{u}}{Dt} = \rho\mathbf{g} - \nabla p + +\mu\nabla^2\mathbf{u}.$$

In the incompressible Newtonian fluid, this equation is known as the Navier-Stokes equation.

1.5.3 Potential Flow and Boundary Conditions

The surface gravity waves propagating at an air-water interface where the force of gravity is the main reinstating force is considered. The fluid volume is acted upon by the gravitational field, which is assumed to be constant, and it is the only available body force acting on the fluid volume. The gravity force is conservative and can be expressed as follows

$$\mathbf{g} = \nabla\Phi,$$

where ϕ represents the potential function. By considering the positive $z-$axis, Φ is given as $-gz$, where g is the acceleration due to gravity. Using the assumption that the flow is inviscid and incompressible, the Euler equation is used to represent the conservation of mass and linear momentum, as given below

$$\nabla \cdot \mathbf{u} = 0, \tag{1.5}$$

$$\frac{\partial \mathbf{u}}{\partial t} + (\mathbf{u} \cdot \nabla)\,\mathbf{u} = -\frac{1}{\rho}\nabla p - g\mathbf{k}, \tag{1.6}$$

where $\mathbf{k}$ represents the $z-$direction's unit vector. For an irrotational flow, curl $\mathbf{u} = 0$, the velocity vector of the flow can be written as a potential vector, that is, $\mathbf{u} = \nabla\phi$. Substituting $\mathbf{u} = \nabla\phi$ into (1.5), we have

$$\Delta\phi = 0.$$

This expression is called the Laplace's equation. Integrating expression (1.6) with respect to $\mathbf{x}$, and follow the principles in [49, 57] yields the Bernoulli's law

$$\phi_t + \frac{1}{2}(\nabla\phi)^2 + \frac{p - p_0}{\rho} + gz = C(t), \tag{1.7}$$

where p_0 is an arbitrary constant and $C(t)$ is a constant of integration which is independent of $\mathbf{x}$.

Let the interface of air-water be defined as $f(x, y, z, t) = 0$ and let $z = \eta(x, y, t)$ defined the free surface, where the vertical elevation of the free surface is represented by $\eta(x, y, t)$. With the assumption that the fluid cannot leave the interface, the surface boundary condition is given as

$$(\mathbf{n} \cdot \mathbf{u})_{z=\eta} = \mathbf{n} \cdot \mathbf{U}_{\text{interface}},$$

where $\mathbf{U}_{\text{interface}}$ represents the interface velocity and $\mathbf{n}$ denotes the surface normal. The velocity of the interface is assumed to be

$$\mathbf{U}_{\text{interface}} = \eta_t\mathbf{k}.$$

At the free surface, the second boundary condition, that is, the dynamic boundary condition can be derived by assuming no mass at the interface. It means there is equal force in the fluids above and beneath the surface. This is equivalent to saying that

on both sides of the boundary, the pressure must be equal. We neglected the effect of the surface tension in this case. The air motion will cause a change in pressure. However, the changes are negligible due to how small they are. Hence, the constant p_0 is considered to be the atmospheric pressure. At the bottom, the third boundary condition, that is, the solid fixed boundary, can be derived. The undisturbed water surface is at $z = 0$, and the distance to the sea bed is given as $h(x, t)$. Since no fluid can cross the boundary, we have $\mathbf{n} \cdot \mathbf{u} = 0$. Finally, the three boundary conditions are given as

$$\eta_t + \phi_x \eta_x + \phi_y \eta_y = \phi_z \qquad \text{at} \quad z = \eta(x, y, t), \tag{1.8}$$

$$\phi_t + \frac{1}{2}\left(\phi_x^2 + \phi_y^2 + \phi_z^2\right) + g\eta = 0 \qquad \text{at} \quad z = \eta(x, y, t), \tag{1.9}$$

$$\phi_z + \phi_x h_x + \phi_y h_y = 0 \qquad \text{at} \quad z = -h(x, y). \tag{1.10}$$

1.5.4 Shallow water waves

The shallow water theory leads to the hyperbolic equations [17], and it is fit to investigate the non-dispersive long waves. The shorter waves and the waves with more dominant dispersion effects can be studied using the Boussinesq theory [57].

In shallow water, the wavelength λ is presumed to be far larger than the undisturbed water depth h_0 in the theory of nonlinear long waves by using the assumption in [36, 49] which stated that a wave is considered a shallow-water wave if

$$\frac{\lambda}{h_0} \gg 1.$$

This can be written in terms of the wave number $k = \dfrac{2\pi}{\lambda}$ as $kh_0 \to 0$. By applying this assumption to the dispersion relation $c = \sqrt{\dfrac{g}{k}\tanh(kh_0)}$ (derived in (2.16) in connection to the linear wave theory) yields

$$c = \sqrt{gh_0}.$$

This expression demonstrated that the waves are non-dispersive. According to [33, 49], the nonlinear theory can be combined with the assumption of long wave to arrive at the propagation speed as

$$c = \sqrt{g(h_0 + \eta)},$$

where the elevation of the free surface is denoted by $\eta(x, t)$.

The shallow water equation is derived using the two-dimensional flows over a constant depth. Without any assumption, the Euler equations given in (1.5) and

(1.6) can be expanded as

$$\begin{aligned} &u_x + w_z = 0, \\ &\frac{Du}{Dt} = u_t + uu_x + wu_z = -\frac{p_x}{\rho}, \\ &\frac{Dw}{Dt} = w_t + uw_x + ww_z = -\frac{p_z}{\rho} - g, \end{aligned}$$

where $u(x, z, t)$ and $w(x, z, t)$ represent the velocity components, $p(x, z, t)$ represents the pressure, and g denotes the gravitational constant. The shallow-water approximation requires the assumption that the vertical acceleration is smaller than the horizontal acceleration. Hence, we neglected the material derivative of w, and the vertical component of the momentum gives

$$-\frac{p_z}{\rho} - g = 0.$$

The integration of this equation with respect to z from the limit z to η gives the hydrostatic law as

$$p - p_0 = \rho g(\eta - z). \tag{1.11}$$

This is in agreement with the free surface dynamic boundary condition. Differentiating equation (1.11) with respect to x and substituting it into the horizontal momentum equation gives the system of equations

$$u_x + w_z = 0, \tag{1.12}$$

$$u_t + uu_x + wu_z + g\eta_x = 0. \tag{1.13}$$

We can derive the Benney equations from equation (1.12) and (1.13) using the free surface boundary condition [25]. At water equilibrium location $z = 0$, there exists a constant depth h_0. The boundary condition at the surface is given by

$$(\mathbf{n} \cdot \mathbf{u})_{z=\eta} = \mathbf{n} \cdot \mathbf{U}_{\text{interface}}.$$

The air-water interface is defined as $f(x, z, t) = \eta(x, t) - z$, where the surface elevation is denoted as $\eta(x, t)$. At $z = \eta(x, t)$, the boundary condition can be written as

$$w = \eta_t + \eta_x u.$$

To obtain the first Benney equation, use the boundary condition we just defined and the integration of equation (1.12) with respect to z over the water depth from $-h_0$ to $\eta(x, t)$, we have

$$\eta_t + \frac{\partial}{\partial x} \int_{-h_0}^{\eta} u \, dz = 0.$$

The second Benney equation is represented by equation (1.13). The third Benney equation can be derived by combining the bottom boundary condition and the integration of equation (1.12) with respect to z from the limit $-h_0$ to z, that is,

$$\int_{-h_0}^{z} (u_x + w_z) \, dz = 0.$$

The vertical velocity component is equal to zero at $z = -h_0$, and the integral equation gives

$$w = -\int_{-h_0}^{z} u_x \, dz.$$

It is worth mentioning that these Benney equations are also referred to as the shallow water models for shear flows due to the dependency of velocity components on both x and z. The Benney equations reduce to the classical shallow water equations using the assumption that the horizontal velocity is not dependent on z. The resulting equations are

$$\begin{aligned} &\eta_t + [u(\eta + h_0)]_x = 0, \\ &u_t + uu_x + g\eta_x = 0. \end{aligned}$$

Chapter 2

Linear and nonlinear wave theory

2.1 Linear wave theory

The problem presented in the subsection 1.5.3 can be linearized to obtain a solution to the problem and to obtain the dispersion relation for propagating water waves with small amplitude. The assumption for this theory is that the amplitude a of the wave must be far smaller than the wavelength λ. In addition, the velocity components quantities, the surface elevation $\eta(x, z, t)$, and their respective derivatives should be smaller.

2.1.1 Linear waves model

The task here is to investigate the two dimensional waves, (x, z), propagating in the linear wave model. The interesting case considered is when the waves propagate in one direction only (that is, in the x direction) as seen in Figure 2.1. The displacement

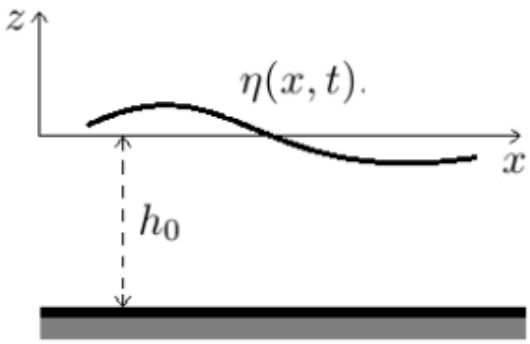

Figure 2.1: Surface wave profile with elevation $\eta(x, t)$ and the constant water depth h_0.

at the free surface is denoted by $\eta(x, t)$. The velocity potential $\phi(x, z, t)$ for an

irrotational flow ($\bigtriangledown \times \mathbf{u} = 0$, where $\mathbf{u} = (u(x,z,t), v(x,z,t))$) is defined by

$$u = \frac{\partial \phi}{\partial x}, \qquad v = \frac{\partial \phi}{\partial z}. \tag{2.1}$$

In connection with the continuity equation

$$\frac{\partial u}{\partial x} + \frac{\partial v}{\partial z} = 0, \tag{2.2}$$

the Laplace equation is obtain as

$$\frac{\partial^2 \phi}{\partial x^2} + \frac{\partial^2 \phi}{\partial z^2} = 0, \quad \text{for } x \in \mathbb{R}, \quad -h_0 < z < \eta(x,t). \tag{2.3}$$

The kinematic boundary condition at the bottom is given as a zero normal vector so that the particles may not penetrate the bottom, that is

$$v = \frac{\partial \phi}{\partial z} = 0, \quad \text{at} \quad z = -h_0. \tag{2.4}$$

The simplified kinematic boundary condition at the surface is given by

$$\left(\frac{\partial \phi}{\partial z}\right)_{z=\eta} = \left(\frac{\partial \eta}{\partial t}\right). \tag{2.5}$$

The right-hand side is expanded around $z = 0$, and the higher-order terms are neglected, so we are left with the linearized form of the kinematic boundary condition

$$\frac{\partial \phi}{\partial z} = \frac{\partial \eta}{\partial t}, \quad \text{at} \quad z = 0. \tag{2.6}$$

The linearized Bernoulli equation from the linearized momentum balance equation is given as

$$\frac{\partial \phi}{\partial t} + \frac{P}{\rho} + gz = 0, \tag{2.7}$$

where P is the pressure and ρ is the density of water. From the dynamic condition, the pressure just below the free surface is always equal to the ambient pressure. Using the assumption that the ambient pressure is zero, we have

$$P = 0 \quad \text{at} \quad z = \eta. \tag{2.8}$$

Using (2.8), simplifying the linearized Bernoulli equation at the surface $z = \eta$ yields

$$\frac{\partial \phi}{\partial t} + g\eta = 0 \quad \text{at} \quad z = \eta. \tag{2.9}$$

The expansion around $z = 0$ gives

$$\frac{\partial \phi}{\partial t} = -g\eta \quad \text{at} \quad z = 0. \tag{2.10}$$

2.1.2 Solution to the linear problem

The form of $\eta(x,t)$ is assumed in order to make use of the boundary conditions given. A sinusoidal component which is consider as a simplest case is considered and it is given as

$$\eta(x,t) = a\cos(kx - \omega t). \tag{2.11}$$

Since η described a cosine function which depends on the phase $(kx - \omega t)$, then the solution to Laplace's equation must be a sine function of the phase $(kx - \omega t)$. However, a solution is assumed and simplified as

$$\phi(x,z,t) = \left(Ae^{kz} + Be^{-kz}\right)\sin(kx - \omega t). \tag{2.12}$$

Using the no-flow condition, kinematic boundary condition, and taking some assumptions into consideration, the velocity potential is obtained as

$$\phi(x,z,t) = \frac{a\omega}{k}\frac{\cosh(k(z+h_0))}{\sinh(kh_0)}\sin(kx - \omega t). \tag{2.13}$$

From expression (2.13), the velocities in the x- and z- direction are obtained respectively as

$$\begin{aligned} u &= \frac{\partial\phi}{\partial x} = a\omega\frac{\cosh(k(z+h_0))}{\sinh(kh_0)}\cos(kx - \omega t), \\ v &= \frac{\partial\phi}{\partial z} = a\omega\frac{\sinh(k(z+h_0))}{\sinh(kh_0)}\sin(kx - \omega t). \end{aligned} \tag{2.14}$$

Substituting (2.11) and (2.13) into the free surface dynamic condition (2.10) yields the dispersion relation

$$\omega = \sqrt{gk\tanh(kh_0)}. \tag{2.15}$$

The phase velocity c at arbitrary depth is obtained by the formula $c = \dfrac{\omega}{k}$, which is given as

$$c = \sqrt{\frac{g}{k}\tanh(kh_0)}, \tag{2.16}$$

where $k = \dfrac{2\pi}{\lambda}$. In deep water approximation, as $kh_0 \to \infty$, relation (2.16) becomes

$$c = \sqrt{\frac{g}{k}}.$$

In shallow water approximation, as $kh_0 \to 0$, relation (2.16) becomes

$$c = \sqrt{gh_0},$$

this demonstrates that under shallow water approximation, the waves are non-dispersive.

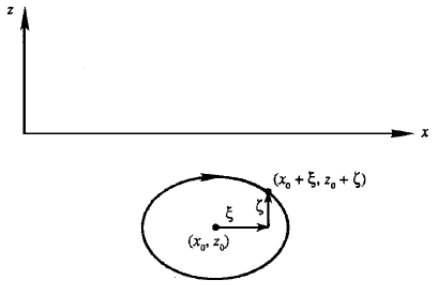

Figure 2.2: Orbit of a fluid particle with an average position of (x_0, z_0) and the displacement $(\xi(t), \zeta(t))$.

2.1.3 Particle paths

The investigation of the particle orbits required the use of Lagrangian coordinates. As shown in Figure 2.2, the fluid particle at rest (that is, at $t = 0$) is positioned at (x_0, z_0) and its coordinates are represented as $(x_0 + \xi, z_0 + \zeta)$ [36].

The particle paths is identified by (x_0, z_0) which represent the center of the orbit, and the path is denoted by the Lagrangian form $\xi(x_0, z_0, t)$ and $\zeta(x_0, z_0, t)$. Then the velocity components are given in the form of differential equations

$$\begin{aligned} \frac{\partial \xi}{\partial t} &= u(\xi(t), \zeta(t), t), \\ \frac{\partial \zeta}{\partial t} &= v(\xi(t), \zeta(t), t). \end{aligned} \tag{2.17}$$

When the small-amplitude waves are considered, the smaller particle excursion (ξ, ζ) is recorded, and at that instant, the velocity of a particle along its path is almost equal to the velocity of the fluid at the mean position (x_0, z_0). Now, the velocity components are evaluated by $\frac{\partial \xi}{\partial t} = u(x_0, z_0, t)$ and $\frac{\partial \zeta}{\partial t} = v(z_0, z_0, t)$. Substituting expression (2.14) into relation (2.17), and integration in time gives

$$\begin{aligned} \xi &= -a\frac{\cosh(k(z_0 + h_0))}{\sinh(kh_0)} \sin(kx_0 - \omega t), \\ \zeta &= a\frac{\sinh(k(z_0 + h_0))}{\sinh(kh_0)} \cos(kx_0 - \omega t). \end{aligned} \tag{2.18}$$

Adding the square of the expressions in (2.18) together, after the simplification, the term $(kx_0 - \omega t)$ is eliminated and we are left with the equation which can be use to describe an ellipse

$$\frac{\xi^2}{\left[a\frac{\cosh(k(z_0 + h_0))}{\sinh(kh_0)}\right]^2} + \frac{\zeta^2}{\left[a\frac{\sinh(k(z_0 + h_0))}{\sinh(kh_0)}\right]^2} = 1. \tag{2.19}$$

Hence, the numerical experimentation shows that the particle path computed is not a closed loop.

2.2 Nonlinear wave theory

The linear wave theory ceases to be valid when the wave becomes too steep or when the wave propagates toward shore into shallow water. In this case, the high-order wave theories are needed to describe the wave behaviors. Note that several theories have been applied to examine the properties embedded in nonlinear waves. In this subsection, the procedure used to obtain the nonlinear theory used in this thesis is presented.

2.2.1 Nonlinear waves model

The background of this study can be traced back to Whitham [57]. Derivation of the KdV equation required the assumption of fluid been incompressible and inviscid in a constant gravitational field as well as assuming small amplitude shallow water. Let the vertical surface be denoted as $z = \eta + h_0$, note that z represents the distance measured from the horizontal bottom. Then the velocity potential ϕ satisfies the Laplace equation

$$\phi_{xx} + \phi_{zz} = 0, \tag{2.20}$$

with

$$\phi_z = 0 \quad \text{on} \quad z = 0, \tag{2.21}$$

and the surface boundary conditions

$$\left.\begin{aligned} &\eta_t + \phi_x \eta_x - \phi_z = 0, \\ &\phi_t + \frac{1}{2}(\phi_x^2 + \phi_z^2) + g\eta = 0, \end{aligned}\right\} \quad \text{on} \quad z = \eta(x,t). \tag{2.22}$$

For the shallow water theory and the small total depth, we have an expansion

$$\phi = \sum_{n=0}^{\infty} z^n f_n(x,t). \tag{2.23}$$

2.2.2 Derivation of the Boussinesq system

Substituting relation (2.23) into Laplace's equation (2.20) and the boundary condition given in (2.21) yields

$$\phi = \sum_{m=0}^{\infty} (-1)^m \frac{z^{2m}}{(2m)!} \frac{\partial^{2m} f}{\partial x^{2m}}, \tag{2.24}$$

where $f = f_0$. Next, the expansion is substituted into the boundary conditions on the free surface. For convenience, normalizing the variables from the start is considered by using the following parameters

$$x = lx', \quad z = h_0 z', \quad t = \frac{lt'}{c_0}, \quad \eta = a\eta', \quad \phi = \frac{gla\phi'}{c_0},$$

where a and c_0 are the amplitude and the phase velocity, respectively. The primed variables are normalized variables, while the ones without primed are original variables. In normalized form, equation (2.20), (2.21) and boundary conditions yield

$$\beta\phi'_{x'x'} + \phi'_{z'z'} = 0, \quad 0 < z' < 1 + \alpha\eta', \tag{2.25}$$

$$\phi'_z = 0, \quad z' = 0, \tag{2.26}$$

$$\eta'_{t'} + \alpha\phi'_{x'}\eta'_{x'} - \frac{1}{\beta}\phi'_{z'} = 0, \tag{2.27}$$

$$\eta' + \phi'_{t'} + \frac{1}{2}\alpha\phi'^2_{x'} + \frac{1}{2}\frac{\alpha}{\beta}\phi'^2_{z'} = 0, \quad \text{at} \quad z' = 1 + \alpha\eta',$$

where $\alpha = \dfrac{a}{h_0}$ and $\beta = \dfrac{h_0^2}{l^2}$. Hence, the expression (2.24) becomes

$$\phi = \sum_{m=0}^{\infty} (-1)^m \frac{z'^{2m}}{(2m)!} \frac{\partial^{2m} f}{\partial x'^{2m}} \beta^m. \tag{2.28}$$

Using equation (2.28) in the boundary conditions at the free surface resulting to

$$\eta'_{t'} + \left\{(1+\alpha\eta')f_{x'}\right\}_{x'} - \left\{\frac{1}{6}(1+\alpha\eta')^3 f_{x'x'x'x'} + \frac{1}{2}\alpha(1+\alpha\eta')^2\eta'_{x'}f_{x'x'x'}\right\}\beta + O(\beta^2) = 0, \tag{2.29}$$

$$\eta' + f_{t'} + \frac{1}{2}\alpha f^2_{x'} - \frac{1}{2}(1+\alpha\eta')^2\left\{f_{x'x't'} + \alpha f_{x'}f_{x'x'x'} - \alpha f^2_{x'x'}\right\}\beta + O(\beta^2) = 0. \tag{2.30}$$

If the terms in the first power of β are retained, but the term of $O(\alpha\beta)$ are dropped and differentiating equation (2.30) with respect to x', we obtain

$$\eta'_{t'} + \left\{(1+\alpha\eta')w\right\}_{x'} - \frac{1}{6}\beta w_{x'x'x'} + O(\alpha\beta, \beta^2) = 0, \tag{2.31}$$

$$w_{t'} + \alpha w w_{x'} + \eta'_{x'} - \frac{1}{2}\beta w_{x'x't'} + O(\alpha\beta, \beta^2) = 0, \quad w = f_{x'}. \tag{2.32}$$

Equations (2.31) and (2.32) are variants of Boussinesq's equations. However, the velocity $\phi'_{x'}$ is derived as

$$\phi'_{x'} = w - \beta\frac{z'^2}{2}w_{x'x'} + O(\beta^2).$$

The value averaged over the depth is

$$\tilde{u} = w - \frac{1}{6}\beta w_{x'x'} + O(\alpha\beta, \beta^2),$$

inverting this expression yields

$$w = \tilde{u} + \frac{1}{6}\beta\tilde{u}_{x'x'} + O(\alpha\beta, \beta^2).$$

2.2.3 Derivation of the KdV equation

The Korteweg-de Vries (KdV) equation can be derived from any of these equations by focusing on the wave moving to the right only. If the terms of order α and β are neglected from equations (2.31) and (2.32), we have

$$w = \eta', \quad \eta'_{t'} + \eta'_{x'} = 0.$$

The aim is to obtain a solution in the form which is to the first order in α and β as

$$w = \eta' + \alpha A + \beta B + O(\alpha^2 + \beta^2),$$

where functions of η' and its x' derivatives are represented by A and B. Substituting this in equations (2.31) and (2.32) gives

$$\eta'_{t'} + \eta'_{x'} + \alpha \{A_{x'} + 2\eta'\eta'_{x'}\} + \beta \left(B_{x'} - \frac{1}{6}\eta'_{x'x'x'}\right) + O(\alpha^2 + \beta^2) = 0, \tag{2.33}$$

$$\eta'_{t'} + \eta'_{x'} + \alpha \{A_{t'} + \eta'\eta'_{x'}\} + \beta \left(B_{t'} - \frac{1}{2}\eta'_{x'x't'}\right) + O(\alpha^2 + \beta^2) = 0. \tag{2.34}$$

After dropping the terms of α and β, we have

$$\eta'_{t'} = -\eta'_{x'} + O(\alpha, \beta).$$

Equations (2.33) and (2.34) are consistent if

$$A = -\frac{1}{4}\eta'^2, \quad B = \frac{1}{3}\eta'_{x'x'}.$$

Substituting A and B into equations (2.33) and (2.34) gives

$$\eta'_{t'} + \eta'_{x'} + \frac{3}{2}\alpha\eta'\eta'_{x'} + \frac{1}{6}\beta\eta'_{x'x'x'} + O(\alpha^2 + \beta^2) = 0, \tag{2.35}$$

$$w = \eta' - \frac{1}{4}\alpha\eta'^2 + \frac{1}{3}\beta\eta'_{x'x'} + O(\alpha^2 + \beta^2), \tag{2.36}$$

Equation (2.36) is similar to Riemann invariant and expression (2.35) is the normalized form of the KdV equation. Using the parameters defined earlier, the normalized variables is change into the original variables, and the terms α and β are dropped to obtain

$$w = \eta - \frac{1}{4}\eta^2 + \frac{1}{3}\eta_{xx}, \tag{2.37}$$

and the KdV equation in the form [8]

$$\eta_t + c_0\eta_x + \frac{3}{2}\frac{c_0}{h_0}\eta\eta_x + \frac{1}{6}c_0h_0^2\eta_{xxx} = 0. \tag{2.38}$$

2.2.4 Derivation of the BBM equation

The BBM equation is derived by neglecting the nonlinear and higher order terms in the KdV equation (2.38) to yields

$$\eta_x = -\frac{1}{c_0}\eta_t.$$

Using this expression in the last term of equation (2.38) gives

$$\eta_t + c_0\eta_x + \frac{3}{2}\frac{c_0}{h_0}\eta\eta_x - \frac{1}{6}h_0^2\eta_{xxt} = 0. \tag{2.39}$$

Equation (2.39) is the associated BBM equation to the KdV equation (2.38). The non-dimensional form of the BBM equation is given as

$$\eta_t + \eta_x + \frac{3}{2}\eta\eta_x - \frac{1}{6}\eta_{xxt} = 0. \tag{2.40}$$

2.2.5 Solitary wave solution of the BBM equation

The solitary wave solution of BBM equation

$$\eta_t + \eta_x + \frac{3}{2}\eta\eta_x - \frac{1}{6}\eta_{xxt} = 0, \tag{2.41}$$

is derived as follows. Let's make use of the traveling wave solution as the solution to equation (2.41)

$$\eta(x,t) = f(\xi) = f(x - ct), \tag{2.42}$$

that is,

$$f(\xi) = f(x - ct), \tag{2.43}$$

By differentiating equation (2.43) with respect to t, we get

$$f_t = -c\frac{df}{d\xi}. \tag{2.44}$$

Again, differentiating equation (2.43) with respect to x twice, then with respect to t, we obtain

$$f_x = \frac{df}{d\xi},\ f_{xx} = \frac{d^2f}{d\xi^2},\ f_{xxt} = -c\frac{d^3f}{d\xi^3}. \tag{2.45}$$

Substituting equation (2.43), (2.44) and (2.45) into equation (2.41), we obtain

$$-c\frac{df}{d\xi} + \frac{df}{d\xi} + \frac{3}{2}f\frac{df}{d\xi} + \frac{c}{6}\frac{d^3f}{d\xi^3} = 0,$$

this is written as

$$(1-c)\frac{df}{d\xi}+\frac{3}{2}f\frac{df}{d\xi}+\frac{c}{6}\frac{d^3f}{d\xi^3}=0. \tag{2.46}$$

Integrating directly since the resulting equation is total derivative, we obtain

$$(1-c)f+\frac{3}{4}f^2+\frac{c}{6}\frac{d^2f}{d\xi^2}=k_1, \tag{2.47}$$

where k_1 is the constant of integration. Our focus is to obtain a first order differential equation for function f, to achieve this, multiply equation (2.47) by $\frac{df}{d\xi}$, we have

$$(1-c)f\frac{df}{d\xi}+\frac{3}{4}f^2\frac{df}{d\xi}+\frac{c}{6}\frac{d^2f}{d\xi^2}\frac{df}{d\xi}=k_1\frac{df}{d\xi},$$

this can be written as

$$(1-c)fdf+\frac{3}{4}f^2df+\frac{c}{6}\frac{d^2f}{d\xi^2}df=k_1df,$$

integrating both side with respect to f yields

$$\frac{(1-c)}{2}f^2+\frac{1}{4}f^3+\frac{c}{12}\left(\frac{df}{d\xi}\right)^2=k_1f+k_2, \tag{2.48}$$

where k_2 is the constant of integration. To obtain the value of constant k_1 and k_2, we have to consider the condition that $f(\xi)\to 0$ when $\xi\to\pm\infty$, then we will have

$$f\to 0,\quad \frac{df}{d\xi}\to 0,\quad \frac{d^2f}{d\xi^2}\to 0.$$

Using these conditions, we obtain $k_1=0$ and $k_2=0$. Hence, equation (2.48) becomes

$$\frac{c}{12}\left(\frac{df}{d\xi}\right)^2=-\frac{(1-c)}{2}f^2-\frac{1}{4}f^3,$$

therefore,

$$\left(\frac{df}{d\xi}\right)^2=\frac{1}{c}\left[3f^2\left[2(c-1)-f\right]\right].$$

By separation of variable

$$\frac{df}{f\sqrt{\frac{3}{c}\left[2(c-1)-f\right]}}=d\xi, \tag{2.49}$$

integrate both sides of equation (2.49)

$$\int_0^f\frac{d\psi}{\psi\sqrt{\frac{6(c-1)}{c}-\frac{3}{c}\psi}}=\int_0^\xi d\kappa, \tag{2.50}$$

In order to proceed, we have to do the transformation of left hand side of Equation (2.50) by

$$m := \frac{6(c-1)}{c} \div \frac{3}{c}\text{sech}^2 p = 2(c-1)\text{sech}^2 p. \tag{2.51}$$

Here ψ will play the role of m i.e $\psi = m$. Let us use this to simplify the denominator of equation (2.50), we have

$$\frac{6(c-1)}{c} - \frac{3}{c}\psi = \frac{6(c-1)}{c} - \frac{3}{c}\left[2(c-1)\text{sech}^2 p\right] = \frac{6(c-1)}{c}\left[1 - \text{sech}^2 p\right].$$

Recall that $\tanh^2 p = 1 - \text{sech}^2 p$, therefore

$$\frac{6(c-1)}{c} - \frac{3}{c}\psi = \frac{6(c-1)}{c}\tanh^2 p. \tag{2.52}$$

In addition, differentiate equation (2.51) with respect to p, we obtain

$$\frac{d\psi}{dp} = -4(c-1)\frac{\sinh p}{\cosh^3 p}. \tag{2.53}$$

Next, we transform the upper integration limit of LHS of equation (2.50), i.e.

$$f = 2(c-1)\text{sech}^2 p,$$

making p the subject of the relation

$$p = \text{sech}^{-1}\sqrt{\frac{f}{2(c-1)}}. \tag{2.54}$$

Substituting equations (2.52), (2.53), and (2.54) into equation (2.50) gives

$$\int_0^f \left(\frac{1}{2(c-1)\text{sech}^2 p\sqrt{\frac{6(c-1)}{c}\tanh^2 p}}\right)\left(-4(c-1)\frac{\sinh p}{\cosh^3 p}\right)dp = \int_0^\xi d\kappa.$$

After simplification, we have

$$-\frac{2}{\sqrt{\frac{6(c-1)}{c}}}p = \xi.$$

Since $p = \text{sech}^{-1}\sqrt{\frac{f}{2(c-1)}}$ in equation (2.54), we have

$$-\frac{2}{\sqrt{\frac{6(c-1)}{c}}}\text{sech}^{-1}\sqrt{\frac{f}{2(c-1)}} = \xi.$$

By making f the subject of the relation, we have

$$f(\xi) = 2(c-1)\text{sech}^2\left(\frac{\sqrt{1}}{2}\sqrt{\frac{6(c-1)}{c}}\xi\right).$$

By using equation (2.42), we finally obtain

$$\eta(x,t) = 2(c-1)\text{sech}^2\left(\frac{1}{2}\sqrt{\frac{6(c-1)}{c}}(x-ct)\right) \tag{2.55}$$

From equation (2.55),

$$\eta(x,t) = 2(c-1)\text{sech}^2\left(\frac{1}{2}\sqrt{\frac{6(c-1)}{c}}(x-x_0-ct)\right) = \eta_0\text{sech}^2\left(\frac{1}{2}\sqrt{\frac{6\eta_0}{2+\eta_0}}(x-x_0-ct)\right), \tag{2.56}$$

where η_0 is the amplitude, x_0 is the initial point of the wave crest, and the phase velocity c is given by

$$c = 1 + \frac{\eta_0}{2}. \tag{2.57}$$

Chapter 3

Methodology

3.1 Particle trajectories in the BBM approximation

After the derivation of the Boussinesq system and the BBM model in section 2.2, to investigate the particle paths, the following considerations follow

3.1.1 Horizontal and vertical velocity

Differentiating equation (2.28) with respect to x', the horizontal velocity is expressed as

$$u(x,z,t) = \phi_{x'} = w - \frac{z'^2}{2} w_{x'x'}\beta + \mathcal{O}(\beta^2). \tag{3.1}$$

Similarly, the vertical velocity can be written as

$$v(x,z,t) = \phi_{z'} = -z' w_{x'}\beta + \mathcal{O}(\beta^2). \tag{3.2}$$

Dropping the prime and β in equations (3.1) and (3.2), the expression for the horizontal velocity of the fluid particle is given in non-dimensional variable as

$$u(x,z,t) = w - \frac{z^2}{2} w_{xx}, \tag{3.3}$$

which is improved to read

$$u(x,z,t) = \eta - \frac{1}{4}\eta^2 + \left(\frac{1}{3} - \frac{z^2}{2}\right)\eta_{xx}. \tag{3.4}$$

Similarly, the vertical velocity is given as

$$v(x,z,t) = -z w_x. \tag{3.5}$$

3.1.2 Particle paths

Let the functions $\xi(t)$ and $\zeta(t)$ denote the x-coordinate and z-coordinate, respectively, of a particle initially positioned at the point $(x, z) = (\xi_0, \zeta_0)$. Then, the particle movement is given by the differential equations

$$\frac{\partial \xi}{\partial t} = u(\xi(t), \zeta(t), t), \quad \frac{\partial \zeta}{\partial t} = v(\xi(t), \zeta(t), t), \tag{3.6}$$

with the initial conditions $\xi(0) = \xi_0$ and $\zeta(0) = \zeta_0$. The solutions to these equations is obtained numerically using fourth-order Runge-Kutta method.

3.1.3 Particle trajectories in solitary-wave solutions

Here, the focus is centered on the particle trajectories in the fluid due to the passage of a solitary wave at the surface. The exact solution of the BBM equation in connection to the solitary-wave is given by

$$\eta(x,t) = \eta_0 \text{sech}^2\left(\frac{1}{2}\sqrt{\frac{6\eta_0}{2+\eta_0}}(x - x_0 - ct)\right), \tag{3.7}$$

where η_0 represents the amplitude, x_0 denotes the initial point of the wave crest, and the phase velocity c is given by

$$c = 1 + \frac{\eta_0}{2}. \tag{3.8}$$

Substituting the solitary-wave solution of the BBM equation given in (3.7) into the relation (2.37), then we got the expression

$$w = \eta_0 \text{sech}^2(\mathcal{A})\left\{1 - \frac{\eta_0}{4}\text{sech}^2(\mathcal{A}) - \frac{\eta_0}{2+\eta_0}\left[3\text{sech}^2(\mathcal{A}) - 2\right]\right\}, \tag{3.9}$$

for the horizontal velocity, where the argument $\mathcal{A} = \frac{1}{2}\sqrt{\frac{6\eta_0}{2+\eta_0}}(x - ct)$. Using equations (3.4) and (3.5) in connection to the relations (3.7) and (3.9), the velocity components, that is, the horizontal and vertical velocities at an arbitrary point (x, z) in the fluid, and at a given time t are computed as

$$u(x,z,t) = \eta_0 \text{sech}^2(\mathcal{A})\left\{1 - \frac{\eta_0}{4}\text{sech}^2(\mathcal{A}) - \frac{3\eta_0}{2+\eta_0}\left(\frac{1}{3} - \frac{z^2}{2}\right)\left[3\text{sech}^2(\mathcal{A}) - 2\right]\right\}, \tag{3.10}$$

$$v(x,z,t) = -z\frac{\eta_0}{2}\sqrt{\frac{6\eta_0}{2+\eta_0}}\text{sech}^2(\mathcal{A})\tanh(\mathcal{A})\left\{-2 + \eta_0\text{sech}^2(\mathcal{A}) + \frac{4\eta_0}{2+\eta_0}\left(3\text{sech}^2(\mathcal{A}) - 1\right)\right\}. \tag{3.11}$$

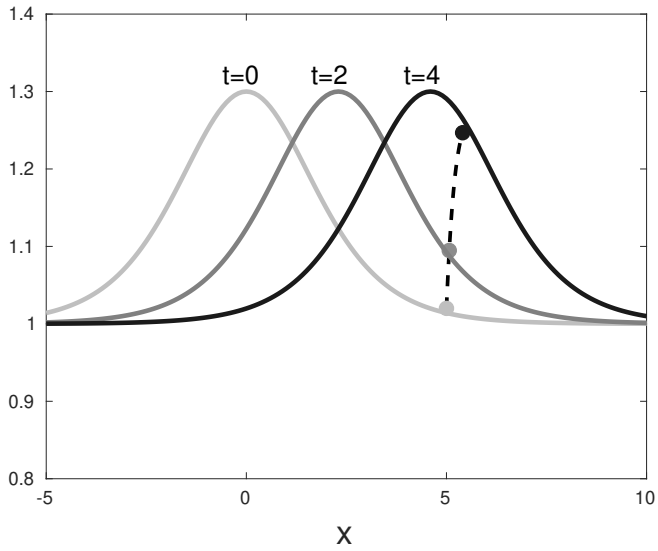

Figure 3.1: The wave profile is shown at $t = 0$ (light-gray), $t = 2$ (dark-gray) and $t = 4$ (black) as indicated in the figure. The particle trajectory originally located on the surface at (5, 1.02) is denoted by the dashed curve.

The surface profile and the particle trajectories throughout the propagation of the solitary wave with amplitude $\eta_0 = 0.3$ are shown in figures 3.1 and 3.2. Figure 3.1 reveals the time evolution of the fluid particle at the surface of the fluid, and the wave profile is displayed at $t = 0$ (light-gray), $t = 2$ (dark-gray) and $t = 4$ (black). Different color is used to denotes the position of the particle on the wave profile; the light-gray spot shows the particle location at time $t = 0$, while the dark-gray spot and the black spot show the particle position at time $t = 4$ and $t = 6$ respectively. It worth noting from these figures that if the fluid particles are positioned to the right side of the crest, they tend to go towards the right and upwards as shown in figure 3.1, while the fluid particles go towards the right and downwards if they are positioned to the left of the crest. This concurred with the discoveries of Borluk and Kalisch [8] and Constantin and Escher [16]. Figure 3.2 demonstrates the particle trajectories during one complete wave cycle. It is evident that the particles which are closer to the bed produce a smaller total excursion. It is regarded that the vertical excursion is smaller when compared to its horizontal displacement and decreases quickly with the depth of the trajectory beneath the free surface. Hence, the particles near the bottom possess a smaller amplitude and the path becomes more or less a straight line at the bottom since the vertical motion of the particle is zero, and just a horizontal displacement remains in existence. These results are in agreement with the results obtained by Khorsand [35] as well as Borluk and Kalisch [8].

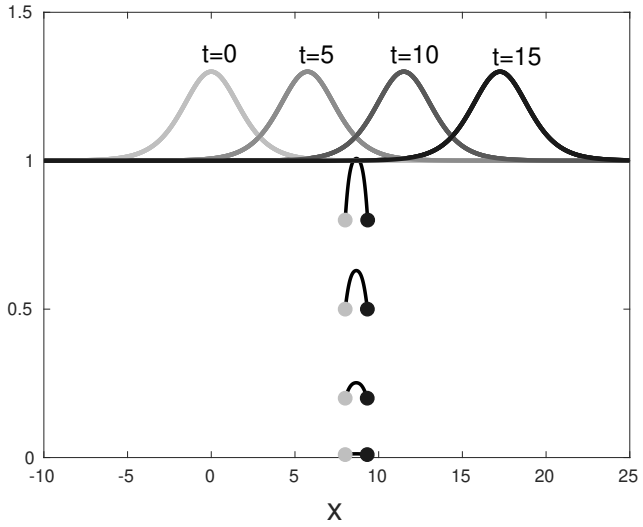

Figure 3.2: The wave profile is shown at $t = 0$, $t = 5$, $t = 10$ and $t = 15$. The paths of the fluid particles shown were initially located at (8, 0.8),(8, 0.5),(8, 0.2) (8, 0.01). The light-gray dots describe the particle positions at time $t = 0$, and the black dots describe the particle positions at time $t = 6$. The curves indicate the paths traced out by particles during the transition from the left to the right.

3.1.4 Particle trajectories in periodic waves

In [22], the periodic wavetrains of KdV approximation are defined by exact solutions of which are expressed as cnoidal functions. The same concept is used here for BBM approximation. The periodic solutions of BBM equation (2.40) are given by

$$\eta = f_2 + (f_1 - f_2)\mathrm{cn}^2(\mathcal{B}), \tag{3.12}$$

where the constants f_1, f_2 and f_3 which are given in the order $f3 < f2 < f1$ are used to described the solution. The argument of equation (3.12) is given by $\mathcal{B}(x,t) = \frac{1}{2}\sqrt{\frac{6}{2+(f_1-f_3)}}(f_1-f_3)^{1/2}(x-ct)$, cn is one of the Jacobian elliptic functions defined by the incomplete elliptic integral of the first kind [8, 39], and the modulus m of this Jacobian elliptic function is given by $m = \frac{f_1-f_2}{f_1-f_3}$. The phase speed and the wavelength of the wave are given by $c = 1 + \frac{(f_1+f_2+f_3)}{2}$ and $\lambda = 4\sqrt{\frac{2+(f_1-f_3)}{6}}K(m)\frac{1}{\sqrt{f_1-f_3}}$ respectively, where $K(m)$ is the complete elliptic integral of the first kind.

Upon substituting (3.12) into relation (2.37), the horizontal velocity in terms of

the Jacobian elliptic functions is given as

$$
\begin{aligned}
w &= f_2 - \frac{1}{4}f_2^2 + (f_1 - f_2)\left(1 - \frac{f_2}{2}\right)\mathrm{cn}^2(\mathcal{B}) \\
&- \frac{1}{4}(f_1 - f_2)^2\mathrm{cn}^4(\mathcal{B}) - \frac{1}{2 + (f_1 - f_3)}(f_1 - f_2)(f_1 - f_3)\times \\
&\Big\{ - \mathrm{sn}^2(\mathcal{B})\mathrm{dn}^2(\mathcal{B}) + \mathrm{cn}^2(\mathcal{B})\mathrm{dn}^2(\mathcal{B}) - m\ \mathrm{sn}^2(\mathcal{B})\mathrm{cn}^2(\mathcal{B})\Big\}.
\end{aligned}
$$

Hence, for the periodic-wave solutions of the BBM equation, the horizontal and vertical velocities at an arbitrary point (x, z) in the fluid, and at a time t are computed as

$$
\begin{aligned}
u(x,z,t) &= f_2 - \frac{1}{4}f_2^2 + (f_1 - f_2)\left(1 - \frac{f_2}{2}\right)\mathrm{cn}^2(\mathcal{B}) \\
&- \frac{1}{4}(f_1 - f_2)^2\mathrm{cn}^4(\mathcal{B}) - \frac{1}{2 + (f_1 - f_3)}(f_1 - f_2)(f_1 - f_3)\times \\
&\Big\{ - \mathrm{sn}^2(\mathcal{B})\mathrm{dn}^2(\mathcal{B}) + \mathrm{cn}^2(\mathcal{B})\mathrm{dn}^2(\mathcal{B}) - m\ \mathrm{sn}^2(\mathcal{B})\mathrm{cn}^2(\mathcal{B})\Big\} \\
&- \frac{\zeta^2}{4}\cdot\frac{3}{2 + (f_1 - f_3)}(f_1 - f_3)\Big\{ - (f_1 - f_2)(2 - f_2)\times \\
&(\mathrm{cn}^2(\mathcal{B})\mathrm{dn}^2(\mathcal{B}) - \mathrm{sn}^2(\mathcal{B})\mathrm{dn}^2(\mathcal{B}) - \mathrm{m}\ \mathrm{sn}^2(\mathcal{B})\mathrm{cn}^2(\mathcal{B})) \\
&+ (f_1 - f_2)^2(\mathrm{cn}^4(\mathcal{B})\mathrm{dn}^2(\mathcal{B}) - 3\mathrm{sn}^2(\mathcal{B})\mathrm{cn}^2(\mathcal{B})\mathrm{dn}^2(\mathcal{B}) \\
&- \mathrm{m}\ \mathrm{sn}^2(\mathcal{B})\mathrm{cn}^4(\mathcal{B})) + \left(\frac{4}{2 + (f_1 - f_3)}(f_1 - f_2)(f_1 - f_3)\right)\times \\
&[(\mathrm{cn}^2(\mathcal{B})\mathrm{dn}^2(\mathcal{B}) - \mathrm{sn}^2(\mathcal{B})\mathrm{dn}^2(\mathcal{B}) - \mathrm{m}\ \mathrm{sn}^2(\mathcal{B})\mathrm{cn}^2(\mathcal{B}))[\mathrm{dn}^2(\mathcal{B}) \\
&+ \mathrm{m}\ \mathrm{cn}^2(\mathcal{B}) - \mathrm{m}\ \mathrm{sn}^2(\mathcal{B})] - 6\mathrm{m}\ \mathrm{sn}^2(\mathcal{B})\mathrm{cn}^2(\mathcal{B})\mathrm{dn}^2(\mathcal{B})]\Big\},
\end{aligned}
\tag{3.13}
$$

$$
\begin{aligned}
v(x,z,t) = &- \frac{\zeta}{2}\sqrt{\frac{6}{2 + (f_1 - f_3)}}(f_1 - f_3)^{1/2}\mathrm{sn}(\mathcal{B})\mathrm{cn}(\mathcal{B})\mathrm{dn}(\mathcal{B})\times \\
&\Big\{ - (f_1 - f_2)(2 - f_2) + (f_1 - f_2)^2\mathrm{cn}^2(\mathcal{B}) \\
&+ \frac{4}{2 + (f_1 - f_3)}(f_1 - f_2)(f_1 - f_3)(\mathrm{dn}^2(\mathcal{B}) \\
&+ \mathrm{m}\ \mathrm{cn}^2(\mathcal{B}) - \mathrm{m}\ \mathrm{sn}^2(\mathcal{B}))\Big\}.
\end{aligned}
\tag{3.14}
$$

Some of the results obtained are presented below

In Figure 3.3, the particle trajectories (ξ, ζ) for periodic waves for one complete cycle using the fourth-order Runge–Kutta method are shown. The closeup in the lower panel shows the importance of periodicity. It is seen that the particle accomplishes a small elliptic cycle prior to its up turning and riding into the next wave.

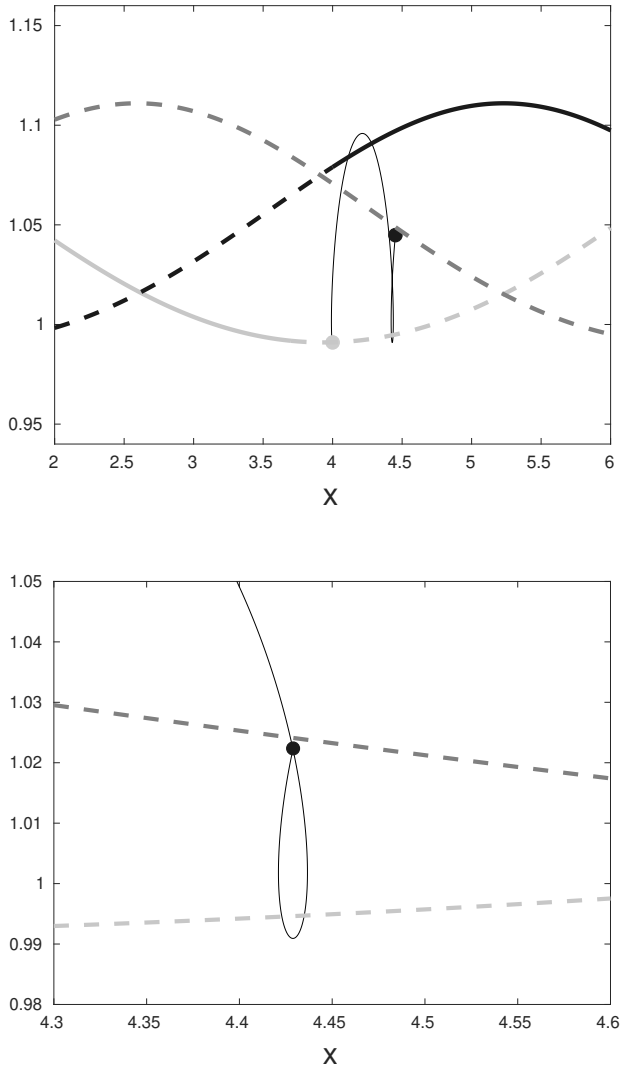

Figure 3.3: The upper panel shows a periodic wave with wavelength 7.3208, period 7.6980 and phase speed $c = 0.9510$ at time $t = 0$ (light-gray), $t = 5$ (dark-gray) and $t = 10$ (black). The motion of the surface is indicated by the solid part which is kept constant in the curve. The path of a particle originated from $(x, z) = (4, 1)$ is shown. A close-up of the lower turning point is shown in the lower panel.

In Figure 3.4, a train of cnoidal waves is presented. The vertical speed and the total vertical excursion of the particles closer to the bed are smaller compared to others. This is pretty much the same as the results obtained for the particle trajectories below the solitary waves.

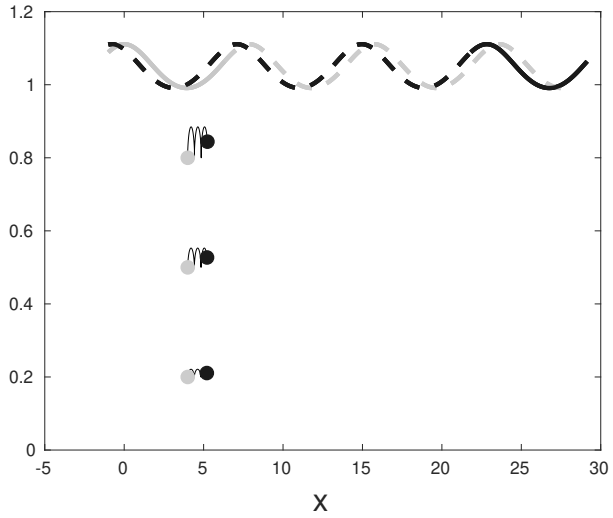

Figure 3.4: The figure shows a periodic wave with wavelength 7.3208, period 7.6980 and phase speed $c = 0.9510$ at time $t = 0$ (light-gray) and $t = 24$ (black). The motion of the surface is indicated by the solid part which is kept constant in the curve. The paths of particles originally located at (4, 0.8), (4, 0.5) and (4, 0.2) are shown.

3.2 Particle trajectories in nonlinear waves on a uniform Shear Flow

3.2.1 The given model

The water-wave problem concerning waves at the surface of an inviscid, incompressible Newtonian fluid is given by the Euler equations with no-penetration conditions at the bed and kinematic and dynamic boundary conditions at the free surface. The sea floor is assumed to be flat. We denote the spatial coordinates by (x, z) where the $x-$axis coincides with the undisturbed free surface, and assume long-crested waves which are uniform in the transverse direction. The gravitational acceleration in the negative $z-$direction is denoted by g, the undisturbed depth is h_0, and $\eta(x, t)$ denotes the departure of the free surface from the rest position. The decisive feature in the present work is the existence of a uniform shear flow with a free surface as shown in Fig. 3.5. In this case, the vorticity is given by a predescribed constant Γ, and the background distribution of the original velocity component before the arrival of the waves is given by

$$\left.\begin{array}{rcl} U & = & U_0 - (z + h_0)\Gamma, \\ V & = & 0. \end{array}\right\} \tag{3.15}$$

For $\Gamma > 0$, we have a shear flow in the direction opposite to the wave propagation. For $\Gamma < 0$, the background flow is in the favorable direction, that is, in the direction

of wave propagation. In most cases, we assume $U_0 = 0$. Assuming a is a typical amplitude, and l is a typical wavelength of the waves to be described, the parameter $\alpha = a/h_0$ represents the amplitude to depth ratio, and the parameter $\beta = h_0^2/l^2$ represents the water depth to wavelength ratio.

In the case of a linear shear flow such as delineated in (3.15), the vorticity is constant. For later reference, we define the unit vectors in the x, y and z directions as $\mathbf{e}_x$, $\mathbf{e}_y$ and $\mathbf{e}_z$, respectively. The vorticity is then given by $\omega = (U_z - V_x)\mathbf{e}_y = -\Gamma \mathbf{e}_y$. In general, one may use Kelvin's circulation theorem together with Stokes theorem and the incompressibility condition to understand that constant vorticity is conserved in inviscid, incompressible flow. In consequence, the flow can be split into a shear flow with uniform vorticity and a pure potential flow. For a uniform shear flow, the perturbation velocity is given in terms of the potential $\phi(x, z, t)$, with $u = \phi_x$ and $v = \phi_z$. The complete velocity field is given by

$$\left.\begin{aligned} U = \phi_x + U_0 - (z + h_0)\Gamma, \\ V = \phi_z. \end{aligned}\right\}$$

Indeed, if we define a three-dimensional velocity field $\mathbf{U} = (U, 0, V)$ for notational convenience, the vorticity is $\omega = \mathrm{curl}(\mathbf{U})$, and it can be checked that the above definition satisfies the vorticity equation

$$\omega_t + (\mathbf{U} \cdot \nabla)\omega = \omega \cdot \nabla \mathbf{U}. \tag{3.16}$$

Using the incompressibility condition $\nabla \cdot \mathbf{U} = 0$ also shows that the velocity potential satisfies Laplace's equation. We can then rewrite the Euler equation

$$\mathbf{U}_t + \frac{1}{2}\nabla |\mathbf{U}|^2 - \mathbf{U} \times \omega + g e_z = 0$$

in terms of the potential ϕ to obtain

$$\nabla\left\{\phi_t + \frac{1}{2}|\mathbf{U}|^2 + gz\right\} \quad = \quad \mathbf{U} \times \omega,$$

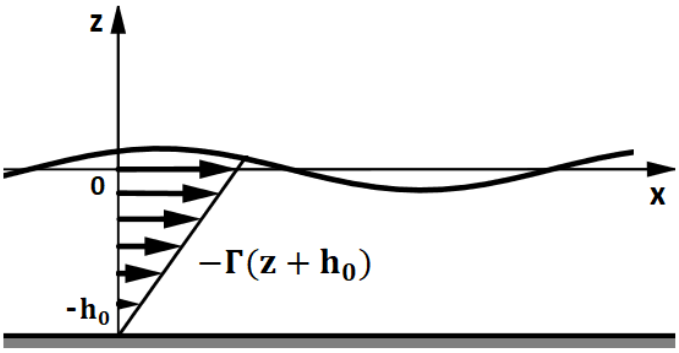

Figure 3.5: Wave propagation over a background shear flow. In this figure, the vorticity Γ is negative.

As the left-hand side is obviously a gradient, the term $\mathbf{U} \times \omega$ must also be the gradient of a function. Following [59] it becomes plain that $\mathbf{u} \times \omega = \nabla G$, where the function G is given by

$$G = -\Gamma \int_{-h_0}^{z} \phi_x \, dz + \Gamma \, U_0 \, z - \frac{\Gamma^2}{2}(z + h_0)^2.$$

The complete problem is written as follows:

$$\Delta\phi = 0 \qquad \text{in} \qquad -h_0 < z < \eta(x,t), \tag{3.17}$$

$$\phi_z = 0 \qquad \text{on} \qquad z = -h_0, \tag{3.18}$$

$$\left.\begin{aligned} \eta_t + U\eta_x - V = 0, \\ \nabla\Big(\phi_t + \tfrac{|\mathbf{u}|^2}{2} + G + g\eta\Big) = 0, \end{aligned}\right\} \qquad \text{on} \qquad z = \eta(x,t). \tag{3.19}$$

3.2.2 Derivation of Boussinesq system

The next goal is to derive a Boussinesq system approximating the wave motion described by (3.17)-(3.19). Here, we follow the development explained in [59]. For starters, the variables are non-dimensionalized using the following scaling

$$\tilde{x} = \frac{x}{l}, \quad \tilde{z} = \frac{z}{h_0}, \quad \tilde{t} = \frac{\sqrt{gh_0}t}{l}, \quad \tilde{\Gamma} = \frac{\Gamma h_0}{\sqrt{gh_0}}, \quad \tilde{\eta} = \frac{\eta}{a}, \quad \tilde{\phi} = \frac{h_0}{al\sqrt{gh_0}}\phi. \tag{3.20}$$

The non-dimensional potential $\tilde{\phi}$ is expressed in powers of $(1 + \tilde{z})$ as

$$\tilde{\phi} = \sum_{n=0}^{\infty} (1 + \tilde{z})^n \phi_n. \tag{3.21}$$

Therefore, we obtain

$$\tilde{\phi} = \phi_0 - \frac{\beta}{2}(1 + \tilde{z})^2 \phi_{0\tilde{x}\tilde{x}} + \frac{\beta^2}{24}(1 + \tilde{z})^4 \phi_{0\tilde{x}\tilde{x}\tilde{x}\tilde{x}} + \mathcal{O}(\beta^3). \tag{3.22}$$

To find a closed system of two evolution equations, we substitute the asymptotic expression for $\tilde{\phi}$ in the associated boundary conditions, and collect all terms of zeroth and first-order in α and β. Then we differentiate dynamic bottom boundary with respect to $\tilde{x}$ and expressed the boundary conditions in terms of the non-dimensional horizontal velocity at the bottom $\phi_{0\tilde{x}} = \tilde{w}$. This procedure yields the system of equations

$$\begin{aligned} \tilde{\eta}_{\tilde{t}} + \tilde{w}_{\tilde{x}} - \tilde{\Gamma}\tilde{\eta}_{\tilde{x}} - \alpha\tilde{\Gamma}\tilde{\eta}\tilde{\eta}_{\tilde{x}} + \alpha(\tilde{\eta}\tilde{w})_{\tilde{x}} - \frac{\beta}{6}\tilde{w}_{\tilde{x}\tilde{x}\tilde{x}} = \mathcal{O}(\alpha\beta, \beta^2), \\ \tilde{w}_{\tilde{t}} + \tilde{\eta}_{\tilde{x}} + \alpha\tilde{w}\tilde{w}_{\tilde{x}} - \frac{\beta}{2}\tilde{w}_{\tilde{x}\tilde{x}\tilde{t}} + \frac{\beta}{3}\tilde{\Gamma}\tilde{w}_{\tilde{x}\tilde{x}\tilde{x}} = \mathcal{O}(\alpha\beta, \beta^2). \end{aligned} \tag{3.23}$$

It is not difficult to derive the following expression as an asymptotic formula for $\tilde{w}$ in terms of $\tilde{w}^\theta$:

$$\tilde{w} = \tilde{w}^\theta + \frac{\beta}{2}\theta^2 \tilde{w}^\theta_{\tilde{x}\tilde{x}} + \mathcal{O}(\alpha\beta, \beta^2). \tag{3.24}$$

Substituting this representation into the system (3.23), this yields the Boussinesq system

$$\begin{aligned}\tilde{\eta}_{\tilde{t}} + \tilde{w}^{\theta}_{\tilde{x}} - \tilde{\Gamma}\tilde{\eta}_{\tilde{x}} - \alpha\tilde{\Gamma}\tilde{\eta}\tilde{\eta}_{\tilde{x}} + \alpha(\tilde{\eta}\tilde{w}^{\theta})_{\tilde{x}} + \frac{\beta}{2}(\theta^2 - \tfrac{1}{3})\tilde{w}^{\theta}_{\tilde{x}\tilde{x}\tilde{x}} = \mathcal{O}(\alpha\beta, \beta^2),\\ \tilde{w}^{\theta}_{\tilde{t}} + \tilde{\eta}_{\tilde{x}} + \alpha\tilde{w}^{\theta}\tilde{w}^{\theta}_{\tilde{x}} + \frac{\beta}{2}(\theta^2 - 1)\tilde{w}^{\theta}_{\tilde{x}\tilde{x}\tilde{t}} + \frac{\beta}{3}\tilde{\Gamma}\tilde{w}^{\theta}_{\tilde{x}\tilde{x}\tilde{x}} = \mathcal{O}(\alpha\beta, \beta^2).\end{aligned} \tag{3.25}$$

3.2.3 Derivation of BBM equation

We now concentrate on unidirectional waves. In the lowest order, the Boussinesq equation is the linear system

$$\tilde{\eta}_{\tilde{t}} + \tilde{w}^{\theta}_{\tilde{x}} - \tilde{\Gamma}\tilde{\eta}_{\tilde{x}} = 0, \quad \tilde{w}^{\theta}_{\tilde{t}} + \tilde{\eta}_{\tilde{x}} = 0. \tag{3.26}$$

Hence, after numerous computations we obtained

$$\tilde{\eta}_{\tilde{t}} + \tilde{c}_{+}\tilde{\eta}_{\tilde{x}} + \alpha\frac{\tilde{c}_{+}(3+\tilde{\Gamma}^2)}{(1+\tilde{c}_{+}^2)}\tilde{\eta}\tilde{\eta}_{\tilde{x}} + \beta\frac{\tilde{c}_{+}+\tilde{\Gamma}}{3(1+\tilde{c}_{+}^2)}\tilde{\eta}_{\tilde{x}\tilde{x}\tilde{x}} = \mathcal{O}(\alpha\beta, \beta^2), \tag{3.27}$$

$$\tilde{w}^{\theta} = -\tilde{c}_{-}\tilde{\eta} + \alpha\frac{\tilde{c}_{-}+\tilde{\Gamma}}{2(1+\tilde{c}_{+}^2)}\tilde{\eta}^2 + \beta\left(\frac{\tilde{c}_{+}+\tilde{\Gamma}}{3(1+\tilde{c}_{+}^2)} - \frac{\tilde{c}_{-}}{6} + \frac{\tilde{c}_{-}}{2}\theta^2\right)\tilde{\eta}_{\tilde{x}\tilde{x}} + \mathcal{O}(\alpha\beta, \beta^2), \tag{3.28}$$

where $c_{+} = \frac{-\Gamma}{2} + \sqrt{\frac{\Gamma^2}{4}+1}$ and $c_{-} = \frac{-\Gamma}{2} - \sqrt{\frac{\Gamma^2}{4}+1}$. Expression (3.27) is the KdV equation with constant vorticity, while Eq. (3.28) denotes the non-dimensional horizontal velocity at the bottom.

It will be convenient to define non-dimensional variables adapted to the problem at hand. In particular, a new non-dimensionalization adapted to the numerical study is defined by

$$x \to h_0 x,\ z \to h_0 z,\ \eta \to h_0\eta,\ t \to \frac{h_0}{\sqrt{gh_0}}t,\ u \to \sqrt{gh_0}u,\ w \to \sqrt{gh_0}w, \text{ and } \Gamma \to \frac{\Gamma\sqrt{gh_0}}{h_0}. \tag{3.29}$$

The Eq. (3.27) can be rewritten in terms of new variables as

$$\eta_t + c_{+}\eta_x + \frac{c_{+}(3+\Gamma^2)}{(1+c_{+}^2)}\eta\eta_x + \frac{c_{+}+\Gamma}{3(1+c_{+}^2)}\eta_{xxx} = 0. \tag{3.30}$$

This equation was also found in [47, 51]. By neglecting the nonlinear term as well as the higher order term, the resulting equation is given as $\eta_t + c_{+}\eta_x = 0$, Upon differentiating both sides, we have $\eta_{xxx} = -\frac{1}{c_{+}}\eta_{xxt}$. Hence, this yields the BBM system

$$\eta_t + c_{+}\eta_x + \frac{c_{+}(3+\Gamma^2)}{(1+c_{+}^2)}\eta\eta_x - \frac{c_{+}+\Gamma}{3c_{+}(1+c_{+}^2)}\eta_{xxt} = 0, \tag{3.31}$$

$$w^{\theta} = -c_{-}\eta + \frac{c_{-}+\Gamma}{2(1+c_{+}^2)}\eta^2 + \frac{c_{+}+\Gamma}{3(1+c_{+}^2)}\eta_{xx} - \frac{c_{-}}{6}\eta_{xx} + \frac{c_{-}}{2}\theta^2\eta_{xx}. \tag{3.32}$$

3.2.4 Horizontal and vertical velocity

From Eq. (3.22), the non-dimensional horizontal velocity and the non-dimensional vertical velocity at the bottom become

$$\begin{aligned}\tilde{u} &= \tilde{w} - \frac{\beta}{2}(1+\tilde{z})^2\tilde{w}_{\tilde{x}\tilde{x}} + \mathcal{O}(\beta^2),\\ \tilde{v} &= -\beta(1+\tilde{z})\tilde{w}_{\tilde{x}\tilde{x}} + \mathcal{O}(\beta^2).\end{aligned} \tag{3.33}$$

From Eq. (3.24) and Eq. (3.33), the non-dimensional horizontal velocity and the non-dimensional vertical velocity at a non-dimensional height $\tilde{z}_\theta = -1 + \theta(\alpha\tilde{\eta}+1)$ become

$$\begin{aligned}\tilde{u} &= \tilde{w}^\theta + \frac{\beta}{2}\left(\theta^2 - (1+\tilde{z}_\theta)^2\right)\tilde{w}^\theta_{\tilde{x}\tilde{x}} + \mathcal{O}(\beta^2),\\ \tilde{v} &= -\beta(1+\tilde{z}_\theta)\tilde{w}^\theta_{\tilde{x}} + \mathcal{O}(\beta^2).\end{aligned} \tag{3.34}$$

The expressions for the horizontal and vertical velocities of a fluid particle at a height $z = -1 + \theta(\eta+1)$ are given in new variables (3.29) as

$$\begin{aligned}u(x,z,t) &= w^\theta(x,t) + \frac{1}{2}\left(\theta^2 - (1+z)^2\right)w^\theta_{xx},\\ v(x,z,t) &= -(1+z)w^\theta_x.\end{aligned} \tag{3.35}$$

3.2.5 Particle paths

The functions $\xi(t)$ and $\zeta(t)$ are taken to represent the x-coordinate and z-coordinate, respectively, of a particle, initially located at the point $(x,z) = (\xi_0,\zeta_0)$, then the dynamical system is recast in the form

$$\begin{aligned}\frac{\partial\xi}{\partial t} &= u(\xi(t),\zeta(t),t) + U_0 - (1+\zeta)\Gamma,\\ \frac{\partial\zeta}{\partial t} &= v(\xi(t),\zeta(t),t),\\ (\xi(0),\zeta(0)) &= (\xi_0,\zeta_0),\end{aligned} \tag{3.36}$$

where the effect of an underlying shear-flow has been added. Finally, the particle trajectories are found by numerically integrating the dynamical system (3.36) using the fourth-order Runge-Kutta method.

3.2.6 Particle trajectories in solitary-wave solutions

The exact solitary-wave solution of the BBM equation (3.31) is derived as

$$\eta(x,t) = \eta_0\,\mathrm{sech}^2\left(\sqrt{\frac{3c_+(1+c_+^2)(3+\Gamma^2)\eta_0}{4(c_++\Gamma)[3(1+c_+^2)+(3+\Gamma^2)\eta_0]}}(x-x_0-ct)\right), \tag{3.37}$$

where η_0 is the initial amplitude, x_0 is the initial location of the wave crest and the phase velocity is defined as

$$c = c_+ + \frac{c_+(3+\Gamma^2)\eta_0}{3(1+c_+^2)}.$$

There is an assumption that when $t = 0$, the wave crest is located at $x = 0$ so that $x_0 = 0$. Hence, the argument is defined as

$$\mathcal{A}(x,t) = \sqrt{\frac{3c_+(1+c_+^2)(3+\Gamma^2)\eta_0}{4(c_+ + \Gamma)[3(1+c_+^2)+(3+\Gamma^2)\eta_0]}}(x - ct).$$

Using equation (3.37), then equation (3.32) yields

$$\begin{aligned} w^\theta = \eta_0 \operatorname{sech}^2(\mathcal{A}) \Bigg\{ & -c_- + \frac{c_- + \Gamma}{2(1+c_+^2)}\eta_0 \operatorname{sech}^2(\mathcal{A}) \\ & + \frac{3c_+(1+c_+^2)(3+\Gamma^2)\eta_0}{4(c_+ + \Gamma)[3(1+c_+^2)+(3+\Gamma^2)\eta_0]} \left(\frac{c_+ + \Gamma}{3(1+c_+^2)} - \frac{c_-}{6} + \frac{c_-}{2}\theta^2 \right) (4 - 6\operatorname{sech}^2(\mathcal{A})) \Bigg\}. \end{aligned} \tag{3.38}$$

The derivatives of Eqn (3.38) are given as

$$\begin{aligned} w_x^\theta = {} & \eta_0 \sqrt{\frac{3c_+(1+c_+^2)(3+\Gamma^2)\eta_0}{4(c_+ + \Gamma)[3(1+c_+^2)+(3+\Gamma^2)\eta_0]}} \operatorname{sech}^2(\mathcal{A}) \tanh(\mathcal{A}) \Bigg\{ 2c_- - \frac{2(c_- + \Gamma)}{(1+c_+^2)}\eta_0 \operatorname{sech}^2(\mathcal{A}) \\ & + \frac{6c_+(1+c_+^2)(3+\Gamma^2)\eta_0}{(c_+ + \Gamma)[3(1+c_+^2)+(3+\Gamma^2)\eta_0]} \left(\frac{c_+ + \Gamma}{3(1+c_+^2)} - \frac{c_-}{6} + \frac{c_-}{2}\theta^2 \right) (-1 + 3\operatorname{sech}^2(\mathcal{A})) \Bigg\}, \\ w_{xx}^\theta = {} & \frac{3c_+(1+c_+^2)(3+\Gamma^2)\eta_0^2}{4(c_+ + \Gamma)[3(1+c_+^2)+(3+\Gamma^2)\eta_0]} \operatorname{sech}^2(\mathcal{A}) \left\{ -4c_- + 6c_- \operatorname{sech}^2(\mathcal{A}) \right. \\ & + \frac{12c_+(1+c_+^2)(3+\Gamma^2)\eta_0}{(c_+ + \Gamma)[3(1+c_+^2)+(3+\Gamma^2)\eta_0]} \left(\frac{c_+ + \Gamma}{3(1+c_+^2)} - \frac{c_-}{6} + \frac{c_-}{2}\theta^2 \right) + \frac{8(c_- + \Gamma)}{(1+c_+^2)}\eta_0 \operatorname{sech}^2(\mathcal{A}) \\ & - \frac{90c_+(1+c_+^2)(3+\Gamma^2)\eta_0}{(c_+ + \Gamma)[3(1+c_+^2)+(3+\Gamma^2)\eta_0]} \left(\frac{c_+ + \Gamma}{3(1+c_+^2)} - \frac{c_-}{6} + \frac{c_-}{2}\theta^2 \right) \operatorname{sech}^2(\mathcal{A}) \\ & - \frac{10(c_- + \Gamma)}{(1+c_+^2)}\eta_0 \operatorname{sech}^4(\mathcal{A}) \\ & \left. + \frac{90c_+(1+c_+^2)(3+\Gamma^2)\eta_0}{(c_+ + \Gamma)[3(1+c_+^2)+(3+\Gamma^2)\eta_0]} \left(\frac{c_+ + \Gamma}{3(1+c_+^2)} - \frac{c_-}{6} + \frac{c_-}{2}\theta^2 \right) \operatorname{sech}^4(\mathcal{A}) \right\}. \end{aligned} \tag{3.39}$$

Therefore, using Eqs. (3.32) and (3.37), the relation (3.35) gives the horizontal and vertical velocities ($u(x,z,t)$ and $v(x,z,t)$, respectively) of the fluid at

$(x, z = -1 + \theta(\eta + 1))$ in the fluid, at a time t as

$$
\begin{aligned}
u = {} & \eta_0 \operatorname{sech}^2(\mathcal{A}) \left\{ -c_- + \frac{3c_+(1+c_+^2)(3+\Gamma^2)\eta_0}{(c_+ + \Gamma)[3(1+c_+^2) + (3+\Gamma^2)\eta_0]} \left(\frac{c_+ + \Gamma}{3(1+c_+^2)} - \frac{c_-}{6} \right) \right. \\
& -(1+z)^2 \frac{3(1+c_+^2)(3+\Gamma^2)}{(c_+ + \Gamma)[3(1+c_+^2) + (3+\Gamma^2)\eta_0]} \frac{\eta_0}{2} \\
& +\eta_0 \operatorname{sech}^2(\mathcal{A}) \left\{ \frac{c_- + \Gamma}{2(1+c_+^2)} - \frac{3}{2} \frac{3c_+(1+c_+^2)(3+\Gamma^2)}{(c_+ + \Gamma)[3(1+c_+^2) + (3+\Gamma^2)\eta_0]} \left(\frac{c_+ + \Gamma}{3(1+c_+^2)} - \frac{c_-}{6} \right) \right. \\
& \left. \left. +\frac{3}{4}(z+1)^2 \frac{3(1+c_+^2)(3+\Gamma^2)}{(c_+ + \Gamma)[3(1+c_+^2) + (3+\Gamma^2)\eta_0]} \right\} \right. \\
& +\frac{1}{2}\left(\theta^2 - (1+z)^2\right) \frac{c_- + \Gamma}{2(1+c_+^2)} \frac{3c_+(1+c_+^2)(3+\Gamma^2)}{(c_+ + \Gamma)[3(1+c_+^2) + (3+\Gamma^2)\eta_0]} \eta_0^2 \operatorname{sech}^2(\mathcal{A}) \times \\
& (4 - 5\operatorname{sech}^2(\mathcal{A})) - \frac{1}{16}\left(\theta^2 - (1+z)^2\right) \frac{9c_+^2(1+c_+^2)^2(3+\Gamma^2)^2\eta_0^2}{(c_+ + \Gamma)^2[3(1+c_+^2) + (3+\Gamma^2)\eta_0]^2} \times \\
& \left. \left(\frac{c_+ + \Gamma}{3(1+c_+^2)} - \frac{c_-}{6} + \frac{c_-}{2}\theta^2 \right) \left(-8 + 60\operatorname{sech}^2 \mathcal{A} - 60\operatorname{sech}^4 \mathcal{A}\right) \right\}, \\
v = {} & -(1+z)(\eta_0)^{3/2} \sqrt{\frac{3c_+(1+c_+^2)(3+\Gamma^2)}{4(c_+ + \Gamma)[3(1+c_+^2) + (3+\Gamma^2)\eta_0]}} \operatorname{sech}^2(\mathcal{A}) \tanh(\mathcal{A}) \left\{ 2c_- - \right. \\
& \frac{2(c_- + \Gamma)}{(1+c_+^2)} \eta_0 \operatorname{sech}^2(\mathcal{A}) + \frac{6c_+(1+c_+^2)(3+\Gamma^2)\eta_0}{(c_+ + \Gamma)[3(1+c_+^2) + (3+\Gamma^2)\eta_0]} \left(\frac{c_+ + \Gamma}{3(1+c_+^2)} - \frac{c_-}{6} + \frac{c_-}{2}\theta^2 \right) \\
& \left. \times(-1 + 3\operatorname{sech}^2(\mathcal{A})) \right\}.
\end{aligned}
\tag{3.40}
$$

Figure 3.6 show particle trajectories during the propagation of a solitary wave with an amplitude of 0.2 (that is, $\eta_0 = 0.2$).The value of θ used throughout is 0.6. It illustrates particle paths during one complete solitary wave cycle, (though the extent of the solitary wave is infinite). It can be seen that the fluid particles closer to the bottom have smaller vertical excursions but nearly the same horizontal extent. Right near the bottom, the particle trajectories become straight lines as the vertical motion becomes zero. The polarity of Γ has a strong influence on the shapes of the particle paths. Indeed, it is apparent from Figure 3.6 (lower panels) that the particles in the center of the fluid column move further to the right when $\Gamma < 0$, while particles in the lower half of the fluid column move further to the right when $\Gamma > 0$.

3.2.7 Particle trajectories in periodic-wave solutions

The BBM equation (3.31) admits the following solution in terms of the three constants f_1, f_2, and f_3 which are arranged as $f_3 < f_2 < f_1$, and in terms of cnoidal functions:

$$
\eta = f_2 + (f_1 - f_2)\operatorname{cn}^2 \left(\sqrt{\frac{3c_+(1+c_+^2)(3+\Gamma^2)}{4(c_+ + \Gamma)[3(1+c_+^2) + (3+\Gamma^2)(f_1 - f_3)]}} (f_1 - f_3)^{1/2}(x - x_0 - ct) \right),
\tag{3.41}
$$

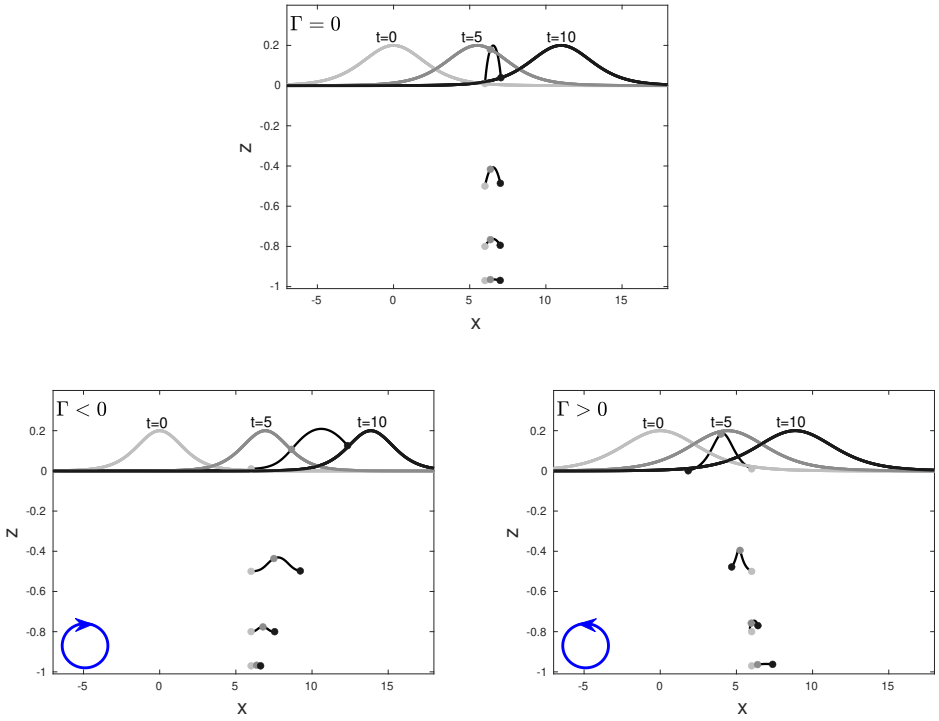

Figure 3.6: The waves are shown at time $t = 0$ (light-gray), $t = 5$ (dark-gray), $t = 10$ (black). The wave crest is initially located at $x = 0$. The path of the fluid particles ($\xi(t)$, $\zeta(t)$) in Eq. (3.36) (u and v corresponds to the Eq. (3.40)) initially located at (6, -0.97), (6, -0.8), (6, -0.5) and (6, 0.01) are shown for different cases (a) $\Gamma = 0$; (b) $\Gamma = -0.5$; (c) $\Gamma = 0.5$. The particle locations at three instances, where the wave profile is shown, are color-coded. The light-gray dot indicates the particle positions at time $t = 0$. The dark-gray dot indicates the particle positions at time $t = 5$. The black dot indicates the particle positions at time $t = 10$. The blue circles indicate the sense of rotation.

where f_1 and f_2 represent the crest and the trough of the wave, respectively. With $x_0 = 0$, the argument is defined as

$$\mathcal{B} = \sqrt{\frac{3c_+(1+c_+^2)(3+\Gamma^2)}{4(c_+ + \Gamma)[3(1+c_+^2)+(3+\Gamma^2)(f_1-f_3)]}}(f_1-f_3)^{1/2}(x-ct).$$

Here, cn is one of the Jacobian elliptic functions defined by the incomplete elliptic integral of the first kind [39], where its modulus is defined as $m = (f_1 - f_2)/(f_1 - f_3)$. The phase speed and the wavelength of the wave is given as

$$c = c_+ + \frac{c_+(3+\Gamma^2)}{3(1+c_+^2)}(f_1+f_2+f_3),$$

and

$$\lambda = 4\sqrt{\frac{(c_+ + \Gamma)[3(1+c_+^2)+(3+\Gamma^2)(f_1-f_3)]}{3c_+(1+c_+^2)(3+\Gamma^2)}}K(m)\frac{1}{\sqrt{f_1-f_3}},$$

respectively, where $K(m)$ is the complete elliptic integral of the first kind.

Using equation (3.41), then equation (3.32) yields

$$\begin{aligned}
w^\theta = &-c_-(f_2+(f_1-f_2)\mathrm{cn}^2(\mathcal{B}))+\frac{c_-+\Gamma}{2(1+c_+^2)}(f_2+(f_1-f_2)\mathrm{cn}^2(\mathcal{B}))^2\\
&+\frac{3c_+(1+c_+^2)(3+\Gamma^2)}{2(c_++\Gamma)[3(1+c_+^2)+(3+\Gamma^2)(f_1-f_3)]}(f_1-f_2)(f_1-f_3)\Big\{\frac{c_++\Gamma}{3(1+c_+^2)}\\
&-\frac{c_-}{6}+\frac{c_-}{2}\theta^2\Big\}\Big\{\mathrm{sn}^2(\mathcal{B})\mathrm{dn}^2(\mathcal{B})-\mathrm{cn}^2(\mathcal{B})\mathrm{dn}^2(\mathcal{B})+m\,\mathrm{sn}^2(\mathcal{B})\mathrm{cn}^2(\mathcal{B})\Big\}. \qquad (3.42)
\end{aligned}$$

Using Eq. (3.42) in the relations (3.35), the horizontal and vertical velocities may be written in terms of the Jacobian elliptic functions cn, sn and dn as

$$\begin{aligned}
u = &-c_-(f_2+(f_1-f_2)\mathrm{cn}^2(\mathcal{B}))+\frac{c_-+\Gamma}{2(1+c_+^2)}(f_2+(f_1-f_2)\mathrm{cn}^2(\mathcal{B}))^2\\
&+\frac{3c_+(1+c_+^2)(3+\Gamma^2)}{2(c_++\Gamma)[3(1+c_+^2)+(3+\Gamma^2)(f_1-f_3)]}(f_1-f_2)(f_1-f_3)\Big\{\frac{c_++\Gamma}{3(1+c_+^2)}\\
&-\frac{c_-}{6}+\frac{c_-}{2}\theta^2\Big\}\Big\{\mathrm{sn}^2(\mathcal{B})\mathrm{dn}^2(\mathcal{B})-\mathrm{cn}^2(\mathcal{B})\mathrm{dn}^2(\mathcal{B})+m\,\mathrm{sn}^2(\mathcal{B})\mathrm{cn}^2(\mathcal{B})\Big\}\\
&+\left(\theta^2-(1+z)^2\right)\frac{3c_+(1+c_+^2)(3+\Gamma^2)}{8(c_++\Gamma)[3(1+c_+^2)+(3+\Gamma^2)(f_1-f_3)]}(f_1-f_3)\\
&\Big\{2c_-(f_1-f_2)\left(\mathrm{cn}^2(\mathcal{B})\mathrm{dn}^2(\mathcal{B})-\mathrm{sn}^2(\mathcal{B})\mathrm{dn}^2(\mathcal{B})-m\mathrm{sn}^2(\mathcal{B})\mathrm{cn}^2(\mathcal{B})\right)+2\frac{c_-+\Gamma}{(1+c_+^2)}\times\\
&\quad f_2(f_1-f_2)\left(\mathrm{sn}^2(\mathcal{B})\mathrm{dn}^2(\mathcal{B})-\mathrm{cn}^2(\mathcal{B})\mathrm{dn}^2(\mathcal{B})+m\mathrm{sn}^2(\mathcal{B})\mathrm{cn}^2(\mathcal{B})\right)\\
&\quad -2\frac{c_-+\Gamma}{(1+c_+^2)}(f_1-f_2)^2\left(-m\mathrm{sn}^2(\mathcal{B})\mathrm{cn}^4(\mathcal{B})+\mathrm{cn}^4(\mathcal{B})\mathrm{dn}^2(\mathcal{B})-3\mathrm{sn}^2(\mathcal{B})\mathrm{cn}^2(\mathcal{B})\mathrm{dn}^2(\mathcal{B})\right)\\
&\quad +\frac{6c_+(1+c_+^2)(3+\Gamma^2)}{(c_++\Gamma)[3(1+c_+^2)+(3+\Gamma^2)(f_1-f_3)]}\left(\frac{c_++\Gamma}{3(1+c_+^2)}-\frac{c_-}{6}+\frac{c_-}{2}\theta^2\right)(f_1-f_2)(f_1-f_3)\times\\
&\quad \left(-9m\mathrm{sn}^2(\mathcal{B})\mathrm{cn}^2(\mathcal{B})\mathrm{dn}^2(\mathcal{B})-m^2\mathrm{sn}^2(\mathcal{B})\mathrm{cn}^4(\mathcal{B})+m\mathrm{cn}^4(\mathcal{B})\mathrm{dn}^2(\mathcal{B})\right.\\
&\qquad \left.+m^2\mathrm{sn}^4(\mathcal{B})\mathrm{cn}^2(\mathcal{B})+m\mathrm{sn}^4(\mathcal{B})\mathrm{dn}^2(\mathcal{B})+\mathrm{cn}^2(\mathcal{B})\mathrm{dn}^4(\mathcal{B})-\mathrm{sn}^2(\mathcal{B})\mathrm{dn}^4(\mathcal{B})\right)\Big\},\\
v = &-(1+z)\sqrt{\frac{3c_+(1+c_+^2)(3+\Gamma^2)}{4(c_++\Gamma)[3(1+c_+^2)+(3+\Gamma^2)(f_1-f_3)]}}(f_1-f_3)^{1/2}\mathrm{sn}(\mathcal{B})\mathrm{cn}(\mathcal{B})\mathrm{dn}(\mathcal{B})\,\{\\
&\quad 2c_-(f_1-f_2)-2\frac{c_-+\Gamma}{(1+c_+^2)}f_2(f_1-f_2)-2\frac{c_-+\Gamma}{(1+c_+^2)}(f_1-f_2)^2\mathrm{cn}^2(\mathcal{B})+\\
&\quad \left(\frac{c_++\Gamma}{3(1+c_+^2)}-\frac{c_-}{6}+\frac{c_-}{2}\theta^2\right)\frac{6c_+(1+c_+^2)(3+\Gamma^2)}{(c_++\Gamma)[3(1+c_+^2)+(3+\Gamma^2)(f_1-f_3)]}(f_1-f_2)(f_1-f_3)\\
&\quad \times\left(-m\mathrm{sn}^2(\mathcal{B})+m\mathrm{cn}^2(\mathcal{B})+\mathrm{dn}^2(\mathcal{B})\right)\}. \qquad (3.43)
\end{aligned}$$

Fig. 3.7 features the particle trajectory during the propagation of the cnoidal wave over three periods, the three instances considered are shown for amplitude 0.4

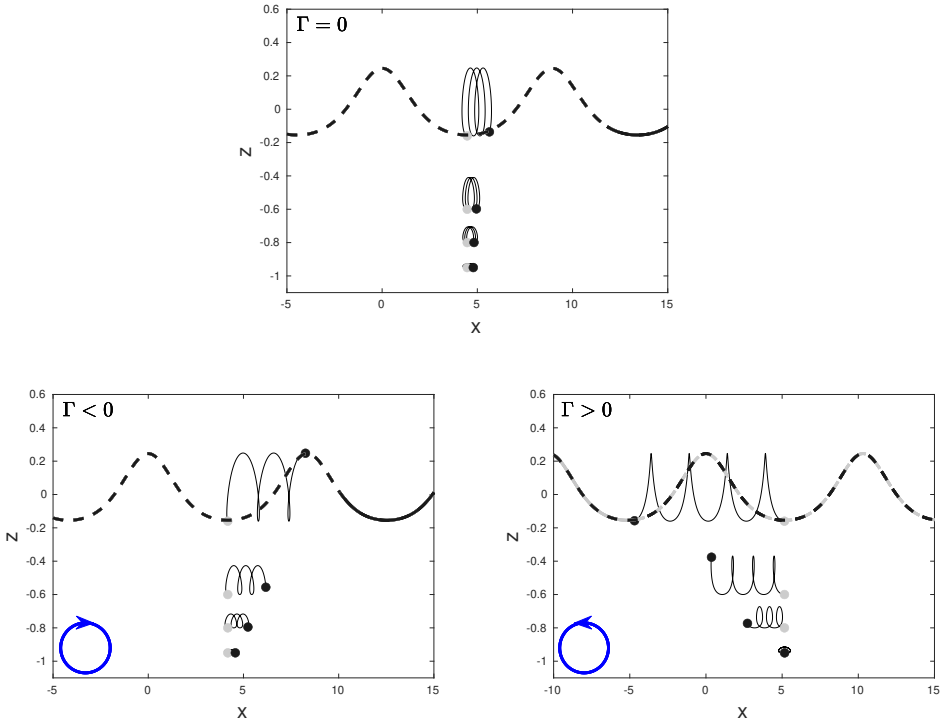

Figure 3.7: The upper panel shows the periodic wave with amplitude 0.4 wavelength 8.9389, period 9.5834, phase speed 0.9327, and $\Gamma = 0$ at $t = 0$ (light-gray) and $t = 28.7501$ (black). The left lower panel shows the periodic wave with amplitude 0.4, wavelength 8.3541, period 8.4016, phase speed 0.9943, and $\Gamma = -0.12$ at $t = 0$ (light-gray) and $t = 25.2047$ (black). The right lower panel shows the periodic wave with amplitude 0.4, wavelength 10.3072, period 12.8613, phase speed 0.8014, and $\Gamma = 0.28$ at $t = 0$ (light-gray) and $t = 38.5840$ (black). The initial particle locations are shown in light-gray curve.

with vorticity $\Gamma = 0, -0.12$. and 0.28. We observe that in the upper and lower panels of Fig. 3.7, for the particles closer to the bottom, the wave effect diminishes, and therefore the effect due to the vorticity can become dominant.

3.3 Fluid transport induced by internal waves

3.3.1 The given model

In the models formulation, two-layer fluids are under consideration, and the waves at the interface between them are the ultimate focus of this study. There is an assumption that the bottom and the upper boundary are flat and rigid.

Moreover, the flows under consideration are assumed to be irrotational in addition to inviscid and incompressible properties. Since the potential flows are the center

of attraction, we start by introducing the velocity potentials $\phi^* = \phi^*((x^*, z^*), t^*)$ in Ω_{t^*} and $\phi^{*'} = \phi^{*'}((x^*, z^*), t^*)$ in Ω'_{t^*}, the associated velocity vectors $\mathbf{v}^*$ and $\mathbf{v}^{*'}$ are described by

$$\mathbf{v}^* = \nabla\phi^*, \tag{3.44}$$

$$\mathbf{v}^{*'} = \nabla\phi^{*'}. \tag{3.45}$$

The continuity equation in the lower and upper layer is given as

$$\phi^*_{x^*x^*} + \phi^*_{z^*z^*} = 0 \quad \text{for } -h < z^* < \eta^*(x^*, t^*), \tag{3.46}$$

$$\phi^{*'}_{x^*x^*} + \phi^{*'}_{z^*z^*} = 0 \quad \text{for } \eta^*(x^*, t^*) < z^* < h'. \tag{3.47}$$

The boundary of the given domain $\{\Omega_{t^*}, \Omega'_{t^*}\}$ consist of two segments, namely, the flat bottom $z^* = -h$ and the flat roof $z^* = h'$. These rigid boundaries with the impermeability conditions along them yield

$$\phi^*_{z^*} = 0 \quad \text{at } z^* = -h, \tag{3.48}$$

$$\phi^{*'}_{z^*} = 0 \quad \text{at } z^* = h'. \tag{3.49}$$

Along the interface, the kinematic conditions are give as

$$\eta^*_{t^*} = \phi^*_{z^*} - \phi^*_x \eta^*_x \quad \text{at } z^* = \eta^*(x^*, t^*), \tag{3.50}$$

$$\eta^*_{t^*} = \phi^{*'}_{z^*} - \phi^{*'}_x \eta^*_x \quad \text{at } z^* = \eta^*(x^*, t^*). \tag{3.51}$$

On the fluids interface, the dynamic boundary condition which is the continuity of pressure because the effects of surface tension are considered to be negligible is given as

$$\rho\left(\frac{\partial\phi^*}{\partial t^*} + \frac{1}{2}|\nabla\phi^*|^2 + gz^*\right) = \rho'\left(\frac{\partial\phi^{*'}}{\partial t^*} + \frac{1}{2}|\nabla\phi^{*'}|^2 + gz^*\right) \quad \text{at } z^* = \eta^*(x^*, t^*), \tag{3.52}$$

where g is the gravitational acceleration.

3.3.2 Derivation of Boussinesq system

The derivation of the Boussinesq system of interfacial waves follows the derivation in [7] for just one layer. Consider the waves with a smaller amplitude, A, compared to the bottom layer depth h, and with a larger wavelength l, compared to the bottom layer depth. In relation to these three parameters (that is, amplitude A, bottom layer depth h, and wavelength l), the non-dimensional numbers are given as

$$\alpha = \frac{A}{h} \ll 1, \quad \beta = \frac{h^2}{l^2} \ll 1, \quad St = \frac{\alpha}{\beta} = \frac{Al^2}{h^3} \approx 1,$$

where St is defined as the Stokes number. The density ratio r and the depth ratio H in dimensionless form are introduced as

$$r = \frac{\rho'}{\rho}, \quad H = \frac{h'}{h}.$$

For convenience, it is important to scale the dependent variables in the problem in such away that they are all of first order. For this purpose, the following scaled dimensionless variables were introduced

$$x^* = lx, \quad z^* = h(z-1), \quad \eta^* = A\eta, \quad t^* = \frac{lt}{c_0}, \quad \phi^* = \frac{gAl\phi}{c_0}, \quad \phi^{*'} = \frac{gAl\phi'}{c_0},$$

where the speed $c_0 = \sqrt{gh}$. By substituting the newly defined variables into the equations (3.46) – (3.52), they transformed to the following equations after the evaluation

$$\beta\phi_{xx} + \phi_{zz} = 0 \quad \text{in } 0 < z < 1 + \alpha\eta, \tag{3.53}$$

$$\phi_z = 0 \quad \text{on } z = 0, \tag{3.54}$$

$$\eta_t + \alpha\phi_x\eta_x - \frac{1}{\beta}\phi_z = 0 \quad \text{on } z = 1 + \alpha\eta, \tag{3.55}$$

$$\beta\phi'_{xx} + \phi'_{zz} = 0 \quad \text{in } 1 + \alpha\eta < z < 1 + H, \tag{3.56}$$

$$\phi'_z = 0 \quad \text{on } z = 1 + H, \tag{3.57}$$

$$\eta_t + \alpha\phi'_x\eta_x - \frac{1}{\beta}\phi'_z = 0 \quad \text{on } z = 1 + \alpha\eta, \tag{3.58}$$

$$\left(\eta + \phi_t + \frac{1}{2}\alpha\phi_x^2 + \frac{1}{2}\frac{\alpha}{\beta}\phi_z^2\right) = r\left(\eta + \phi'_t + \frac{1}{2}\alpha\phi_x'^2 + \frac{1}{2}\frac{\alpha}{\beta}\phi_z'^2\right) \quad \text{on } z = 1 + \alpha\eta. \tag{3.59}$$

Note that these equations were rearranged after the evaluation.

The potential ϕ is denoted as a formal expansion given below

$$\phi((x,z),t) = \sum_{m=0}^{\infty} f_m(x,t)z^m.$$

Hence, after simplification, the potential ϕ yields

$$\phi((x,z),t) = \sum_{k=0}^{\infty} \frac{(-1)^k\beta^k}{(2k)!}\frac{\partial^{2k}F(x,t)}{\partial x^{2k}}z^{2k}.$$

By expanding the above expression, we have

$$\phi((x,z),t) = F - \frac{\beta}{2}F_{xx}z^2 + \frac{\beta^2}{24}F_{xxxx}z^4 - \frac{\beta^3}{720}F_{xxxxxx}z^6 + \mathcal{O}(\beta^4).$$

Likewise, the potential ϕ' is represented as a formal expansion given as

$$\phi'((x,z),t) = \sum_{m=0}^{\infty} f'_m(x,t)(1+H-z)^m.$$

Representing the velocity potential on the roof $z = 1 + H$ as $F'(x,t) = f'_0(x,t)$ and going through the computation as before yields

$$\phi'((x,z),t) = \sum_{k=0}^{\infty} \frac{(-1)^k\beta^k}{(2k)!}\frac{\partial^{2k}F'(x,t)}{\partial x^{2k}}(1+H-z)^{2k}.$$

Expansion of above expression gives

$$\phi'((x,z),t) = F' - \frac{\beta}{2}F'_{xx}(1+H-z)^2 + \frac{\beta^2}{24}F'_{xxxx}(1+H-z)^4 - \frac{\beta^3}{720}F'_{xxxxxx}(1+H-z)^6 + \mathcal{O}(\beta^4). \tag{3.60}$$

By substituting these into the given problem and using $w = \dfrac{\partial F(x,t)}{\partial x}$ and $z = 1+\alpha\eta$, we obtain

$$\eta_t + w_x + \alpha(w\eta)_x - \frac{1}{6}\beta w_{xxx} - \frac{1}{2}\alpha\beta(\eta w_{xx})_x + \frac{1}{120}\beta^2 w_{xxxxx} + \mathcal{O}(\beta^3) = 0. \tag{3.61}$$

Similarly, on the upper layer and using $w' = \dfrac{\partial F'(x,t)}{\partial x}$ and $z = 1+\alpha\eta$, we obtain

$$\eta_t - Hw'_x + \alpha(w'\eta)_x + \frac{1}{6}\beta H^3 w'_{xxx} - \frac{1}{2}\alpha\beta H^2(\eta w'_{xx})_x - \frac{1}{120}\beta^2 H^5 w'_{xxxxx} + \mathcal{O}(\beta^3) = 0. \tag{3.62}$$

Therefore, substituting the expressions ϕ and ϕ' derived into the given dynamic condition and differentiate with respect to x gives

$$\begin{aligned}&(1-r)\eta_x + w_t - rw'_t - \frac{1}{2}\beta(w_{xxt} - rH^2 w'_{xxt}) + \alpha(ww_x - rw'w'_x) - \alpha\beta(\eta w_{xt})_x - \alpha\beta rH(\eta w'_{xt})_x \\ &+ \frac{1}{24}\beta^2(w_{xxxxt} - rH^4 w'_{xxxxt}) - \frac{1}{2}\alpha\beta(ww_{xx} - rH^2 w'w'_{xx})_x + \alpha\beta(w_x w_{xx} - rH^2 w'_x w'_{xx}) \\ &+ \mathcal{O}(\beta^3) = 0.\end{aligned} \tag{3.63}$$

Th relationships between w, w^θ, w', and w'^θ are given as

$$w = w^\theta + \frac{1}{2}\beta\theta^2 w^\theta_{xx} + \frac{5}{24}\beta^2\theta^4 w^\theta_{xxxx} + \mathcal{O}(\beta^3). \tag{3.64}$$

$$w' = w'^\theta + \frac{1}{2}\beta\theta'^2 w'^\theta_{xx} + \frac{5}{24}\beta^2\theta'^4 w'^\theta_{xxxx} + \mathcal{O}(\beta^3). \tag{3.65}$$

However, substituting the equations (3.64) and (3.65) into equations (3.61), (3.62),and (3.63) and neglecting the terms of order α^2, β^2, and $\alpha\beta$ yield

$$\begin{aligned}&\eta_t + w^\theta_x + \alpha(w^\theta\eta)_x + \frac{1}{2}\beta\left(\theta^2 - \frac{1}{3}\right)w^\theta_{xxx} = 0, \\ &\eta_t - Hw'^\theta_x + \alpha(w'^\theta\eta)_x - \frac{1}{2}\beta H\left(\theta'^2 - \frac{1}{3}H^2\right)w'^\theta_{xxx} = 0, \\ &(1-r)\eta_x + w^\theta_t - rw'^\theta_t + \frac{1}{2}\beta\left[(\theta^2-1)w^\theta - r(\theta'^2 - H^2)w'^\theta\right]_{xxt} + \alpha(w^\theta w^\theta_x - rw'^\theta w'^\theta_x) = 0.\end{aligned} \tag{3.66}$$

The systems (3.66) are not suitable for numerical experimentation. However, the system is reduce to a system of two evolution equations and neglecting the nonlinear and higher-order terms to yield

$$\begin{aligned}&\eta_t + \frac{H}{r+H}W^\theta_x + \alpha\frac{H^2-r}{(r+H)^2}(W^\theta\eta)_x + \beta\left(\frac{1}{2}\frac{H^2 S}{(r+H)^2} + \frac{1}{3}\frac{H^2(1+rH)}{(r+H)^2}\right)W^\theta_{xxx} = 0, \\ &W^\theta_t + (1-r)\eta_x + \alpha\frac{H^2-r}{(r+H)^2}W^\theta W^\theta_x + \frac{1}{2}\beta\frac{HS}{r+H}W^\theta_{xxt} = 0.\end{aligned} \tag{3.67}$$

3.3.3 Derivation of the KdV equation

The attention is shifted to the unidirectional waves. Neglecting the nonlinear terms and higher-order derivatives, we have the lowest order of the Boussinesq systems (3.67) given as a linear system

$$\begin{aligned} \eta_t + \frac{H}{r+H} W_x^\theta &= 0, \\ W_t^\theta + (1-r)\eta_x &= 0. \end{aligned} \tag{3.68}$$

The horizontal velocities at the lower and upper layer respectively are given as

$$w^\theta = \frac{H}{r+H} W^\theta + \mathcal{O}(\beta), \qquad w'^\theta = \frac{-1}{r+H} W^\theta + \mathcal{O}(\beta). \tag{3.69}$$

Hence, the simplification yields

$$\eta_t + \sqrt{\frac{H(1-r)}{(r+H)}}\eta_x + \frac{3}{2}\sqrt{\frac{(H^2-r)^2(1-r)}{H(r+H)^3}}\eta\eta_x + \frac{1}{6}\sqrt{\frac{H^3(1+rH)^2(1-r)}{(r+H)^3}}\eta_{xxx} = 0, \tag{3.70}$$

$$\begin{aligned} w'^\theta = -\sqrt{\frac{(1-r)}{H(r+H)}}\eta + \frac{1}{4}\sqrt{\frac{(H^2-r)^2(1-r)}{H^3(r+H)^3}}\eta^2 + \\ \frac{1}{2}\left(\sqrt{\frac{HS^2(1-r)}{(r+H)^3}} + \frac{1}{3}\sqrt{\frac{H(1+rH)^2(1-r)}{(r+H)^3}}\right)\eta_{xx}, \end{aligned} \tag{3.71}$$

where (3.70) and (3.71) is the dimensionless form of the KdV equation and the horizontal velocity, respectively.

3.3.4 Horizontal and vertical velocity

From (3.60), let $F_x' = w'$, the respective non-dimensional horizontal and vertical velocity at the bottom is given as

$$\begin{aligned} u'(x,z,t) &= \phi_x' = w' - \frac{\beta}{2}(1+H-z)^2 w_{xx}' + \mathcal{O}(\beta^2), \\ v'(x,z,t) &= \phi_z' = \beta(1+H-z)w_x' + \mathcal{O}(\beta^2). \end{aligned} \tag{3.72}$$

After scaling back to the physical variable, we have

$$\begin{aligned} u'^*(x,z,t) &= w'^* - \frac{h^2}{2}(H - \frac{z^*}{h})^2 w_{x^*x^*}'^* + \mathcal{O}(\beta^2), \\ v'^*(x,z,t) &= h(H - \frac{z^*}{h})w_{x^*}'^* + \mathcal{O}(\beta^2). \end{aligned} \tag{3.73}$$

The expressions for the non-dimensional horizontal and vertical velocity become

$$\begin{aligned} u'(x,z,t) &= w' - \frac{1}{2}(H-z)^2 w_{xx}' + \mathcal{O}(\beta^2), \\ v'(x,z,t) &= (H-z)w_x' + \mathcal{O}(\beta^2), \end{aligned} \tag{3.74}$$

and after incorporating Eq. (3.65), we have

$$\begin{aligned} u'(x,z,t) &= w'^{\theta} + \frac{1}{2}(\theta'^2 - (H-z)^2)w'^{\theta}_{xx} + \mathcal{O}(\beta^2), \\ v'(x,z,t) &= (H-z)w'^{\theta}_{x} + \mathcal{O}(\beta^2). \end{aligned} \tag{3.75}$$

3.3.5 Particle paths

The x- and z-coordinates of a particle are denoted by the functions $\xi'(t)$ and $\zeta'(t)$ respectively. The particle is originally positioned at the point $(x,z) = (\xi'_0, \zeta'_0)$. Therefore, the motion of the particle is represented by the differential equations

$$\begin{aligned} \frac{\partial \xi'}{\partial t} &= u'(\xi'(t), \zeta'(t), t), \\ \frac{\partial \zeta'}{\partial t} &= v'(\xi'(t), \zeta'(t), t). \end{aligned} \tag{3.76}$$

Hence, the system (3.76) is integrated numerically to compute the associated particle paths.

3.3.6 Particle trajectories in internal solitary-wave solutions

The KdV equation derived in the previous section is used to illustrate the particle paths in the two-layers fluid due to the motion of an internal solitary wave. The exact solution of the internal solitary wave of the KdV equation (3.70) is derived as

$$\eta(x,t) = \eta_0 \operatorname{sech}^2\left(\frac{1}{2}\sqrt{3\eta_0 \frac{(H^2-r)}{H^2(1+rH)}}(x - x_0 - ct)\right), \tag{3.77}$$

where the initial amplitude and the initial position of the wave crest are denoted by η_0 and x_0, respectively. The phase velocity is represented as

$$c = \sqrt{\frac{H(1-r)}{(r+H)}} + \frac{\eta_0}{2\sqrt{\dfrac{H(r+H)^3}{(H^2-r)^2(1-r)}}}.$$

For computational purpose, let argument of (3.77) be represented by

$$\mathcal{A} = \frac{1}{2}\sqrt{3\eta_0 \frac{(H^2-r)}{H^2(1+rH)}}(x - x_0 - ct).$$

Substituting (3.77) into expression (3.71) yields

$$\begin{aligned} w'^{\theta} = \eta_0 \operatorname{sech}^2(\mathcal{A}) \Bigg\{ &- \sqrt{\frac{(1-r)}{H(r+H)}} + \frac{\eta_0}{4}\sqrt{\frac{(H^2-r)^2(1-r)}{H^3(r+H)^3}} \operatorname{sech}^2(\mathcal{A}) \\ &- \frac{3}{2}\eta_0 \frac{(H^2-r)}{H^2(1+rH)} \left[\frac{1}{2}\left(\sqrt{\frac{HS^2(1-r)}{(r+H)^3}} + \frac{1}{3}\sqrt{\frac{H(1+rH)^2(1-r)}{(r+H)^3}}\right)\right] \left[3\operatorname{sech}^2(\mathcal{A}) - 2\right] \Bigg\}. \end{aligned} \tag{3.78}$$

The derivatives of (3.78) are given as

$$
\begin{aligned}
w_x'^{\theta} &= \eta_0\sqrt{3\eta_0\frac{(H^2-r)}{H^2(1+rH)}}\,\mathrm{sech}^2(\mathcal{A})\tanh(\mathcal{A})\Bigg\{\sqrt{\frac{(1-r)}{H(r+H)}}-\frac{\eta_0}{2}\sqrt{\frac{(H^2-r)^2(1-r)}{H^3(r+H)^3}}\,\mathrm{sech}^2(\mathcal{A})\\
&+3\eta_0\frac{(H^2-r)}{H^2(1+rH)}\left[\frac{1}{2}\left(\sqrt{\frac{HS^2(1-r)}{(r+H)^3}}+\frac{1}{3}\sqrt{\frac{H(1+rH)^2(1-r)}{(r+H)^3}}\right)\right]\left[3\,\mathrm{sech}^2(\mathcal{A})-1\right]\Bigg\},\\
w_{xx}'^{\theta} &= \eta_0^2\frac{(H^2-r)}{H^2(1+rH)}\,\mathrm{sech}^2(\mathcal{A})\Bigg\{-3\sqrt{\frac{(1-r)}{H(r+H)}}+\frac{9}{2}\sqrt{\frac{(1-r)}{H(r+H)}}\,\mathrm{sech}^2(\mathcal{A})\\
&+9\eta_0\frac{(H^2-r)}{H^2(1+rH)}\left[\frac{1}{2}\left(\sqrt{\frac{HS^2(1-r)}{(r+H)^3}}+\frac{1}{3}\sqrt{\frac{H(1+rH)^2(1-r)}{(r+H)^3}}\right)\right]\\
&+3\eta_0\sqrt{\frac{(H^2-r)^2(1-r)}{H^3(r+H)^3}}\,\mathrm{sech}^2(\mathcal{A})\\
&-\frac{135}{2}\eta_0\frac{(H^2-r)}{H^2(1+rH)}\left[\frac{1}{2}\left(\sqrt{\frac{HS^2(1-r)}{(r+H)^3}}+\frac{1}{3}\sqrt{\frac{H(1+rH)^2(1-r)}{(r+H)^3}}\right)\right]\mathrm{sech}^2(\mathcal{A})\\
&-\frac{15}{4}\eta_0\sqrt{\frac{(H^2-r)^2(1-r)}{H^3(r+H)^3}}\,\mathrm{sech}^4(\mathcal{A})\\
&+\frac{135}{2}\eta_0\frac{(H^2-r)}{H^2(1+rH)}\left[\frac{1}{2}\left(\sqrt{\frac{HS^2(1-r)}{(r+H)^3}}+\frac{1}{3}\sqrt{\frac{H(1+rH)^2(1-r)}{(r+H)^3}}\right)\right]\mathrm{sech}^4(\mathcal{A})\Bigg\}.
\end{aligned}
\tag{3.79}
$$

Finally, the horizontal velocity $u'(x,z,t)$ and the vertical velocity $v'(x,z,t)$ of the particle paths in the upper layer of the fluid are obtained using the expressions (3.78)

and (3.79) in Eq. (3.75) as

$$u' = \eta_0 \operatorname{sech}^2(\mathcal{A})\Bigg\{ -\sqrt{\frac{(1-r)}{H(r+H)}} + \frac{\eta_0}{4}\sqrt{\frac{(H^2-r)^2(1-r)}{H^3(r+H)^3}}\operatorname{sech}^2(\mathcal{A})$$
$$-\frac{3}{2}\eta_0\frac{(H^2-r)}{H^2(1+rH)}\left[\frac{1}{2}\left(\sqrt{\frac{HS^2(1-r)}{(r+H)^3}}+\frac{1}{3}\sqrt{\frac{H(1+rH)^2(1-r)}{(r+H)^3}}\right)\right](3\operatorname{sech}^2(\mathcal{A})-2)$$
$$+\frac{1}{2}(\theta'^2-(1+H-z)^2)\eta_0\frac{(H^2-r)}{H^2(1+rH)}\Bigg\{-3\sqrt{\frac{(1-r)}{H(r+H)}}+9\eta_0\frac{(H^2-r)}{H^2(1+rH)}\times$$
$$\left[\frac{1}{2}\left(\sqrt{\frac{HS^2(1-r)}{(r+H)^3}}+\frac{1}{3}\sqrt{\frac{H(1+rH)^2(1-r)}{(r+H)^3}}\right)\right]+\Bigg\{\frac{9}{2}\sqrt{\frac{(1-r)}{H(r+H)}}$$
$$+3\eta_0\sqrt{\frac{(H^2-r)^2(1-r)}{H^3(r+H)^3}}$$
$$-\frac{135}{2}\eta_0\frac{(H^2-r)}{H^2(1+rH)}\left[\frac{1}{2}\left(\sqrt{\frac{HS^2(1-r)}{(r+H)^3}}+\frac{1}{3}\sqrt{\frac{H(1+rH)^2(1-r)}{(r+H)^3}}\right)\right]\Bigg\}\operatorname{sech}^2(\mathcal{A})$$
$$+\Bigg\{-\frac{15}{4}\eta_0\sqrt{\frac{(H^2-r)^2(1-r)}{H^3(r+H)^3}}$$
$$+\frac{135}{2}\eta_0\frac{(H^2-r)}{H^2(1+rH)}\left[\frac{1}{2}\left(\sqrt{\frac{HS^2(1-r)}{(r+H)^3}}+\frac{1}{3}\sqrt{\frac{H(1+rH)^2(1-r)}{(r+H)^3}}\right)\right]\Bigg\}\operatorname{sech}^4(\mathcal{A})\Bigg\}\Bigg\}, \tag{3.80}$$

$$v' = (1+H-z)\eta_0\sqrt{3\eta_0\frac{(H^2-r)}{H^2(1+rH)}}\operatorname{sech}^2(\mathcal{A})\tanh(\mathcal{A})\Bigg\{\sqrt{\frac{(1-r)}{H(r+H)}}-$$
$$\frac{\eta_0}{2}\sqrt{\frac{(H^2-r)^2(1-r)}{H^3(r+H)^3}}\operatorname{sech}^2(\mathcal{A})+$$
$$3\eta_0\frac{(H^2-r)}{H^2(1+rH)}\left[\frac{1}{2}\left(\sqrt{\frac{HS^2(1-r)}{(r+H)^3}}+\frac{1}{3}\sqrt{\frac{H(1+rH)^2(1-r)}{(r+H)^3}}\right)\right]\left[3\operatorname{sech}^2(\mathcal{A})-1\right]\Bigg\}. \tag{3.81}$$

The choice of H and r is based on the acceptable value of η_0 as shown in the table 3.1

Table 3.1: The choice of H and r.

$H^2 - r > 0$	$0 < \eta_0 < H$
$H^2 - r < 0$	$-1 < \eta_0 < 0$

It is noted that the solitary waves are of elevation for the upper layer ($H^2 > r$), while for the bottom layers ($H^2 < r$), the solitary waves are of depression. In Figs. 3.8 and 3.9, the solitary wave profiles are shown with an amplitude $\eta_0 = 0.2$ and

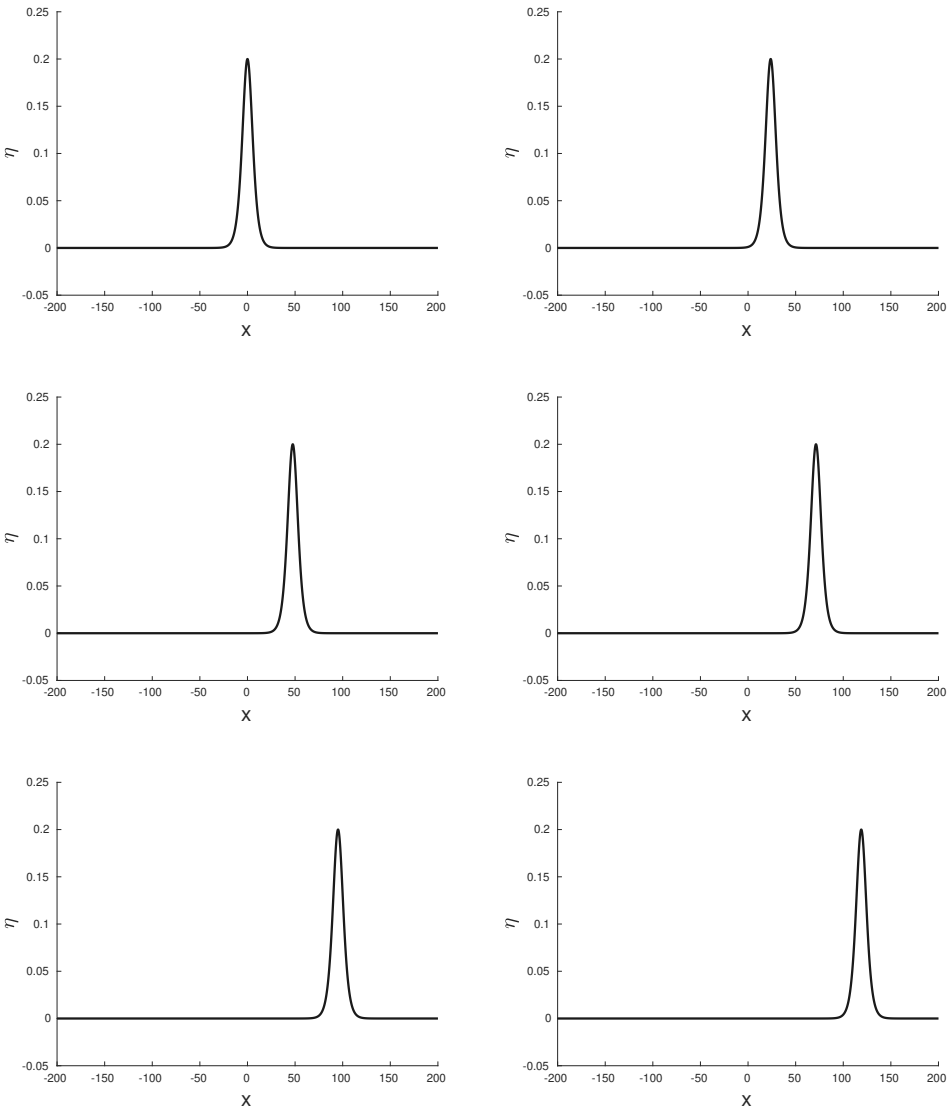

Figure 3.8: The elevation representation of the solitary wave solution propagating in the right direction at different time. This is a given internal solitary wave solution (3.77) to the KdV equation (3.70), with the parameters $\eta_0 = 0.2$, $H = 1.1$, and $r = 0.9$.

$\eta_0 = -0.2$, respectively. As expected, the figures show the right propagation in both cases, that is, for the positive and negative amplitude. In Fig. 3.8, we used $H = 1.1$ and $r = 0.9$, while $H = 0.6$ and $r = 0.85$ in Fig. 3.9. The plots in upper, middle, and lower panels correspond to the time at $t = 0s$, $t = 100s$, $t = 200s$, $t = 300s$, $t = 400s$ and $t = 500s$, respectively. The right propagation of the solitary waves is

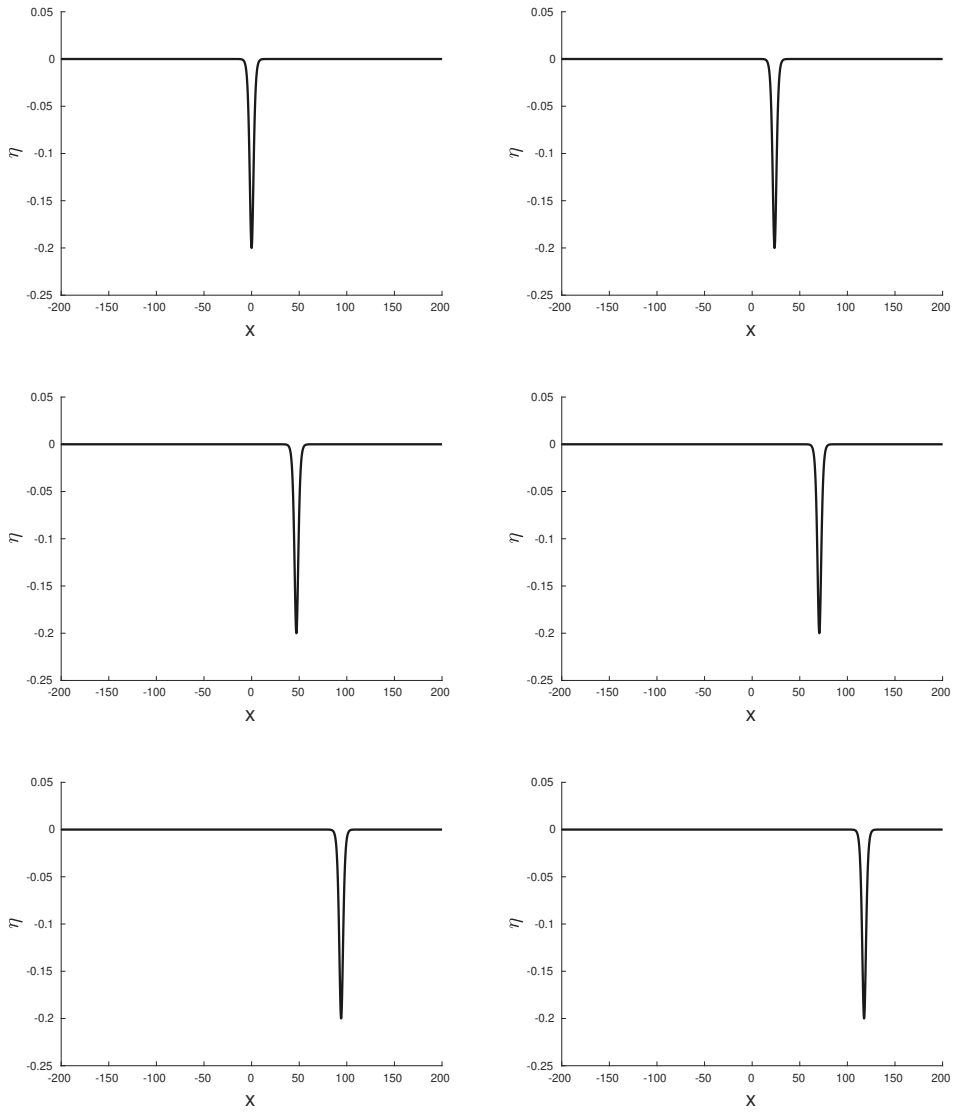

Figure 3.9: The depression representation of the solitary wave solution propagating in the right direction at different time. This is a given internal solitary wave solution (3.77) to the KdV equation (3.70), with the parameters $\eta_0 = -0.2$, $H = 0.6$, and $r = 0.85$.

evident at time $t = 500s$. It is important to mention that the values assigned for r are between 0 and 1. Using $r = 0$ leads to the case that corresponds to water waves, while taking r closer to 1 (that is, $r \approx 1$) leads to the case that corresponds to the situation where two fluids have approximately the same density. The results of the numerical computations of particle paths during the propagation of the internal

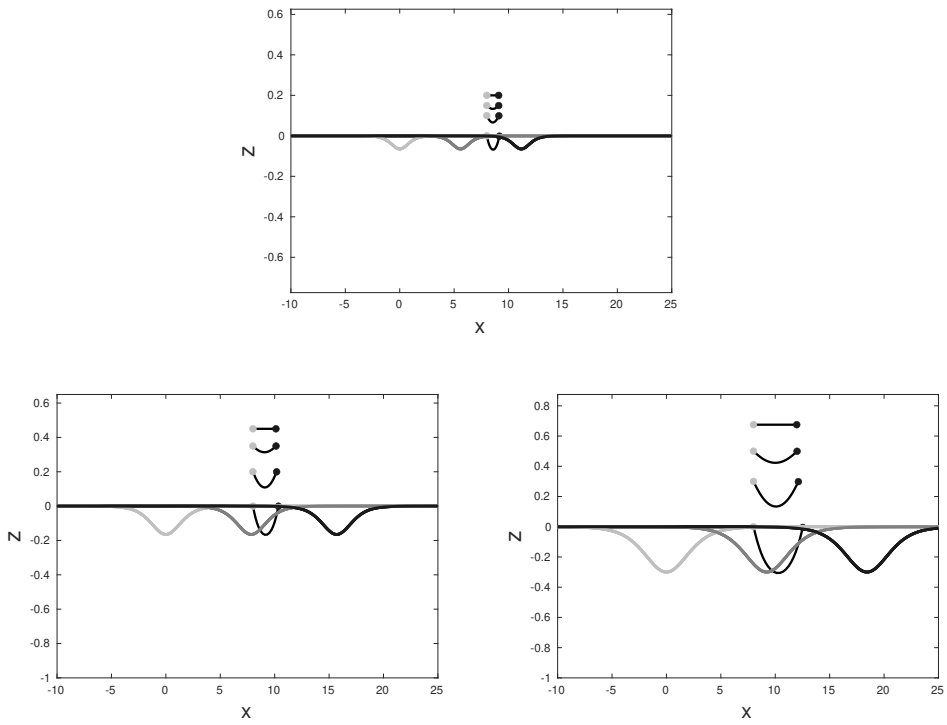

Figure 3.10: The wave profiles are shown beneath the particle trajectories at time $t = 0$ (light-gray), $t = 50$ (dark-gray), and $t = 100$ (black). In the left upper panel, the particle paths were located at $(8.0, 0.0)$, $(8.0, 0.1)$, and $(8.0, 0.2)$ with the parameter $\eta_0 = -0.065$, $h = 2.0$, $h' = 0.4$. The right upper panel were located at $(8.0, 0.0)$, $(8.0, 0.2)$, $(8.0, 0.35)$, and $(8.0, 0.45)$ with the parameter $\eta_0 = -0.165$, $h = 2.0$, $h' = 0.9$, while the lower panel were located at $(8.0, 0.0)$, $(8.0, 0.3)$, $(8.0, 0.5)$, and $(8.0, 0.675)$ with the parameter $\eta_0 = -0.165$, $h = 2.0$, $h' = 0.9$. In all the instances, $\rho = 1.1$ and $\rho' = 1.0$.

solitary waves are presented in Fig. 3.10. The wave profiles are shown beneath the particle trajectories at time $t = 0$ (light-gray), $t = 50$ (dark-gray), and $t = 100$ (black). The particle motion given in expression (3.76) with the help of the horizontal and vertical velocities given in relations (3.80) and (3.81), respectively, is denoted by the black-solid curve at a different depth as shown in the Figures. Three instances are investigated in the two-layers fluid. In all three demonstrations, the depth ratio H varies due to different combinations of the lower fluid depth h and the upper fluid depth h'.

3.4 Particle trajectories in the Gardner equation

3.4.1 The given model

Based on the domain $\Omega_t = \{(x,z) \in \mathbb{R} \times \mathbb{R}, -h_0 < z < \eta(x,t)\}$, the two-dimensional Euler equations are given as

$$\begin{aligned} &\mathbf{u}_t + (\mathbf{u} \cdot \nabla)\mathbf{u} + \nabla p = \mathbf{g}, \\ &\nabla \cdot \mathbf{u} = 0, \end{aligned}$$

where $\mathbf{u} = (u, v)$ represents the velocity field, $\mathbf{g} = (0, -g)$ denotes the body force gravitational acceleration, and $p(x,t,z)$ represents the pressure.

Moreover, the flows under consideration are also assumed to be irrotational in addition to inviscid and incompressible properties. Since the potential flows are the center of attraction, we start by introducing the velocity potentials $\phi = \phi((x,z),t)$ in Ω_t which satisfies the Laplace's equation in the given domain as

$$\phi_{xx} + \phi_{zz} = 0 \quad \text{for} \quad -h_0 < z < \eta(x,t). \tag{3.82}$$

The boundary of the given domain Ω_t consists the flat bottom $z = -h_0$. This rigid boundary, with the impermeability conditions, along them yield

$$\phi_z = 0 \quad \text{at } z = -h_0. \tag{3.83}$$

The kinematic conditions are given as

$$\eta_t = \phi_z - \phi_x \eta_x \quad \text{at } z = \eta(x,t). \tag{3.84}$$

The dynamic boundary condition is given as

$$\phi_t + \frac{1}{2}|\nabla\phi|^2 + gz = 0 \quad \text{at } z = \eta(x,t), \tag{3.85}$$

where g is the acceleration due to gravity.

3.4.2 Derivation of Bussinesq system

The next task is to compute the Boussinesq system, which follows the derivation in [7, 57]. The waves with a smaller amplitude, a, the bottom layer depth h_0, and a larger wavelength l is under consideration. However, the non-dimensional numbers are given as

$$\alpha = \frac{a}{h_0} \ll 1, \quad \beta = \frac{h_0^2}{l^2} \ll 1, \quad St = \frac{\alpha}{\beta} = \frac{al^2}{h_0^3} \approx 1,$$

where St is defined as the Stokes number.

For convenience, it is important to scale the dependent variables in the problem in such a way that they are all of the first order. For this purpose, the following scaled dimensionless variables were introduced

$$\tilde{x} = \frac{x}{l}, \quad \tilde{z} = \frac{z + h_0}{h_0}, \quad \tilde{t} = \frac{c_0 t}{l}, \quad \tilde{\eta} = \frac{\eta}{a}, \quad \tilde{\phi} = \frac{c_0}{gal}\phi.$$

where the speed $c_0 = \sqrt{gh_0}$. By substituting the newly defined variables into the equations (3.82) – (3.85), they are transformed to the following equations after the evaluation

$$\beta\tilde{\phi}_{\tilde{x}\tilde{x}} + \tilde{\phi}_{\tilde{z}\tilde{z}} = 0 \quad \text{in } 0 < \tilde{z} < 1 + \alpha\tilde{\eta}, \tag{3.86}$$

$$\tilde{\phi}_{\tilde{z}} = 0 \quad \text{on } \tilde{z} = 0, \tag{3.87}$$

$$\tilde{\eta}_{\tilde{t}} + \alpha\tilde{\phi}_{\tilde{x}}\tilde{\eta}_{\tilde{x}} - \frac{1}{\beta}\tilde{\phi}_{\tilde{z}} = 0 \quad \text{on } \tilde{z} = 1 + \alpha\tilde{\eta}, \tag{3.88}$$

$$\tilde{\eta} + \tilde{\phi}_{\tilde{t}} + \frac{1}{2}\alpha\tilde{\phi}_{\tilde{x}}^2 + \frac{1}{2}\frac{\alpha}{\beta}\tilde{\phi}_{\tilde{z}}^2 = 0 \quad \text{on } \tilde{z} = 1 + \alpha\tilde{\eta}. \tag{3.89}$$

The potential ϕ is represented as a formal expansion given as

$$\tilde{\phi}((\tilde{x}, \tilde{z}), \tilde{t}) = \sum_{m=0}^{\infty} f_m(\tilde{x}, \tilde{t})\tilde{z}^m.$$

Using the same procedure as before and using ϕ and other assumptions together with Eq. (3.88), and dynamic condition (3.89) and differentiate with respect to $\tilde{x}$, and using $\tilde{w} = \dfrac{\partial F(\tilde{x}, \tilde{t})}{\partial \tilde{x}}$ and $\tilde{z} = 1 + \alpha\tilde{\eta}$, we obtain

$$\begin{aligned} \tilde{\eta}_{\tilde{t}} + \tilde{w}_{\tilde{x}} + \alpha(\tilde{\eta}\tilde{w})_{\tilde{x}} - \frac{\beta}{6}\tilde{w}_{\tilde{x}\tilde{x}\tilde{x}} &= \mathcal{O}(\alpha\beta, \beta^2), \\ \tilde{w}_{\tilde{t}} + \tilde{\eta}_{\tilde{x}} + \alpha\tilde{w}\tilde{w}_{\tilde{x}} - \frac{\beta}{2}\tilde{w}_{\tilde{x}\tilde{x}\tilde{t}} &= \mathcal{O}(\alpha\beta, \beta^2). \end{aligned} \tag{3.90}$$

To be able to choose the fluid levels, we need to introduce θ to the horizontal velocity. Denoting the $\tilde{w}^\theta$ as the non-dimensional velocity with $0 \le \theta \le 1$, and using Taylor's formula and other transformation, we have

$$\tilde{w} = \tilde{w}^\theta + \frac{\beta}{2}\theta^2\tilde{w}^\theta_{\tilde{x}\tilde{x}} + \mathcal{O}(\alpha\beta, \beta^2). \tag{3.91}$$

Substituting the expression (3.91) into (3.90) yields the system

$$\begin{aligned} \tilde{\eta}_{\tilde{t}} + \tilde{w}^\theta_{\tilde{x}} + \alpha(\tilde{\eta}\tilde{w}^\theta)_{\tilde{x}} + \frac{\beta}{2}(\theta^2 - \tfrac{1}{3})\tilde{w}^\theta_{\tilde{x}\tilde{x}\tilde{x}} &= \mathcal{O}(\alpha\beta, \beta^2), \\ \tilde{w}^\theta_{\tilde{t}} + \tilde{\eta}_{\tilde{x}} + \alpha\tilde{w}^\theta\tilde{w}^\theta_{\tilde{x}} + \frac{\beta}{2}(\theta^2 - 1)\tilde{w}^\theta_{\tilde{x}\tilde{x}\tilde{t}} &= \mathcal{O}(\alpha\beta, \beta^2). \end{aligned} \tag{3.92}$$

Hence, the Boussinesq system is represented by the system (3.92), which is correct to first order in α and β.

3.4.3 Derivation of the Gardner equation

Neglecting the nonlinear terms and higher-order derivatives, we have the lowest order of the Boussinesq systems (3.92) given as a linear system

$$\begin{aligned} \tilde{\eta}_{\tilde{t}} + \tilde{w}^\theta_{\tilde{x}} &= 0, \\ \tilde{w}^\theta_{\tilde{t}} + \tilde{\eta}_{\tilde{x}} &= 0. \end{aligned} \tag{3.93}$$

Further simplification yields

$$\eta_t + \eta_x + \frac{3}{2}\eta\eta_x + \frac{1}{6}\eta_{xxx} - \frac{3}{8}\eta^2\eta_x = 0, \tag{3.94}$$

$$w^\theta = \eta - \frac{1}{4}\eta^2 + \left(\frac{1}{3} - \frac{\theta^2}{2}\right)\eta_{xx} + \frac{1}{8}\eta^3, \tag{3.95}$$

where (3.94) and (3.95) are the dimensionless form of the eKdV equation and the horizontal velocity, respectively.

3.4.4 Horizontal and vertical velocity components

The expressions for the non-dimensional horizontal and vertical velocities become

$$\begin{aligned} u(x,z,t) &= \phi_x = w^\theta + \frac{1}{2}(\theta^2 - (1+z)^2)w^\theta_{xx}, \\ v(x,z,t) &= \phi_z = -(1+z)w^\theta_x. \end{aligned} \tag{3.96}$$

Substituting Eqn. (3.95) into the horizontal and vertical velocity obtained in Eqn. (3.96) yields

$$\begin{aligned} u(x,z,t) &= \eta - \frac{1}{4}\eta^2 + \left(\frac{1}{3} - \frac{(1+z)^2}{2}\right)\eta_{xx} + \frac{1}{8}\eta^3, \\ v(x,z,t) &= -(1+z)\eta_x. \end{aligned} \tag{3.97}$$

3.4.5 Particle paths

The x- and z-coordinates of a particle are denoted by the functions $\xi(t)$ and $\zeta(t)$ respectively. The particle is originally positioned at the point $(x,z) = (\xi_0, \zeta_0)$. Therefore, the motion of the particle is represented by the differential equations

$$\begin{aligned} \frac{\partial \xi}{\partial t} &= u(\xi(t), \zeta(t), t), \\ \frac{\partial \zeta}{\partial t} &= v(\xi(t), \zeta(t), t). \end{aligned} \tag{3.98}$$

Hence, Eqn. (3.98) is integrated numerically to compute the associated particle paths.

3.4.6 Particle trajectories in solitary-wave solutions

The goal of this section is to compute the particle trajectories in the fluid. The area of interest is to consider the passage of a solitary wave at the surface of the fluid. The solitary wave solution of the eKdV equation (3.94) is derived as

$$\eta(x,t) = \frac{A}{b + (1-b)\cosh^2(k(x-ct))}, \tag{3.99}$$

where

$$A = 4\left[1-\sqrt{2-c}\right], \quad k = 2^{-\frac{1}{2}}3^{\frac{1}{2}}\sqrt{c-1}, \quad b = \frac{A^2}{16(c-1)}, \quad c = 1+\frac{A}{2}-\frac{A^2}{16}. \tag{3.100}$$

Here, A is the amplitude, k is wave-number, c is the phase velocity, and b is a constant. The argument is represented as $\mathcal{B} = k(x-ct)$.

Using equation (3.97) and the solitary wave solution (3.99), the velocity fields, that is, the horizontal and the vertical velocities, respectively, at an arbitrary point (x,z) in the fluid, and at a time t are derived as

$$u = \frac{A}{b+(1-b)\cosh^2(\mathcal{B})}\left\{1-\frac{1}{4}\frac{A}{\left[b+(1-b)\cosh^2(\mathcal{B})\right]}+\frac{1}{8}\frac{A^2}{\left[b+(1-b)\cosh^2(\mathcal{B})\right]^2}\right.$$
$$-\left(\frac{1}{3}-\frac{(1+z)^2}{2}\right)\times$$
$$\left.\frac{2k^2(1-b)\left[[b-3(1-b)\cosh^2(\mathcal{B})]\sinh^2(\mathcal{B})+(1-b)\cosh^4(\mathcal{B})+b\cosh^2(\mathcal{B})\right]}{\left[b+(1-b)\cosh^2(\mathcal{B})\right]^2}\right\}, \tag{3.101}$$

$$v = (1+z)\frac{2kA(1-b)\cosh(\mathcal{B})\sinh(\mathcal{B})}{\left[b+(1-b)\cosh^2(\mathcal{B})\right]^2}. \tag{3.102}$$

In Figure 3.11, the particle trajectories of the eKdV equation during the solitary wave propagation with an amplitude of 0.2243 were shown. Using the motion of the particle, which is represented by the differential equations (3.98) with the velocity components (3.101) and (3.102), the particle trajectories below the solitary waves were constructed.

Considering the fluid at different depths, it is observed that the fluid particles have smaller vertical excursions as they approach the flat bottom compared to its associated horizontal displacement. The rapid decrease of fluid particles is evident with every depth of the trajectory underneath the free surface. Consequently, the particle path very close to the bottom becomes a nearly straight line since there exists a horizontal displacement as the vertical propagation becomes zero. In addition, it is important to note that in Fig. 3.11, the fluid particles propagate to the right and upwards if their position is towards the right of the crest, and particles positioned on the left of the crest propagates to the right and downwards.

3.4.7 The maximum wave-height of the solitary waves

Next, the derivation of the maximum analytical height of the solitary wave using the conducive breaking criterion is considered. The conductive breaking criterion implies that the wave breaks if the horizontal particle velocity at the top of the leading wave exceeds the wave's local phase speed. Using the horizontal velocity component derived in Eqn. (3.97), the horizontal particle velocity at the top of the leading wave for the eKdV equation when $z = \eta$ is given by

$$U = \eta - \frac{1}{4}\eta^2 + \frac{1}{8}\eta^3 + \left(\frac{1}{3}-\frac{(1+\eta)^2}{2}\right)\eta_{xx}. \tag{3.103}$$

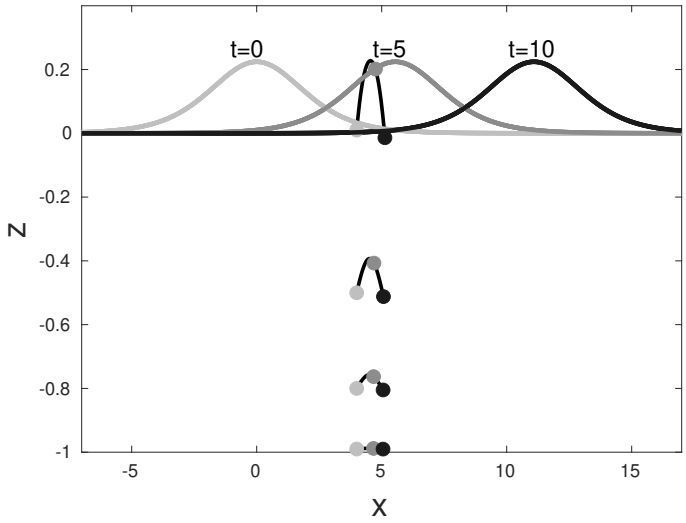

Figure 3.11: Here, the waves' surface profiles are shown at time $t = 0$ (light-gray), $t = 5$ (dark-gray), $t = 10$ (black). As before, the wave crest is initially located at $x = 0$. The particle path $(\xi(t), \zeta(t))$ given in Eqn. (3.98), where u and v are expressed in Eqns. (3.101) and (3.102) is represented by the curve, and it is initially located at (6, -0.97), (6, -0.8), (6, -0.5), and (6, 0.01). The color-coded is used to indicate the particle positions at the three instances where the wave surface profile is shown. The particle position at time $t = 0$ is represented by the light-gray dot, while the particle positions at time $t = 5$ and $t = 10$ are indicated by the dark-gray dot and black dot, respectively.

The breaking criterion is given as

$$U \geq c_{phase}, \tag{3.104}$$

where c_{phase} is the phase speed. Eqns. (3.103) and (3.104) yields

$$\eta - \frac{1}{4}\eta^2 + \frac{1}{8}\eta^3 + \left(\frac{1}{3} - \frac{(1+\eta)^2}{2}\right)\eta_{xx} \geq c_{phase}. \tag{3.105}$$

The second derivative of the solitary wave solution (3.99) is given as

$$\eta_{xx} = -\frac{2Ak^2(1-b)\left[[b-3(1-b)\cosh^2(\mathcal{B})]\sinh^2(\mathcal{B}) + (1-b)\cosh^4(\mathcal{B}) + b\cosh^2(\mathcal{B})\right]}{\left[b+(1-b)\cosh^2(\mathcal{B})\right]^3}. \tag{3.106}$$

The shape of a solitary wave is constant, this means that the wave will have the same height as the initial height at all times t. Hence, we evaluated the solitary wave (3.99) and its second derivative (3.106) at $(x, t) = (0, 0)$, to get

$$\eta = A, \quad \text{and} \quad \eta_{xx} = -\frac{3}{16}\left(8A^2 - 2A^3\right). \tag{3.107}$$

Substituting the phase speed derived in Eqn. (3.100) and Eqn. (3.107) into expression (3.105) gives

$$A - \frac{1}{4}A^2 + \frac{1}{8}A^3 - \frac{3}{16}\left(\frac{1}{3} - \frac{(1+A)^2}{2}\right)\left(8A^2 - 2A^3\right) \geq 1 + \frac{A}{2} - \frac{A^2}{16}. \tag{3.108}$$

The inequality is set to equality to compute the critical value of the wave-height, and after evaluating and rearranging the terms, the result is obtained as fifth-order polynomial

$$P(A) = 3A^5 - 6A^4 - 25A^3 - A^2 - 8A + 16 = 0. \tag{3.109}$$

One of the roots of this polynomial is 0.7078, and it can be inferred that the solitary wave of that waveheight starts breaking. We thus find that the maximum possible waveheight for the solitary wave is

$$A_{max} = 0.7078. \tag{3.110}$$

This is in contrast to the value 0.6879 in the KdV equation found in [10], and we see that the value for the eKdV (Gardner) equation is closer to the theoretical value of 0.78 [40, 41].

Chapter 4

Overview of the papers

In this chapter, an overview of the research papers which contribute to this thesis is presented. The overview shows how the methods presented in the papers are related.

4.1 PAPER A

Particle trajectories in the BBM approximation.

In paper A, a systematic asymptotic derivation of the BBM equation which is the regularized version of the KdV equation is used as a model equation for long waves in shallow water. The behavior of the waves at the surface of the fluid is studied using this model. The horizontal and vertical velocity field components are reconstructed during the derivation, and they were used to compute the particle trajectories numerically using the exact solutions of the BBM equation. However, using this concept, the solutions of the solitary wave and the periodic traveling wave were considered. The approximate analytical solutions of the particle trajectories were also computed for comparison purposes.

4.2 PAPER B

Particle trajectories in a weakly nonlinear long-wave model on shear flow.

In paper B, we proposed a BBM model in shallow water waves regime to study the particle trajectories associated with the propagation of nonlinear water waves on linear shear flow over a flat bottom. The Boussinesq-type system for two-dimensional water waves with constant vorticity is derived using the assumption that the dispersive and nonlinear terms are small and of the same magnitude. Focusing on the waves going in one direction, the KdV equation in the presence of a shear flow is derived. However, further computation led to the derivation of the BBM equation

with the coefficients that depend on the vorticity. Furthermore, we derived the approximate velocity field associated with the exact solutions of the BBM equation over a shear flow to study the particle trajectories of the flow. However, the particle trajectories of the solitary waves and periodic traveling waves were studied using numerical computation.

4.3 PAPER C

Fluid transport induced by internal waves.

In paper C, the investigation is based on the interfacial waves in the two-layer fluid of different densities using the KdV equation. Originally, three equations representing the Boussinesq-type system were derived. For numerical suitability, it is reduced to the two systems of equation. However, the KdV equation is derived as a result of the waves propagating in one direction within the two-layer fluids. The velocity field associated with the exact solutions of the KdV equation is derived to study the particle trajectories of the flow. The study is centered on the solitary wave solution.

4.4 PAPER D

Particle trajectories and wave breaking in the Gardner equation

In paper D, we considered the numerical computation of the particle paths of the solitary wave solution of the eKdV equation. We paid attention to the one-directional waves to derive the eKdV equation (also known as the Gardner equation) from the Boussinesq-type model derived earlier for water waves. This model is used to study the particle paths of the flows. In addition, the velocity components (i.e., the horizontal and vertical velocity) were derived. Furthermore, a solitary wave solution of the Gardner equation is obtained, and it is used in connection to the velocity components to study the particle paths of the flow. In addition, the maximum height of the solitary wave solution of the eKdV equation is computed.

Bibliography

[1] Ali, A. and Kalisch, H. Reconstruction of the pressure in long-wave models with constant vorticity. *Eur. J. Mech. B Fluids*, 2013, **37**, 187–194. 3

[2] Bakhoday-Paskyabi, M. Particle motions beneath irrotational water waves. *Ocean Dynamics*, 2015, **65 (8)**, 1063–1078. 3

[3] Barros, R., Gavrilyuk, S. L., and Teshukov, V. M. Dispersive nonlinear waves in two-layer flows with free surface. I. Model derivation and general properties. *Stud. Appl. Math.*, 2007, **119**, 191–211. 4

[4] Benjamin, T. B., Bona, J. L., and Mahony, J. J. Model equations for long waves in nonlinear dispersive systems. *Philosophical Transactions of the Royal Society of London. Series A, Mathematical and Physical Sciences*, 1972, **272 (1220)**, 47–78. 5

[5] Bjørkavåg, M. and Kalisch, H. Wave breaking in Boussinesq models for undular bores. *Phys. Lett. A*, 2011, **375**, 1570–1578. 4

[6] Bjørnestad, M., Buckley, M., Kalisch, H., Streßer, M., Horstmann, J., Frøysa, H. G., Ige, O. E., Cysewski, M. and Carrasco-Alvarez, R. Lagrangian measurements of orbital velocities in the surf zone. *Geophys. Res. Lett.*, 2021, **48**, e2021GL095722. 3

[7] Bona, J. L., Chen, M., and Saut, J.-C. Boussinesq equations and other systems for small-amplitude long waves in nonlinear dispersive media. I: Derivation and linear theory. *J. Nonlinear Sci.*, 2002, **12**, 283–318. 41, 51

[8] Borluk, H. and Kalisch, H. Particle dynamics in the KdV approximation. *Wave Motion*, 2012, **49**, 691–709. 3, 4, 6, 19, 27, 28

[9] Boussinesq, J. Essai sur la theorie des eaux courantes. *Impr. nationale*, 1877. 5

[10] Brun, M. K. and Kalisch, H. Convective wave breaking in the KdV equation. *Anal. Math. Phys.*, **8**, 2018, 57–75. 4, 56

[11] Burns, J. C. Long waves in running water. *Mathematical Proceedings of the Cambridge Philosophical Society*, 1953, **49 (4)**, 695–706. 3

[12] Carr, M., Sutherland, P., Haase, A., Evers, K.-U., Fer, I., Jensen, A., et al. Laboratory experiments on internal solitary waves in ice-covered waters. *Geophysical Research Letters*, 2019, **46**, 12,230–12,238. 3

[13] Choi, W. Strongly nonlinear long gravity waves in uniform shear flows. *Physical review E*, 2003, **68**. 3

[14] Choi, W., and Camassa, R. Fully nonlinear internal waves in a two-fluid system. *J. Fluid Mech.*, 1999, **396**, 1–36. 4

[15] Constantin, A. The trajectories of particles in Stokes waves. *Invent. Math.*, 2006, **166 (3)**, 523–535. 3

[16] Constantin, A. and Escher, J. Particle trajectories in solitary water waves. *Bull. Amer. math. soc.*, 2007, **44**, 423–431. 27

[17] Courant, R. and Friedrichs, K. O. Supersonic flow and shock waves. *Springer-Verlag*, 1999. 10

[18] Darrigol, O. Worlds of flow: A history of hydrodynamics from the Bernoullis to Prandtl. *Oxford University Press*, 2005. 5

[19] Debnath, L. Nonlinear Water Waves. *Academic Press Inc.*, 1994. 3

[20] Dias, F., and Vanden-Broeck, J.-M. On internal fronts. *J. Fluid Mech.*, 2003, **479**, 145–154. 4

[21] Dias, F., and Vanden-Broeck, J.-M. Two-layer hydraulic falls over an obstacle. *Europ. J. Mech. B Fluids*, 2004, **23**, 879–898. 4

[22] Drazin, P. G. and Johnson, R. S. Solitons: an introduction, volume 2. *Cambridge university press*, 1989. 5, 28

[23] Flamarion, M. V. Stagnation points beneath rotational solitary waves in gravity-capillary flows. *Trends in Computational and Applied Mathematics*, 2023, **24**, 265–274. 4

[24] Funakoshi, M., and Oikawa, M. Long internal waves of large amplitude in a two-layer fluid. *J. Phys. Soc. Japan*, 1986, **55**, 128–144. 4

[25] Gavrilyuk, S. L., Makarenko, N. I., and Sukhinin, S. V. Waves in Continuous Media. *Springer International Publishing*, 2017. 11

[26] Grimshaw, R., Pelinovsky, D., Pelinovsky, E., and Slunyaev, A. Generation of large-amplitude solitons in the extended Korteweg-de Vries equation. *Chaos*, 2002, **12**, 1070–1076. 4

[27] Hatland, S., and Kalisch, H. Wave breaking in undular bores generated by a moving bottom. *Phys. Fluids*, 2019, **31**, 033601. 4

[28] Holand, K., Kalisch, K., Bjørnestad, M., Streßer, M., Buckley, M. Horstmann, J., Roeber, V., Carrasco-Alvarez, R., Cysewski, M. and Frøysa, H. G. Identification of wave breaking from nearshore wave-by-wave records. *Phys. Fluids*, 2023, **35**, 9. 4

[29] Hsu, H. C. Particle trajectories for waves on a linear shear current. *Nonlinear Analysis: Real World Applications*, 2013, **14** 3

[30] Ige, O. E., and Kalisch, H. Particle trajectories in a weakly nonlinear long-wave model on a shear flow. *Applied Num. Math.*, 2023.

[31] Ige, O. E. and Khorsand, Z. Particle Trajectories in the BBM Approximation. *IAENG International Journal of Applied Mathematics*, 2020, **50 (3)**, 589–600.

[32] Itay, U. and Liberzon, D. Lagrangian kinematic criterion for the breaking of shoaling waves, *J. Phys. Ocean*, 2017, **47**, 827–833. 4

[33] Johnson, R. S. A modern introduction to the mathematical theory of water waves. *Cambridge University Press*, 1997. 10

[34] Khait, A. and Shemer L. On the kinematic criterion for the inception of breaking in surface gravity waves: Fully nonlinear numerical simulations and experimental verification. *Phys. Fluids*, 2018, **30**, 057103. 4

[35] Khorsand, Z. Particle trajectories in the serre equations. *Applied Mathematics and Computation*, 2014, **230**, 35–42. 27

[36] Kundu, P. K. and Cohen, I. M. Fluid mechanics, Fourth edition. *Elsevier*, 2007. 6, 10, 16

[37] Laget, O. and Dias, F. Numerical computation of capillary-gravity interfacial solitary waves. *J. Fluid Mech.*, 1997, **349**, 221–251. 4

[38] Lamb, H. Hydrodynamics. *Dover Publications, New York*, 1945. 3

[39] Lawden, D. F. Elliptic functions and applications. *Springer, New York*, 1989. 28, 38

[40] Massel, S. R. On the largest wave height in water of constant depth. *Ocean Engineering*, 1996, **23**, 553–573. 4, 56

[41] McCowan, J. On the highest wave of permanent type. *The London, Edinburgh, and Dublin Philosophical Magazine and Journal of Science*, 1894, **38**, 351–358. 56

[42] Munk, W. H. The solitary wave theory and its application to surf problems. *Annals of the New York Academy of Sciences*, 1949, **51**, 376–424. 3

[43] Nachbin, A. and Ribeiro-Junior, R. A boundary integral formulation for particle trajectories in Stokes waves. *Discrete and continuous dynamical systems*, 2014, **34 (8)**, 3135–3153. 3

[44] Nguyen, H. Y. and Dias, F. A Boussinesq system for two-way propagation of interfacial waves. *Physica D: Nonlinear Phenomena*, 2008, **237**, 2365–2389. 4

[45] Postacchini, M. and Brocchini, M. A wave-by-wave analysis for the evaluation of the breaking-wave celerity. *Applied Ocean Research*, 2014, **46**, 15–27. 4

[46] Stansell, P. and MacFarlane, C. Experimental investigation of wave breaking criteria based on wave phase speeds. *J. Phys. Oceanography*, 2002, **32**, 1269–1283. 4

[47] Senthilkumar, A. and Kalisch, H. Wave breaking in the KdV equation on a flow with constant vorticity. *European Journal of Mechanics-B/Fluids*, 2019, **73**, 48–54. 4, 34

[48] Shatah, J., Walsh, S., and Zeng, C. Travelling water waves with compactly supported vorticity. *Nonlinearity*, 2013, **26**, 1529.

[49] Stoker, J. J. Water Waves. The Mathematical Theory with Applications. *New York: Interscience Publ. Inc.*, 1957. 3, 6, 9, 10

[50] Stokes, G. G. On the theory of oscillatory waves. *Trans. Camb. Phil.Soc.*, 441–455, 1847. Reprinted in: Stokes, G. G. *Mathematical and Physical Papers, Volume I. Cambridge University Press*, 197–229, 1880. 3

[51] Stuhlmeier, R. Effects of shear flow on KdV balance - applications to tsunami. *Comm. Pure Applied Anal.*, 2012, **11**, 1549–1561. 34

[52] Teles da Silva, A. F. and Peregrine, D. H. Steep, steady surface waves on water of finite depth with constant vorticity. *J. Fluid Mech.*, 1988, **195**, 281–302. 3

[53] Thomas, R., Kharif, C., and Manna, M. A nonlinear Schroedinger equation for water waves on finite depth with constant vorticity. *Phys. Fluids*, 2012, **24**, 127102. 3

[54] Ursell, F. Mass transport in gravity waves. *Proc. Cambridge Phil. Soc*, 1953, **40**, 145–150. 3

[55] Vasan, V. and Oliveras, K. Pressure beneath a traveling wave with constant vorticity. *Discrete Contin. Dyn. Syst*, 2014, **34**, 3219–3239. 3

[56] Wang, Z., Guan, X. and Vanden-Broeck, J. M. Progressive flexural-gravity waves with constant vorticity. *Journal of Fluid Mechanics*, 2020, **905**. 3

[57] Whitham, G. B. Linear and Nonlinear Waves. *Wiley, New York*, 1974. 9, 10, 17, 51

[58] Wu, C. H. and Nepf, H. M. Breaking criteria and energy losses for three-dimensional wave breaking. *J. Geophys. Res.*, 2002, **107**, 3177–3195. 4

[59] Yaosong, C., Guocan, L., and Tao, J. Non-linear water waves on shearing flows. *Acta Mechanica Sinica*, 1994, **10 (2)**, 97–102. 33

[60] Zabusky, N. J. and Kruskal, M. D. Interaction of "solitons" in a collisionless plasma and the recurrence of initial states. *Physical review letters*, 1965, **15(6)**, 240. 5

Part II

Included papers

Paper A

Particle Trajectories in the BBM Approximation.

Olufemi Elijah Ige and Zahra Khorsand

IAENG International Journal of Applied Mathematics, (2020), **50** (3), 589–600.

Paper B

Particle Trajectories in a Weakly Nonlinear Long-Wave Model on a Shear Flow.

Olufemi Elijah Ige and Henrik Kalisch

Applied Numerical Mathematics, (2023).

ARTICLE IN PRESS

Applied Numerical Mathematics ••• (••••) •••–•••

Contents lists available at ScienceDirect

Applied Numerical Mathematics

journal homepage: www.elsevier.com/locate/apnum

Particle trajectories in a weakly nonlinear long-wave model on a shear flow

Olufemi Elijah Ige, Henrik Kalisch *

Department of Mathematics, University of Bergen, Postbox 7800, 5020 Bergen, Norway

ARTICLE INFO

Article history:
Received 31 July 2022
Received in revised form 12 December 2022
Accepted 19 January 2023
Available online xxxx

Keywords:
Surface waves
Particle trajectories
Shear flow
Vorticity
Solitary waves
Cnoidal waves
BBM equation

ABSTRACT

This work centers on the numerical examination of particle trajectories associated with the propagation of long water waves of small but finite amplitude on a background shear flow over a flat bottom. Taking into consideration the assumption that the nonlinear and dispersive effects are small and of the same magnitude, the Boussinesq-type equations for two-dimensional water waves on a background flow with constant vorticity are derived. Restricting attention to waves propagating in a single direction, we find a new version of the Benjamin-Bona-Mahony (BBM) equation which takes into account the effect of vorticity. In order to investigate the particle trajectories of the flow, an approximate velocity field associated with the derivation of the BBM equation over a shear flow is obtained. Several cases of particle paths under surface waves profiles such as solitary waves and periodic traveling waves are examined.

1. Introduction

Boussinesq-type equations are widely used for the simulation of ocean waves in the nearshore zone, where both nonlinear and dispersive effects influence the wave evolution. While these simplified model equations are most often derived in the context of irrotational flow, in coastal waters, the presence of vorticity may also be an important factor. Indeed, a variety of currents exists in the coastal zone, such as for example tidal currents and currents due to river discharge (see [26] for example). In this situation, using the assumption that the flows are irrotational when gravity waves travel on the surface of shear flows is no longer valid [4]. The inclusion of the vorticity to the shallow-water theory was first considered by Burns [7], who modified the shallow-water theory by incorporating the effects of the vorticity and studied the range of wave speeds for general velocity profiles. Following the publication of [37], constant background shear has been used in many works (see for example, [1,11,17,23,38,40,41] and the references therein). A linear shear flow avoids many of the mathematical complications of more general current profiles and may be seen as a first approximation to more general shear currents, especially in the case of long wavelength.

Recently, more general shear profiles have been used for the description of flow properties associated with surface waves (see [9,21,31] for example) in steady form. Other examples of surface waves interacting with vorticity include the case of compactly supported vorticity, such as vortex patches [35] and point vortices [16,18]. One recent work addresses the problem of vorticity creation by the waves itself in the transient case [8], though the resulting mathematical model is rather complex.

* Corresponding author.
E-mail addresses: olufemi.ige@uib.no (O.E. Ige), henrik.kalisch@uib.no (H. Kalisch).

https://doi.org/10.1016/j.apnum.2023.01.016
0168-9274/

Please cite this article as: O.E. Ige and H. Kalisch, Particle trajectories in a weakly nonlinear long-wave model on a shear flow, Applied Numerical Mathematics, https://doi.org/10.1016/j.apnum.2023.01.016

In the present work, the goal is to use a simple model equation in order to describe particle trajectories associated with surface wave patterns in the presence of constant vorticity. A series of derivations is carried out, resulting in a BBM-type equation that is valid in the presence of background constant vorticity. The BBM model will be examined in the non-dimensional form

$$\eta_t + c_+\eta_x + \frac{c_+(3+\Gamma^2)}{(1+c_+^2)}\eta\eta_x - \frac{c_+ + \Gamma}{3c_+(1+c_+^2)}\eta_{xxt} = 0,$$

where $\eta(x,t)$ is the surface profile, Γ is the prescribed vorticity, and the constants c_+ and c_- are given by $c_+ = \frac{-\Gamma}{2} + \sqrt{\frac{\Gamma^2}{4}+1}$ and $c_- = \frac{-\Gamma}{2} - \sqrt{\frac{\Gamma^2}{4}+1}$. Except for the coefficients, this equation is similar to the standard BBM equation and can be reduced to a first-order equation for both solitary and periodic (cnoidal) traveling waves in terms of surface elevation. Furthermore, as will be shown presently, a rigorous review of the derivation of the BBM equation as a surface water-wave model in the presence of a background shear flow reveals that the reconstruction of an approximate fluid velocity field below the free surface is possible. This process yields expressions for the horizontal and vertical velocity components in terms of the principal unknown variable η, which represents the deflection of the free surface from the equilibrium position.

To the first order in the perturbation parameter, it is observed that the horizontal velocity is not connected to its measuring depth, and we have $u = -c_-\eta$. However, considering the fact that the BBM equation is accurate to the second order, this term is revised to an expression that holds to the second-order as given below

$$u = -c_-\eta + \frac{c_- + \Gamma}{2(1+c_+^2)}\eta^2 + \left(\frac{c_+ + \Gamma}{3(1+c_+^2)} - \frac{c_-}{6}\right)\eta_{xx}. \tag{1}$$

In (1), the horizontal velocity at the flat bottom is denoted by u. It is also possible to obtain an equation for this horizontal velocity at an arbitrary depth in the fluid column. This theory will be presented in the next section. After establishing the velocity field connected to the surface wave, a great number of the dynamic features of the flow can be exploited, especially the construction of the approximate representations of the trajectories mapped out by the particles of the fluid beneath the surface.

The investigation of particle paths underneath a surface wave can be traced back to the late nineteenth century [30]. In linear wave theory, a standard first-order approximation suggests that all particle paths are closed [19,27,33]. However, Stokes [34] showed that particle trajectories are not closed for periodic waves (see also [10,15]). Indeed, the movement of a periodic surface wave is associated with particle trajectories that are not closed and lead to net mass transport in the direction of the wave. This result is known today as the Stokes drift. Stokes drift in channels of finite depth was reviewed by Ursell [39]. Constantin [12] gave firm mathematical proof that the particle paths are not closed. Other effects, such as infragravity wave motion and inertia, may also affect the particle motion [2,6]. We finally mention the work of Munk who considered particle motion under waves in the surf zone and applied a backward current in order to describe nearly closed particle paths which were observed under some conditions [29].

The first work which made use of Lagrangian coordinates for the examination of periodic surface gravity waves with finite vorticity was Gerstner [20]. In the Gerstner wave, particles travel in circles, and the surface curve is of trochoidal form. The mathematical approach used in [22] shows that Gerstner's flow is dynamically possible: the particles never collide despite moving in a circle and occupy the whole region beneath the surface wave. Later, Constantin and Strauss [14] showed that a closed particle path in the presence of current is possible. There have also been numerical studies of several orbit patterns. Indeed, Nachbin and Ribeiro-Junior [30] investigated a case of a closed orbit when a stokes wave propagates in the presence of an adverse current. Particle paths in shear flow have been studied in various situations using the full Euler equations in a steady formulation [9,21,31]. More recently, physical phenomena such as wave breaking, and undular bores were considered in this context [25,32].

The present study focuses on providing a clear qualitative view of the particle paths throughout the fluid domain of the nonlinear water waves on the shear flows. The article is organized as follows: a thorough review of the derivation of the Boussinesq system that features shear flow is presented in Section 2. Afterward, we sketch the derivation of the BBM equation and its corresponding approximate velocity field in terms of the free surface η and constant vorticity Γ. In Section 3, we study the surface solitary wave. Here, the velocity field expressions derived in Section 2 in connection with the exact solutions of the BBM equation are used to examine the particle trajectories numerically by considering different values of vorticity. Similarly, Section 4 is dedicated to the numerical investigation of the particle trajectories in connection to the propagation of the periodic wave. Lastly, Section 5 is devoted to the conclusion.

2. Formulation of the mathematical problem

The water-wave problem concerning waves at the surface of an inviscid, incompressible Newtonian fluid is given by the Euler equations with no-penetration conditions at the bed and kinematic and dynamic boundary conditions at the free surface. The sea floor is assumed to be flat. We denote the spatial coordinates by (x, z) where the x-axis coincides with the

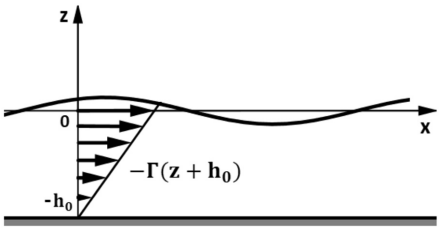

Fig. 1. Wave propagation over a background shear flow. In this figure, the vorticity Γ is negative.

undisturbed free surface, and assume long-crested waves which are uniform in the transverse direction. The gravitational acceleration in the negative z-direction is denoted by g, the undisturbed depth is h_0, and $\eta(x,t)$ denotes the departure of the free surface from the rest position. The decisive feature in the present work is the existence of a uniform shear flow with a free surface as shown in Fig. 1. In this case, the vorticity is given by a predescribed constant Γ, and the background distribution of the original velocity component before the arrival of the waves is given by

$$\left.\begin{array}{rcl} U &=& U_0-(z+h_0)\Gamma, \\ V &=& 0. \end{array}\right\} \tag{2}$$

For $\Gamma>0$, we have a shear flow in the direction opposite to the wave propagation. For $\Gamma<0$, the background flow is in the favorable direction, that is, in the direction of wave propagation. Without loss of generality, we may assume $U_0=0$. Assuming a is a typical amplitude, and l is a typical wavelength of the waves to be described, the parameter $\alpha=a/h_0$ represents the amplitude to depth ratio, and the parameter $\beta=h_0^2/l^2$ represents the water depth to wavelength ratio.

In the case of a linear shear flow such as delineated in (2), the vorticity is constant. For later reference, we define the unit vectors in the x, y and z directions as $\mathbf{e}_x$, $\mathbf{e}_y$ and $\mathbf{e}_z$, respectively. The vorticity is then given by $\omega=(U_z-V_x)\mathbf{e}_y=-\Gamma\mathbf{e}_y$. In general, one may use Kelvin's circulation theorem together with Stokes theorem and the incompressibility condition to understand that constant vorticity is conserved in inviscid, incompressible flow. In consequence, the flow can be split into a shear flow with uniform vorticity and a pure potential flow. For a uniform shear flow, the perturbation velocity is given in terms of the potential $\phi(x,z,t)$, with $u=\phi_x$ and $v=\phi_z$. The complete velocity field is given by

$$\left.\begin{array}{c} U=\phi_x-(z+h_0)\Gamma, \\ V=\phi_z. \end{array}\right\}$$

Indeed if we define a three-dimensional velocity field $\mathbf{U}=(U,0,V)$ for notational convenience, the vorticity is $\omega=\mathrm{curl}(\mathbf{U})$, and it can be checked that the above definition satisfies the vorticity equation

$$\omega_t+(\mathbf{U}\cdot\nabla)\omega=\omega\cdot\nabla\mathbf{U}. \tag{3}$$

Using the incompressibility condition $\nabla\cdot\mathbf{U}=0$ also shows that the velocity potential satisfies Laplace's equation. We can then rewrite the Euler equations

$$\mathbf{U}_t+\frac{1}{2}\nabla|\mathbf{U}|^2-\mathbf{U}\times\omega+ge_z=0$$

with the help of the velocity potential ϕ to obtain

$$\nabla\left\{\phi_t+\frac{1}{2}|\mathbf{U}|^2+gz\right\}=\mathbf{U}\times\omega.$$

As the left-hand side is obviously a gradient, the term $\mathbf{U}\times\omega$ must also be the gradient of a function. Following [42] it becomes plain that $\mathbf{U}\times\omega=\nabla G$, where the function G is given by

$$G=-\Gamma\int_{-h_0}^{z}\phi_x\,dz+\frac{\Gamma^2}{2}(z+h_0)^2.$$

The complete problem is written as follows:

$$\Delta\phi=0 \qquad \text{in } -h_0<z<\eta(x,t), \tag{4}$$

$$\phi_z=0 \qquad \text{on } z=-h_0, \tag{5}$$

$$\left.\begin{array}{c} \eta_t+U\eta_x-V=0, \\ \phi_t+\frac{1}{2}|\mathbf{U}|^2-G+g\eta=0, \end{array}\right\} \quad \text{on } z=\eta(x,t). \tag{6}$$

The next goal is to derive a Boussinesq system approximating the wave motion described by (4)-(6). To this end, we follow the development explained in [42]. For starters, the variables are non-dimensionalized using the following scaling:

$$\tilde{x}=\frac{x}{l},\ \ \tilde{z}=\frac{z}{h_0},\ \ \tilde{t}=\frac{\sqrt{gh_0}t}{l},\ \ \tilde{\Gamma}=\frac{\Gamma h_0}{\sqrt{gh_0}},\ \ \tilde{\eta}=\frac{\eta}{a},\ \ \tilde{\phi}=\frac{h_0}{al\sqrt{gh_0}}\phi.$$

Then we get the equation

$$\beta\tilde{\phi}_{\tilde{x}\tilde{x}}+\tilde{\phi}_{\tilde{z}\tilde{z}}=0\quad -1<\tilde{z}<\alpha\tilde{\eta}, \tag{7}$$

and at the bottom $\tilde{z}=-1$, we have the following boundary condition

$$\tilde{\phi}_{\tilde{z}}=0. \tag{8}$$

At the free surface $\tilde{z}=\alpha\tilde{\eta}$, the non-dimensional kinematic condition is

$$\beta\left\{\tilde{\eta}_{\tilde{t}}+\left[-(1+\alpha\tilde{\eta})\tilde{\Gamma}+\alpha\tilde{\phi}_{\tilde{x}}\right]\tilde{\eta}_{\tilde{x}}\right\}=\tilde{\phi}_{\tilde{z}}. \tag{9}$$

The non-dimensional dynamic condition may be expressed as

$$\beta(\tilde{\phi}_{\tilde{t}}+\tilde{\eta})+\frac{\alpha\beta}{2}\left[\tilde{\phi}_{\tilde{x}}-\frac{\tilde{\Gamma}}{\alpha}(1+\alpha\tilde{\eta})\right]^2+\frac{\alpha}{2}\left[\tilde{\phi}_{\tilde{z}}\right]^2-\frac{\beta}{ag}G=0. \tag{10}$$

The non-dimensional potential $\tilde{\phi}$ is expressed in powers of $(1+\tilde{z})$ as

$$\tilde{\phi}=\sum_{n=0}^{\infty}(1+\tilde{z})^n\phi_n. \tag{11}$$

Using Eq. (7), Eq. (11) and Eq. (8), we have

$$\tilde{\phi}=\phi_0-\frac{\beta}{2}(1+\tilde{z})^2\phi_{0\tilde{x}\tilde{x}}+\frac{\beta^2}{24}(1+\tilde{z})^4\phi_{0\tilde{x}\tilde{x}\tilde{x}\tilde{x}}+\mathcal{O}(\beta^3). \tag{12}$$

To find a closed system of two evolution equations, we substitute the asymptotic expression for $\tilde{\phi}$ in the boundary conditions Eq. (9) and Eq. (10) and collect all terms of zeroth and first-order in α and β. Then we differentiate the dynamic bottom boundary with respect to $\tilde{x}$ and expressed the boundary conditions in terms of the non-dimensional horizontal velocity at the bottom $\phi_{0\tilde{x}}=\tilde{w}$. This procedure yields the system of equations

$$\begin{aligned}\tilde{\eta}_{\tilde{t}}+\tilde{w}_{\tilde{x}}-\tilde{\Gamma}\tilde{\eta}_{\tilde{x}}-\alpha\tilde{\Gamma}\tilde{\eta}\tilde{\eta}_{\tilde{x}}+\alpha(\tilde{\eta}\tilde{w})_{\tilde{x}}-\frac{\beta}{6}\tilde{w}_{\tilde{x}\tilde{x}\tilde{x}}&=\mathcal{O}(\alpha\beta,\beta^2),\\ \tilde{w}_{\tilde{t}}+\tilde{\eta}_{\tilde{x}}+\alpha\tilde{w}\tilde{w}_{\tilde{x}}-\frac{\beta}{2}\tilde{w}_{\tilde{x}\tilde{x}\tilde{t}}+\frac{\beta}{3}\tilde{\Gamma}\tilde{w}_{\tilde{x}\tilde{x}\tilde{x}}&=\mathcal{O}(\alpha\beta,\beta^2).\end{aligned} \tag{13}$$

Next, a family of Boussinesq systems is derived using the standard technique of describing the horizontal velocity component at different heights in the fluid column. If we let $\tilde{w}^\theta$ be the non-dimensional velocity at a non-dimensional height $\tilde{z}_\theta=-1+\theta(\alpha\tilde{\eta}+1)$, with $0\le\theta\le1$, then Taylor's formula shows that

$$\tilde{w}^\theta=\tilde{w}-\frac{\beta}{2}(1+\tilde{z}_\theta)^2\tilde{w}_{\tilde{x}\tilde{x}}+\mathcal{O}(\beta^2)=\tilde{w}-\frac{\beta}{2}\theta^2\tilde{w}_{\tilde{x}\tilde{x}}+\mathcal{O}(\alpha\beta,\beta^2).$$

By applying the standard techniques of inversion, it is not difficult to derive the following expression as an asymptotic formula for $\tilde{w}$ in terms of $\tilde{w}^\theta$:

$$\tilde{w}=\tilde{w}^\theta+\frac{\beta}{2}\theta^2\tilde{w}^\theta_{\tilde{x}\tilde{x}}+\mathcal{O}(\alpha\beta,\beta^2). \tag{14}$$

Substituting this representation into the system (13), this yields

$$\begin{aligned}\tilde{\eta}_{\tilde{t}}+\tilde{w}^\theta_{\tilde{x}}-\tilde{\Gamma}\tilde{\eta}_{\tilde{x}}-\alpha\tilde{\Gamma}\tilde{\eta}\tilde{\eta}_{\tilde{x}}+\alpha(\tilde{\eta}\tilde{w}^\theta)_{\tilde{x}}+\frac{\beta}{2}(\theta^2-\tfrac{1}{3})\tilde{w}^\theta_{\tilde{x}\tilde{x}\tilde{x}}&=\mathcal{O}(\alpha\beta,\beta^2),\\ \tilde{w}^\theta_{\tilde{t}}+\tilde{\eta}_{\tilde{x}}+\alpha\tilde{w}^\theta\tilde{w}^\theta_{\tilde{x}}+\frac{\beta}{2}(\theta^2-1)\tilde{w}^\theta_{\tilde{x}\tilde{x}\tilde{t}}+\frac{\beta}{3}\tilde{\Gamma}\tilde{w}^\theta_{\tilde{x}\tilde{x}\tilde{x}}&=\mathcal{O}(\alpha\beta,\beta^2).\end{aligned} \tag{15}$$

For any real λ and μ, the above system is a special case of the more general system

$$\tilde{\eta}_{\tilde{t}} + \tilde{w}^{\theta}_{\tilde{x}} - (1+\alpha\tilde{\eta})\tilde{\Gamma}\tilde{\eta}_{\tilde{x}} + \alpha(\tilde{\eta}\tilde{w}^{\theta})_{\tilde{x}} + \frac{\beta}{2}(\theta^2 - \tfrac{1}{3})\lambda\tilde{w}^{\theta}_{\tilde{x}\tilde{x}\tilde{x}} - \tfrac{\beta}{2}(\theta^2 - \tfrac{1}{3})(1-\lambda)\tilde{\eta}_{\tilde{x}\tilde{x}\tilde{t}} + \frac{\beta}{2}(\theta^2 - \tfrac{1}{3})(1-\lambda)\tilde{\Gamma}\tilde{\eta}_{\tilde{x}\tilde{x}\tilde{x}} = \mathcal{O}(\alpha\beta, \beta^2),$$

$$\tilde{w}^{\theta}_{\tilde{t}} + \tilde{\eta}_{\tilde{x}} + \alpha\tilde{w}^{\theta}\tilde{w}^{\theta}_{\tilde{x}} + \frac{\beta}{2}(1-\theta^2)\mu\tilde{\eta}_{\tilde{x}\tilde{x}\tilde{x}} - \frac{\beta}{2}(1-\theta^2)(1-\mu)\tilde{w}^{\theta}_{\tilde{x}\tilde{x}\tilde{t}} + \frac{\beta}{3}\tilde{\Gamma}\tilde{w}^{\theta}_{\tilde{x}\tilde{x}\tilde{x}} = \mathcal{O}(\alpha\beta, \beta^2).$$

The concentration is now on the unidirectional waves. In the lowest order, the Boussinesq equation is the linear system

$$\tilde{\eta}_{\tilde{t}} + \tilde{w}^{\theta}_{\tilde{x}} - \tilde{\Gamma}\tilde{\eta}_{\tilde{x}} = 0, \quad \tilde{w}^{\theta}_{\tilde{t}} + \tilde{\eta}_{\tilde{x}} = 0. \tag{16}$$

The system can be diagonalized by introducing characteristic coordinates. Introduce new variables r and s defined by $(r,s) = P^{-1}(\tilde{\eta}, \tilde{w}^{\theta})$ where

$$P^{-1} = \frac{1}{1+(\tilde{c}_+)^2}\begin{pmatrix} \tilde{c}_+ & 1 \\ -1 & \tilde{c}_+ \end{pmatrix},$$

with $\tilde{c}_+ = \frac{-\tilde{\Gamma}}{2} + \sqrt{\frac{\tilde{\Gamma}^2}{4}+1}$. A simple calculation shows that

$$\begin{pmatrix} r_t \\ s_t \end{pmatrix} + \begin{pmatrix} \tilde{c}_+ & 0 \\ 0 & \tilde{c}_- \end{pmatrix}\begin{pmatrix} r_x \\ s_x \end{pmatrix} = 0 \tag{17}$$

where $\tilde{c}_- = \frac{-\tilde{\Gamma}}{2} - \sqrt{\frac{\tilde{\Gamma}^2}{4}+1}$ is the conjugate of $\tilde{c}_+$. The solutions of system (17) are

$$r = r_0(x - \tilde{c}_+ t) \text{ and } s = s_0(x - \tilde{c}_- t).$$

The solution to Eq. (16) is, therefore,

$$\tilde{w}^{\theta}(x,t) = \frac{1}{1+\tilde{c}_+^2}\Big[\tilde{c}_+\tilde{\eta}_0(x-\tilde{c}_+t) + \tilde{w}^{\theta}_0(x-\tilde{c}_+t) - \tilde{c}_+\tilde{\eta}_0(x-\tilde{c}_-t) + \tilde{c}_+^2\tilde{w}^{\theta}_0(x-\tilde{c}_-t)\Big],$$

$$\tilde{\eta}(x,t) = \frac{1}{1+\tilde{c}_+^2}\Big[\tilde{c}_+^2\tilde{\eta}_0(x-\tilde{c}_+t) + \tilde{c}_+\tilde{w}^{\theta}_0(x-\tilde{c}_+t) + \tilde{\eta}_0(x-\tilde{c}_-t) - \tilde{c}_+\tilde{w}^{\theta}_0(x-\tilde{c}_-t)\Big].$$

The unidirectional KdV equation is derived from the system (15) by specializing to waves moving to the right with speed $\tilde{c}_+$.

$$\tilde{w}^{\theta} = -\tilde{c}_-\tilde{\eta} + \alpha A + \beta B + \mathcal{O}(\alpha\beta, \beta^2),$$

where A and B are functions of $\tilde{\eta}$ and its $\tilde{x}$ derivatives. Then the system (15) becomes

$$\tilde{\eta}_{\tilde{t}} + \tilde{c}_+\tilde{\eta}_{\tilde{x}} + \alpha(-2\tilde{c}_-\tilde{\eta}\tilde{\eta}_{\tilde{x}} - \tilde{\Gamma}\tilde{\eta}\tilde{\eta}_{\tilde{x}} + A_{\tilde{x}}) + \beta(B_{\tilde{x}} - \tfrac{1}{2}\tilde{c}_-(\theta^2 - \tfrac{1}{3})\tilde{\eta}_{\tilde{x}\tilde{x}\tilde{x}}) = \mathcal{O}(\alpha\beta, \beta^2),$$

$$\tilde{\eta}_{\tilde{t}} + \tilde{c}_+\tilde{\eta}_{\tilde{x}} + \alpha(\tilde{c}_+A_{\tilde{t}} - \tilde{c}_-\tilde{\eta}\tilde{\eta}_{\tilde{x}}) + \beta(\tilde{c}_+B_{\tilde{t}} + \tfrac{1}{2}(\theta^2-1)\tilde{\eta}_{\tilde{x}\tilde{x}\tilde{t}} + \tfrac{\tilde{\Gamma}}{3}\tilde{\eta}_{\tilde{x}\tilde{x}\tilde{x}}) = \mathcal{O}(\alpha\beta, \beta^2).$$

Since $\tilde{\eta}_{\tilde{t}} = -\tilde{c}_+\tilde{\eta}_{\tilde{x}}$, all derivatives in the first order terms may be replaced by $-\tilde{c}_+$ times the x derivatives. Then the two equations are consistent if

$$A = \frac{\tilde{c}_- + \tilde{\Gamma}}{2(1+\tilde{c}_+^2)}\tilde{\eta}^2 \text{ and } B = \left(\frac{\tilde{c}_+ + \tilde{\Gamma}}{3(1+\tilde{c}_+^2)} - \frac{\tilde{c}_-}{6} + \frac{\tilde{c}_-}{2}\theta^2\right)\tilde{\eta}_{\tilde{x}\tilde{x}}.$$

Hence, we have

$$\begin{aligned} \tilde{w}^{\theta} &= -\tilde{c}_-\tilde{\eta} + \alpha\frac{\tilde{c}_- + \tilde{\Gamma}}{2(1+\tilde{c}_+^2)}\tilde{\eta}^2 + \beta\left(\frac{\tilde{c}_+ + \tilde{\Gamma}}{3(1+\tilde{c}_+^2)} - \frac{\tilde{c}_-}{6} + \frac{\tilde{c}_-}{2}\theta^2\right)\tilde{\eta}_{\tilde{x}\tilde{x}} + \mathcal{O}(\alpha\beta, \beta^2), \\ \tilde{\eta}_{\tilde{t}} &+ \tilde{c}_+\tilde{\eta}_{\tilde{x}} + \alpha\frac{\tilde{c}_+(3+\tilde{\Gamma}^2)}{(1+\tilde{c}_+^2)}\tilde{\eta}\tilde{\eta}_{\tilde{x}} + \beta\frac{\tilde{c}_+ + \tilde{\Gamma}}{3(1+\tilde{c}_+^2)}\tilde{\eta}_{\tilde{x}\tilde{x}\tilde{x}} = \mathcal{O}(\alpha\beta, \beta^2). \end{aligned} \tag{18}$$

From Eq. (14), the non-dimensional horizontal velocity at the bottom is

$$\tilde{w} = -\tilde{c}_-\tilde{\eta} + \alpha\frac{\tilde{c}_- + \tilde{\Gamma}}{2(1+\tilde{c}_+^2)}\tilde{\eta}^2 + \beta\frac{\tilde{c}_+ + \tilde{\Gamma}}{3(1+\tilde{c}_+^2)}\tilde{\eta}_{\tilde{x}\tilde{x}} - \tilde{c}_-\frac{\beta}{6}\tilde{\eta}_{\tilde{x}\tilde{x}} + \mathcal{O}(\alpha\beta, \beta^2). \tag{19}$$

From Eq. (12), the non-dimensional horizontal velocity and the non-dimensional vertical velocity at the bottom become

$$\tilde{u} = \tilde{w} - \frac{\beta}{2}(1+\tilde{z})^2 \tilde{w}_{\tilde{x}\tilde{x}} + \mathcal{O}(\beta^2),$$
$$\tilde{v} = -\beta(1+\tilde{z})\tilde{w}_{\tilde{x}\tilde{x}} + \mathcal{O}(\beta^2). \tag{20}$$

From Eq. (14) and Eq. (20), the non-dimensional horizontal velocity and the non-dimensional vertical velocity at a non-dimensional height $\tilde{z}_\theta = -1 + \theta(\alpha\tilde{\eta}+1)$ become

$$\tilde{u} = \tilde{w}^\theta + \frac{\beta}{2}\left(\theta^2 - (1+\tilde{z}_\theta)^2\right)\tilde{w}^\theta_{\tilde{x}\tilde{x}} + \mathcal{O}(\beta^2),$$
$$\tilde{v} = -\beta(1+\tilde{z}_\theta)\tilde{w}^\theta_{\tilde{x}} + \mathcal{O}(\beta^2).$$

From Eq. (19) and Eq. (20), we have

$$\tilde{u} = -\tilde{c}_-\tilde{\eta} + \alpha\frac{\tilde{c}_- + \tilde{\Gamma}}{2(1+\tilde{c}_+^2)}\tilde{\eta}^2 + \beta\frac{\tilde{c}_+ + \tilde{\Gamma}}{3(1+\tilde{c}_+^2)}\tilde{\eta}_{\tilde{x}\tilde{x}} - \tilde{c}_-\frac{\beta}{6}\tilde{\eta}_{\tilde{x}\tilde{x}} + \tilde{c}_-\frac{\beta}{2}(1+\tilde{z})^2\tilde{\eta}_{\tilde{x}\tilde{x}} + \mathcal{O}(\alpha\beta,\beta^2),$$
$$\tilde{v} = \beta\tilde{c}_-\tilde{\eta}_{\tilde{x}}(1+\tilde{z}) + \mathcal{O}(\alpha\beta,\beta^2).$$

After neglecting the second-order term, the dimensional form of the velocities is given by

$$u = \sqrt{\frac{g}{h_0}}\left\{-\tilde{c}_-\eta + \frac{\tilde{c}_- + \tilde{\Gamma}}{2(1+\tilde{c}_+^2)}\frac{\eta^2}{h_0} + \frac{\tilde{c}_+ + \tilde{\Gamma}}{3(1+\tilde{c}_+^2)}h_0^2\eta_{xx} - \frac{\tilde{c}_-}{6}{h_0}^2\eta_{xx} + \frac{\tilde{c}_-}{2}h_0^2(1+\frac{z}{h_0})^2\eta_{xx}\right\},$$
$$v = \sqrt{gh_0}\,\tilde{c}_-\,\eta_x\left(1+\frac{z}{h_0}\right). \tag{21}$$

In the following, it will be convenient to define non-dimensional variables adapted to the problem at hand. In particular, a new non-dimensionalization adapted to the numerical study is defined by

$$x \to h_0 x,\ z \to h_0 z,\ \eta \to h_0\eta,\ t \to \frac{h_0}{\sqrt{gh_0}}t,\ u \to \sqrt{gh_0}u,\ w \to \sqrt{gh_0}w,\ \text{ and } \Gamma \to \frac{\Gamma\sqrt{gh_0}}{h_0}.$$

Then Eq. (21) can be rewritten in terms of new variables as

$$u = -c_-\eta + \frac{c_- + \Gamma}{2(1+c_+^2)}\eta^2 + \frac{c_+ + \Gamma}{3(1+c_+^2)}\eta_{xx} - \frac{c_-}{6}\eta_{xx} + \frac{c_-}{2}(1+z)^2\eta_{xx},$$
$$v = c_-\eta_x\,(1+z).$$

The coefficients are given as $c_+ = \frac{-\Gamma}{2} + \sqrt{\frac{\Gamma^2}{4}+1}$ and $c_- = \frac{-\Gamma}{2} - \sqrt{\frac{\Gamma^2}{4}+1}$. The Eq. (18) can be rewritten in terms of new variables as

$$\eta_t + c_+\eta_x + \frac{c_+(3+\Gamma^2)}{(1+c_+^2)}\eta\eta_x + \frac{c_+ + \Gamma}{3(1+c_+^2)}\eta_{xxx} = 0. \tag{22}$$

This equation was also found in [32,36]. By neglecting the nonlinear term as well as the higher-order term, the resulting equation is given as $\eta_t + c_+\eta_x = 0$. Upon differentiating both sides, we have $\eta_{xxx} = -\frac{1}{c_+}\eta_{xxt}$. Using this in equation (22) yields the BBM equation with vorticity

$$\eta_t + c_+\eta_x + \frac{c_+(3+\Gamma^2)}{(1+c_+^2)}\eta\eta_x - \frac{c_+ + \Gamma}{3c_+(1+c_+^2)}\eta_{xxt} = 0. \tag{23}$$

This equation is the main model used in this article. The expressions for the horizontal and vertical velocities of a fluid particle at a height $z = -1 + \theta(\eta+1)$ are given in new variables as

$$u(x,z,t) = w^\theta(x,t) + \frac{1}{2}\left(\theta^2 - (1+z)^2\right)w^\theta_{xx},$$
$$v(x,z,t) = -(1+z)w^\theta_x, \tag{24}$$

where

$$w^\theta = -c_-\eta + \frac{c_- + \Gamma}{2(1+c_+^2)}\eta^2 + \frac{c_+ + \Gamma}{3(1+c_+^2)}\eta_{xx} - \frac{c_-}{6}\eta_{xx} + \frac{c_-}{2}\theta^2\eta_{xx}. \tag{25}$$

The functions $\xi(t)$ and $\zeta(t)$ are taken to represent the x-coordinate and z-coordinate, respectively, of a particle, initially located at the point $(x,z) = (\xi_0,\zeta_0)$, then the dynamical system is recast in the form

$$\begin{aligned}
&\frac{\partial \xi}{\partial t} = u(\xi(t),\zeta(t),t) - (1+\zeta)\Gamma,\\
&\frac{\partial \zeta}{\partial t} = v(\xi(t),\zeta(t),t),\\
&(\xi(0),\zeta(0)) = (\xi_0,\zeta_0),
\end{aligned} \tag{26}$$

where the effect of an underlying shear-flow has been added. Finally, the particle trajectories are found by numerically integrating the dynamical system (26) using the fourth-order Runge-Kutta method. As explained in [5], for all values of θ, the outcomes will be qualitatively the same in as much as waves are in the validity of the Boussinesq scaling. To get more accurate results in particular cases, Eq. (24) can be used.

3. Particle trajectories in solitary-wave solutions

In this section, we aim to describe the particle trajectories in the fluid owing to the passage of a solitary wave at the surface. The exact solitary-wave solution of the BBM equation (23) is given by

$$\eta(x,t) = \eta_0 \operatorname{sech}^2\left(\sqrt{\frac{3c_+(1+c_+^2)(3+\Gamma^2)\eta_0}{4(c_++\Gamma)[3(1+c_+^2)+(3+\Gamma^2)\eta_0]}}(x-x_0-ct)\right), \tag{27}$$

where η_0 is the initial amplitude, x_0 is the initial location of the wave crest, and the phase velocity is defined as

$$c = c_+ + \frac{c_+(3+\Gamma^2)\eta_0}{3(1+c_+^2)}.$$

In this study, there is an assumption that when $t=0$, the wave crest is located at $x=0$ so that $x_0=0$. Hence, the argument is defined as

$$\mathcal{A}(x,t) = \sqrt{\frac{3c_+(1+c_+^2)(3+\Gamma^2)\eta_0}{4(c_++\Gamma)[3(1+c_+^2)+(3+\Gamma^2)\eta_0]}}(x-ct).$$

Therefore, using Eqs. (25) and (27), the relation (24) gives the horizontal and vertical velocities ($u(x,z,t)$ and $v(x,z,t)$, respectively) of the fluid at $(x, z=-1+\theta(\eta+1))$ in the fluid, at a time t as

$$\begin{aligned}
u = {}& \eta_0\operatorname{sech}^2(\mathcal{A})\left\{-c_- + \frac{3c_+(1+c_+^2)(3+\Gamma^2)\eta_0}{(c_++\Gamma)[3(1+c_+^2)+(3+\Gamma^2)\eta_0]}\left(\frac{c_++\Gamma}{3(1+c_+^2)} - \frac{c_-}{6}\right)\right.\\
&-(1+z)^2\frac{3(1+c_+^2)(3+\Gamma^2)}{(c_++\Gamma)[3(1+c_+^2)+(3+\Gamma^2)\eta_0]}\frac{\eta_0}{2}\\
&+\eta_0\operatorname{sech}^2(\mathcal{A})\left\{\frac{c_-+\Gamma}{2(1+c_+^2)} - \frac{3}{2}\frac{3c_+(1+c_+^2)(3+\Gamma^2)}{(c_++\Gamma)[3(1+c_+^2)+(3+\Gamma^2)\eta_0]}\left(\frac{c_++\Gamma}{3(1+c_+^2)} - \frac{c_-}{6}\right)\right.\\
&\left.\left.+\frac{3}{4}(z+1)^2\frac{3(1+c_+^2)(3+\Gamma^2)}{(c_++\Gamma)[3(1+c_+^2)+(3+\Gamma^2)\eta_0]}\right\}\right.\\
&+\frac{1}{2}\left(\theta^2-(1+z)^2\right)\frac{c_-+\Gamma}{2(1+c_+^2)}\frac{3c_+(1+c_+^2)(3+\Gamma^2)}{(c_++\Gamma)[3(1+c_+^2)+(3+\Gamma^2)\eta_0]}\eta_0^2\operatorname{sech}^2(\mathcal{A})(4-5\operatorname{sech}^2(\mathcal{A}))\\
&-\frac{1}{16}\left(\theta^2-(1+z)^2\right)\frac{9c_+^2(1+c_+^2)^2(3+\Gamma^2)^2\eta_0^2}{(c_++\Gamma)^2[3(1+c_+^2)+(3+\Gamma^2)\eta_0]^2}\times\\
&\left.\left(\frac{c_++\Gamma}{3(1+c_+^2)} - \frac{c_-}{6} + \frac{c_-}{2}\theta^2\right)(-8+60\operatorname{sech}^2\mathcal{A}-60\operatorname{sech}^4\mathcal{A})\right\},\\
v = {}& -(1+z)(\eta_0)^{3/2}\sqrt{\frac{3c_+(1+c_+^2)(3+\Gamma^2)}{4(c_++\Gamma)[3(1+c_+^2)+(3+\Gamma^2)\eta_0]}}\operatorname{sech}^2(\mathcal{A})\tanh(\mathcal{A})\left\{2c_- - \frac{2(c_-+\Gamma)}{(1+c_+^2)}\times\right.\\
&\left.\eta_0\operatorname{sech}^2(\mathcal{A}) + \frac{6c_+(1+c_+^2)(3+\Gamma^2)\eta_0}{(c_++\Gamma)[3(1+c_+^2)+(3+\Gamma^2)\eta_0]}\left(\frac{c_++\Gamma}{3(1+c_+^2)} - \frac{c_-}{6} + \frac{c_-}{2}\theta^2\right)(-1+3\operatorname{sech}^2(\mathcal{A}))\right\}.
\end{aligned} \tag{28}$$

Figs. 2, 3, and 4 show particle trajectories during the propagation of a solitary wave with an amplitude of 0.2 (that is, $\eta_0 = 0.2$). The value of θ used throughout this study is 0.6. The particle paths beneath the solitary waves were obtained

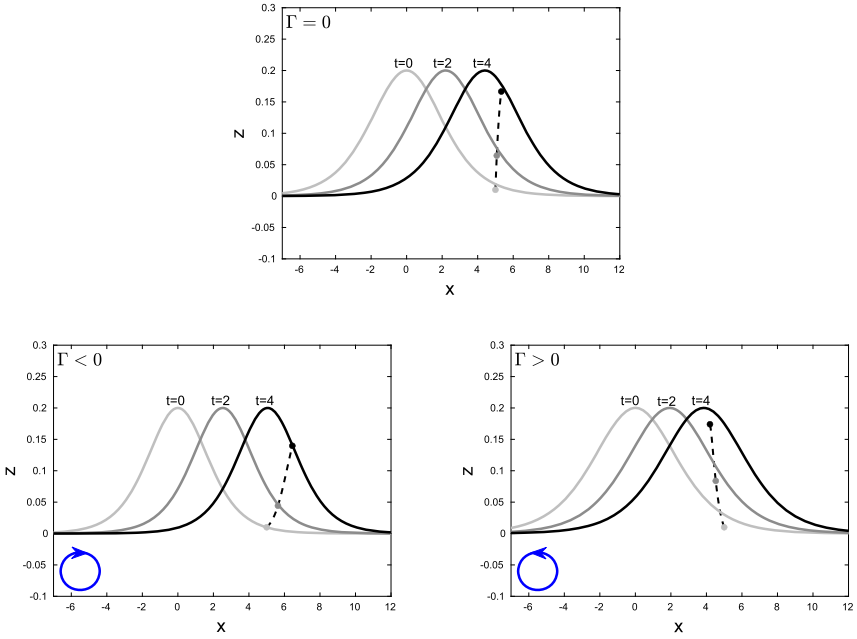

Fig. 2. The waves are shown at time $t = 0$ (light-gray), $t = 2$ (dark-gray), $t = 4$ (black). The wave crest is initially located at $x = 0$. The path of the fluid particles $(\xi(t), \zeta(t))$ of Eq. (26) (u and v corresponds to the Eq. (28)) initially located at $(5, 0.01)$ for different cases of vorticity $\Gamma = 0$; $\Gamma = -0.3$; $\Gamma = 0.3$ are shown. The particle locations at three instances where the wave profile is shown are color coded. The light-gray curve indicates the particle positions at time $t = 0$. The dark-gray curve indicates the particle positions at time $t = 2$. The black curve indicates the particle positions at time $t = 4$. The blue circles indicate the sense of rotation. (For interpretation of the colors in the figure(s), the reader is referred to the web version of this article.)

with the dynamical system (26) where the vector field is given in Eq. (28). In these figures the fluid particle location at the three instances where the wave profile is shown is color-coded: the initial position is indicated by the light-gray dot, the dark-gray dot shows its middle position while the black dot shows its final position. A circle with an arrowhead indicating the sense of rotation of the background shear flow is placed at the bottom of each figure.

Fig. 2 shows the time evolution of a fluid particle located to the right of the crest in the surface for three different vorticity values (a) $\Gamma = 0$; (b) $\Gamma = -0.3$; (c) $\Gamma = 0.3$. The particle path given by equation (26) is represented by the dashed curve. In the case of favorable vorticity ($\Gamma \leq 0$), it can be seen that the fluid particles move to the right and upwards if they are located to the right of the crest, while the fluid particle moves to the left and upwards for the case of vorticity $\Gamma > 0$. This is in agreement with the results of [5,13,24] in the absence of shear flow.

Fig. 3 illustrates particle paths associated to the passage of a solitary wave. It can be seen that the fluid particles closer to the bottom have smaller vertical excursions but nearly the same horizontal extent. Right near the bottom, the particle trajectories become straight lines as the vertical motion becomes zero. The polarity of Γ has a strong influence on the shapes of the particle paths. Indeed, it is apparent from Fig. 3 (lower panels) that the particles in the center of the fluid column move further to the right when $\Gamma < 0$, while particles in the lower half of the fluid column move further to the right when $\Gamma > 0$.

In the upper and left lower panels of Fig. 4, for $\Gamma \leq 0$, fluid particles move to the right and upwards if they are located to the right of the crest and particles located on the left of the crest move to the right and downwards. In the right lower panel of Fig. 4, for $\Gamma > 0$, fluid particles move to the left and upwards if they are located to the right of the crest and particles located on the left of the crest move to the left and downwards. But as can be seen in the right lower panel of Fig. 4, the particles closer to the bottom move to the right and upwards if they are located to the right of the crest and particles located on the left of the crest move to the right and downwards for the case $\Gamma > 0$. It is clear that for particles deeper into the fluid channel, the wave effect diminishes, and therefore the effect due the vorticity can become dominant. Through the numerical simulations, it is apparent that the closer the particle is to the free surface, the stronger it feels the wave effect.

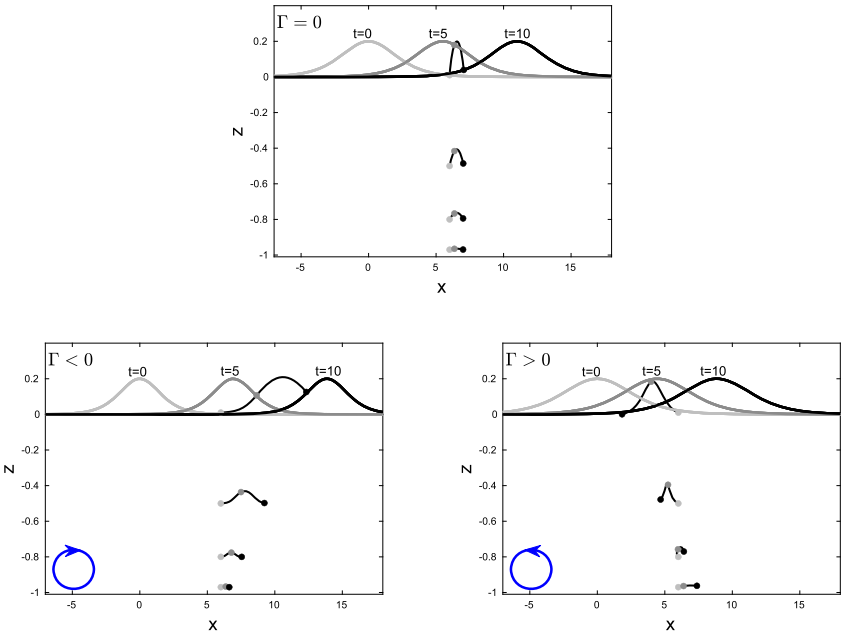

Fig. 3. The waves are shown at time $t = 0$ (light-gray), $t = 5$ (dark-gray), $t = 10$ (black). The wave crest is initially located at $x = 0$. The path of the fluid particles $(\xi(t), \zeta(t))$ in Eq. (26) (u and v corresponds to the Eq. (28)) initially located at (6, -0.97), (6, -0.8), (6, -0.5) and (6, 0.01) are shown for different cases (a) $\Gamma = 0$; (b) $\Gamma = -0.5$; (c) $\Gamma = 0.5$. The particle locations at three instances, where the wave profile is shown, are color-coded. The light-gray dot indicates the particle positions at time $t = 0$. The dark-gray dot indicates the particle positions at time $t = 5$. The black dot indicates the particle positions at time $t = 10$. The blue circles indicate the sense of rotation.

One interesting feature of the present work is that it appears to capture the existence of closed particle orbits in solitary waves such as observed in a field campaign conducted by the Beach Erosion Board on a beach in New Jersey, USA on a gently sloping beach [3]. This finding partially motivated the work of [29], where a solitary wave was coupled with an offshore current in order to capture this phenomenon which is thought to be due to an undertoe. However, an undertoe would more likely be a sheared flow that loses strength in the upper half of the fluid column. If such a flow is introduced in the equation (2), then the resulting flow look like in Fig. 5, where strong beachward transport is seen near the surface, and closed particle orbits exist near the bottom.

4. Particle trajectories in periodic-wave solutions

The focus is now on the particle paths in the fluid flow as a result of the propagation of periodic traveling waves at the surface. The BBM equation (23) admits the following solution in terms of the three constants f_1, f_2, and f_3 which are arranged as $f_3 < f_2 < f_1$, and in terms of cnoidal functions:

$$\eta = f_2 + (f_1 - f_2)\mathrm{cn}^2\left(\sqrt{\frac{3c_+(1+c_+^2)(3+\Gamma^2)}{4(c_++\Gamma)[3(1+c_+^2)+(3+\Gamma^2)(f_1-f_3)]}}(f_1 - f_3)^{1/2}(x - x_0 - ct)\right), \tag{29}$$

where f_1 and f_2 represent the crest and the trough of the wave, respectively. With $x_0 = 0$, the argument is defined as

$$\mathcal{B} = \sqrt{\frac{3c_+(1+c_+^2)(3+\Gamma^2)}{4(c_++\Gamma)[3(1+c_+^2)+(3+\Gamma^2)(f_1-f_3)]}}(f_1 - f_3)^{1/2}(x - ct).$$

Here, cn is one of the Jacobian elliptic functions defined by the incomplete elliptic integral of the first kind [28], where its modulus is defined as $m = (f_1 - f_2)/(f_1 - f_3)$. The phase speed and the wavelength of the wave are given as

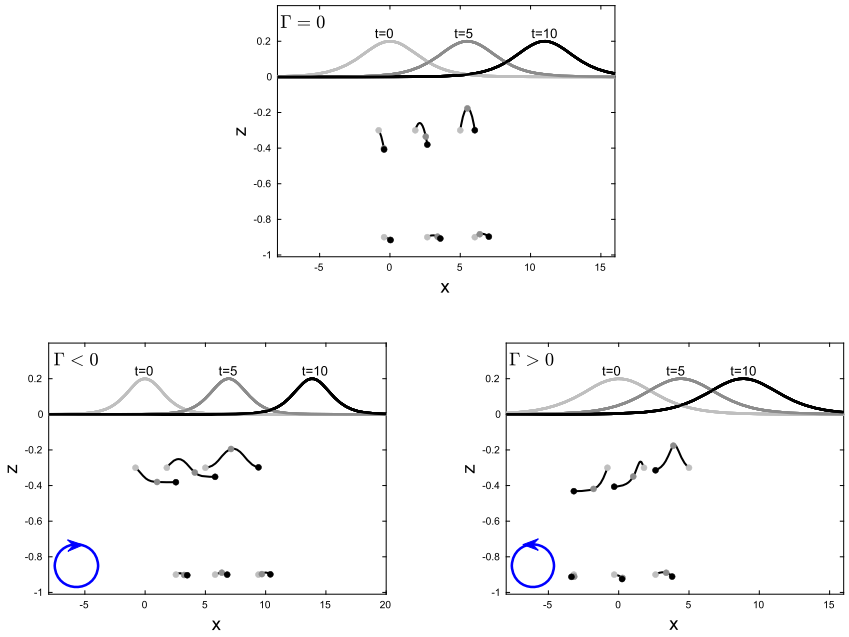

Fig. 4. The waves are shown at time $t = 0$ (light-gray), $t = 5$ (dark-gray), $t = 10$ (black). The wave crest is initially located at $x = 0$. The path of the fluid particles $(\xi(t), \zeta(t))$ in (26) (u and v corresponds to the Eq. (28)) initially located at (-0.8, -0.3), (1.8, -0.3) and (5, -0.3), also (-0.8, -0.9), (1.8, -0.9) and (5, -0.9) are shown for different cases (a) $\Gamma = 0$; (b) $\Gamma = -0.5$; (c) $\Gamma = 0.5$. The particle locations at three instances, where the wave profile is shown, are color-coded. The light-gray curve indicates the particle positions at time $t = 0$. The dark-gray curve indicates the particle positions at time $t = 5$. The black curve indicates the particle positions at time $t = 10$. The blue circles indicate the sense of rotation.

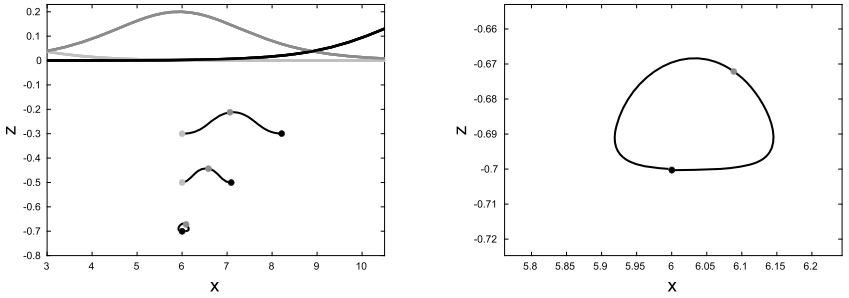

Fig. 5. Solitary-wave solution and particle paths in a shear current. The waves are shown at time $t = 0$ (light-gray), $t = 5$ (dark-gray), $t = 10$ (black). The parameter values are $a = 0.2$, $\Gamma = -0.5$, $U_0 = -0.2$, $c = 1.3859$, $x_0 = 6$. A closed path is visible near the bottom, and a close-up is shown in the right panel.

$$c = c_+ + \frac{c_+(3+\Gamma^2)}{3(1+c_+^2)}(f_1+f_2+f_3),$$

and

$$\lambda = 4\sqrt{\frac{(c_+ + \Gamma)[3(1+c_+^2)+(3+\Gamma^2)(f_1-f_3)]}{3c_+(1+c_+^2)(3+\Gamma^2)}}\,K(m)\frac{1}{\sqrt{f_1-f_3}},$$

respectively, where $K(m)$ is the complete elliptic integral of the first kind. Using Eqs. (25) and (29) in the relations (24), the horizontal and vertical velocities may be written in terms of the Jacobian elliptic functions cn, sn, and dn as

$$
\begin{aligned}
u = {} & -c_-(f_2+(f_1-f_2)\mathrm{cn}^2(\mathcal{B}))+\frac{c_-+\Gamma}{2(1+c_+^2)}(f_2+(f_1-f_2)\mathrm{cn}^2(\mathcal{B}))^2\\
& +\frac{3c_+(1+c_+^2)(3+\Gamma^2)}{2(c_++\Gamma)[3(1+c_+^2)+(3+\Gamma^2)(f_1-f_3)]}(f_1-f_2)(f_1-f_3)\Big\{\frac{c_++\Gamma}{3(1+c_+^2)}\\
& -\frac{c_-}{6}+\frac{c_-}{2}\theta^2\Big\}\Big\{\mathrm{sn}^2(\mathcal{B})\mathrm{dn}^2(\mathcal{B})-\mathrm{cn}^2(\mathcal{B})\mathrm{dn}^2(\mathcal{B})+m\,\mathrm{sn}^2(\mathcal{B})\mathrm{cn}^2(\mathcal{B})\Big\}\\
& +\Big(\theta^2-(1+z)^2\Big)\frac{3c_+(1+c_+^2)(3+\Gamma^2)}{8(c_++\Gamma)[3(1+c_+^2)+(3+\Gamma^2)(f_1-f_3)]}(f_1-f_3)\\
& \Big\{2c_-(f_1-f_2)\Big(\mathrm{cn}^2(\mathcal{B})\mathrm{dn}^2(\mathcal{B})-\mathrm{sn}^2(\mathcal{B})\mathrm{dn}^2(\mathcal{B})-m\mathrm{sn}^2(\mathcal{B})\mathrm{cn}^2(\mathcal{B})\Big)+2\frac{c_-+\Gamma}{(1+c_+^2)}\times\\
& f_2(f_1-f_2)\Big(\mathrm{sn}^2(\mathcal{B})\mathrm{dn}^2(\mathcal{B})-\mathrm{cn}^2(\mathcal{B})\mathrm{dn}^2(\mathcal{B})+m\mathrm{sn}^2(\mathcal{B})\mathrm{cn}^2(\mathcal{B})\Big)\\
& -2\frac{c_-+\Gamma}{(1+c_+^2)}(f_1-f_2)^2\Big(-m\mathrm{sn}^2(\mathcal{B})\mathrm{cn}^4(\mathcal{B})+\mathrm{cn}^4(\mathcal{B})\mathrm{dn}^2(\mathcal{B})-3\mathrm{sn}^2(\mathcal{B})\mathrm{cn}^2(\mathcal{B})\mathrm{dn}^2(\mathcal{B})\Big)\\
& +\frac{6c_+(1+c_+^2)(3+\Gamma^2)}{(c_++\Gamma)[3(1+c_+^2)+(3+\Gamma^2)(f_1-f_3)]}\left(\frac{c_++\Gamma}{3(1+c_+^2)}-\frac{c_-}{6}+\frac{c_-}{2}\theta^2\right)(f_1-f_2)(f_1-f_3)\times\\
& \Big(-9m\mathrm{sn}^2(\mathcal{B})\mathrm{cn}^2(\mathcal{B})\mathrm{dn}^2(\mathcal{B})-m^2\mathrm{sn}^2(\mathcal{B})\mathrm{cn}^4(\mathcal{B})+m\mathrm{cn}^4(\mathcal{B})\mathrm{dn}^2(\mathcal{B})\\
& +m^2\mathrm{sn}^4(\mathcal{B})\mathrm{cn}^2(\mathcal{B})+m\mathrm{sn}^4(\mathcal{B})\mathrm{dn}^2(\mathcal{B})+\mathrm{cn}^2(\mathcal{B})\mathrm{dn}^4(\mathcal{B})-\mathrm{sn}^2(\mathcal{B})\mathrm{dn}^4(\mathcal{B})\Big)\Big\},\\
v = {} & -(1+z)\sqrt{\frac{3c_+(1+c_+^2)(3+\Gamma^2)}{4(c_++\Gamma)[3(1+c_+^2)+(3+\Gamma^2)(f_1-f_3)]}}(f_1-f_3)^{1/2}\mathrm{sn}(\mathcal{B})\mathrm{cn}(\mathcal{B})\mathrm{dn}(\mathcal{B})\,\{2c_-(f_1-f_2)\\
& -2\frac{c_-+\Gamma}{(1+c_+^2)}f_2(f_1-f_2)-2\frac{c_-+\Gamma}{(1+c_+^2)}(f_1-f_2)^2\mathrm{cn}^2(\mathcal{B})+\left(\frac{c_++\Gamma}{3(1+c_+^2)}-\frac{c_-}{6}+\frac{c_-}{2}\theta^2\right)\times\\
& \frac{6c_+(1+c_+^2)(3+\Gamma^2)}{(c_++\Gamma)[3(1+c_+^2)+(3+\Gamma^2)(f_1-f_3)]}(f_1-f_2)(f_1-f_3)\Big(-m\mathrm{sn}^2(\mathcal{B})+m\mathrm{cn}^2(\mathcal{B})+\mathrm{dn}^2(\mathcal{B})\Big)\Big\}.
\end{aligned}
\tag{30}
$$

The particle paths shown in Figs. 6 - 9 are numerical approximations of solutions of Eq. (26) where the vector field is given in Eq. (30). The cnoidal wave of the BBM equations can be specified by fixing the values of the parameters f_1, f_2, and f_3. Of particular interest is the case of an adverse current, and researchers [14,30] predicted the existence of a closed orbit. Fig. 6 illustrates the particle path during one complete periodic cnoidal wave cycle with $m = 0.99$ and $H = f_1 - f_2 = 0.3$ for different values of vorticity $\Gamma = 0, -0.1$ and 0.1. The crest of the wave is centered at $x = 0$, and depths $z = -0.9, -0.4$ and -0.078. The particle paths are nearly elliptic but not closed in the presence of the vorticity $\Gamma \leq 0$. For the case of positive vorticity $\Gamma > 0$, the particle paths are orbit loops.

Next, we present a train of the cnoidal wave for different values of vorticity $\Gamma = 0, -0.4$, and 0.6. A close-up of particle paths initially located at the surface is shown in Fig. 7. The particle path during the propagation of the cnoidal wave over 4 periods at the three cases are shown, and the initial particle locations are shown in light-gray dots. In the upper and left lower panels of Fig. 7, for $\Gamma \leq 0$, fluid particles move to the right and upwards. As can be seen in the right lower panel of Fig. 7, the particles move to the left and upwards for the case $\Gamma > 0$.

In Figs. 8 and 9, the particle paths with different vorticity values are shown for different depths. In Fig. 8, the particle path during the propagation of the cnoidal wave over one period at the three instances are shown for amplitude 0.2 with different values of vorticity $\Gamma = 0, -0.4$, and 0.6, all particles are initially at $x_0 = \text{wavelength}/2 - 0.001$, and depth $z_0 = -0.1, -0.5$ and -0.9. Fig. 9 features the particle trajectory during the propagation of the cnoidal wave over three periods. The three instances considered are shown for amplitude 0.4 with vorticity $\Gamma = 0, -0.12$, and 0.28. We observe that in the upper and lower panels of Fig. 9, for the particles closer to the bottom, the wave effect diminishes, and therefore the effect due to the vorticity can become dominant.

5. Conclusion

This study has focused on the motion of particles in the body of the fluid excited by the combination of wave motion at the free surface and a pre-existing linear shear flow. The waves were assumed to be long and of small amplitude when

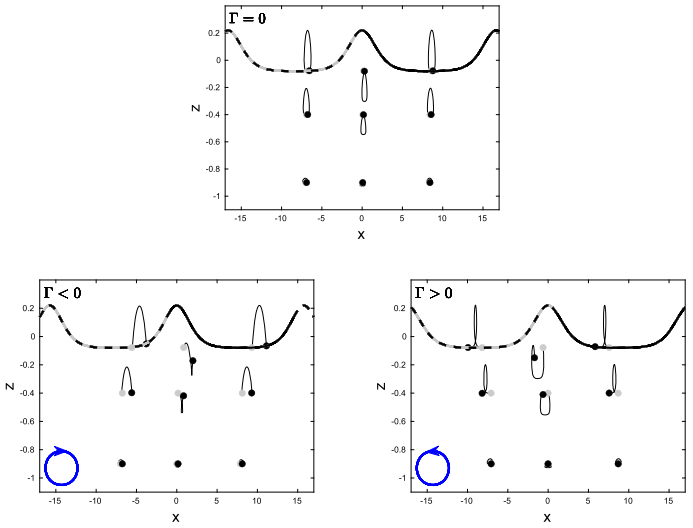

Fig. 6. The upper panel shows the periodic wave with amplitude 0.3, wavelength 16.6372, period 16.1830, phase speed 1.0281 and $\Gamma = 0$ at $t = 0$ (light-gray) and $t = 16.18$ (black). The left lower panel shows the periodic wave with amplitude 0.3, wavelength 15.7511, period 14.5928, phase speed 1.0794 and $\Gamma = -0.1$ at $t = 0$ (light-gray) and $t = 14.59$ (black). The right lower panel shows the periodic wave with amplitude 0.3, wavelength 17.5221, period 17.8910, phase speed 0.9794 and $\Gamma = 0.1$ at $t = 0$ (light-gray) and $t = 17.89$ (black). The paths of fluid particles are located at (x, z), where the initial x-coordinate are $x = -7, 0$ and wavelength$/2 - 0.001$, and depth are $z = -0.9, -0.4$ and -0.078. The blue circles indicate the sense of rotation.

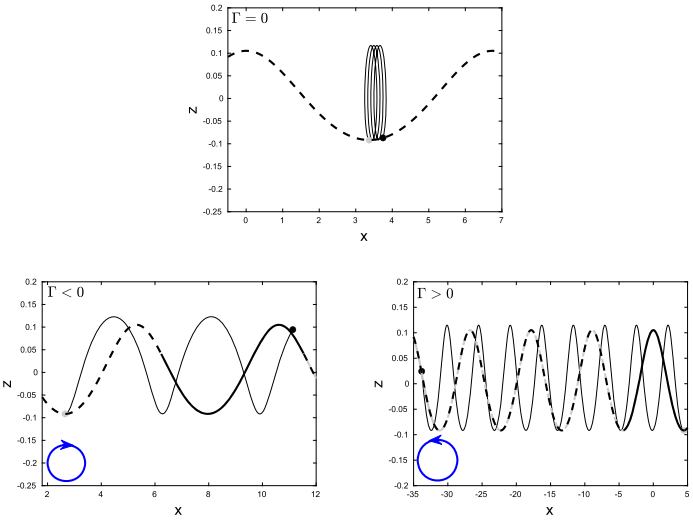

Fig. 7. The upper panel shows the periodic wave with amplitude 0.1968, wavelength 6.7430, period 8.1566, phase speed 0.8267 and $\Gamma = 0$ at $t = 0$ (light-gray) and $t = 4$periods (black), (these values of t are used in all the three cases. This means that the final value of t varies). The left lower panel shows the periodic wave with amplitude 0.1968, wavelength 5.3077, period 5.0997, phase speed 1.0408, and $\Gamma = -0.4$. The right lower panel shows the periodic wave with amplitude 0.1968, wavelength 8.9134, period 15.9709, phase speed 0.5581, and $\Gamma = 0.6$. The initial particle locations at the three cases are shown in light-gray curve. All particles are initially at $x_0 =$ wavelength$/2 - 0.001$ and depth $z_0 = -0.1$. The blue circles indicate the sense of rotation.

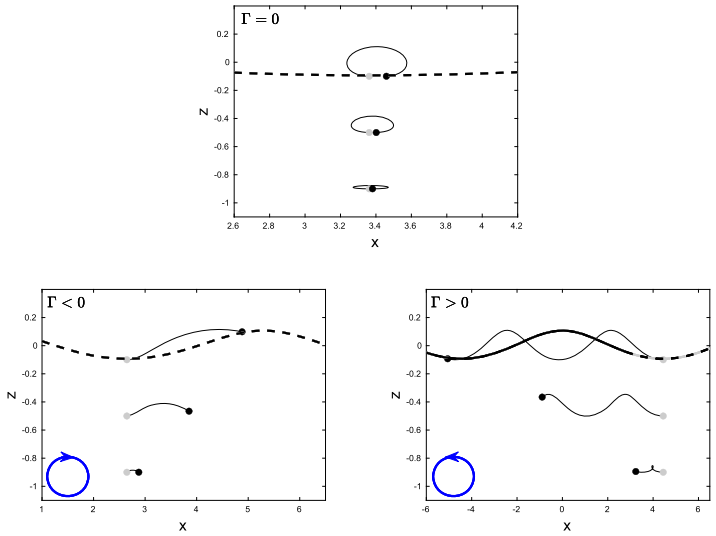

Fig. 8. The upper panel shows the periodic wave with amplitude 0.2, wavelength 6.7264, period 8.1470, phase speed 0.8256, and $\Gamma = 0$ at $t = 0$ (light-gray) and $t = 8.1470$ (black). The left lower panel shows the periodic wave with amplitude 0.2, wavelength 5.2941, period 5.0919, phase speed 1.0397, and $\Gamma = -0.4$ at $t = 0$ (light-gray) and $t = 5.0919$ (black). The right lower panel shows the periodic wave with amplitude 0.2, wavelength 8.8940, period 15.9686, phase speed 0.5570, and $\Gamma = 0.6$ at $t = 0$ (light-gray) and $t = 15.9686$ (black). The initial particle locations in the three cases are shown in the light-gray curve. All particles are initially at $x_0 = \text{wavelength}/2 - 0.001$, and depth $z_0 = -0.1, -0.5$ and -0.9.

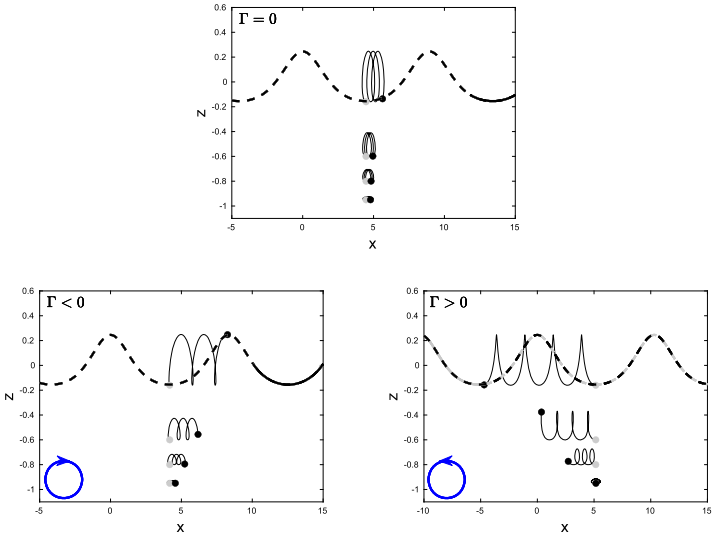

Fig. 9. The upper panel shows the periodic wave with amplitude 0.4 wavelength 8.9389, period 9.5834, phase speed 0.9327, and $\Gamma = 0$ at $t = 0$ (light-gray) and $t = 28.7501$ (black). The left lower panel shows the periodic wave with amplitude 0.4, wavelength 8.3541, period 8.4016, phase speed 0.9943, and $\Gamma = -0.12$ at $t = 0$ (light-gray) and $t = 25.2047$ (black). The right lower panel shows the periodic wave with amplitude 0.4, wavelength 10.3072, period 12.8613, phase speed 0.8014, and $\Gamma = 0.28$ at $t = 0$ (light-gray) and $t = 38.5840$ (black). The initial particle locations are shown in light-gray curve.

compared to the depth of the fluid, so that a weakly nonlinear long-wave equation could be used to describe the wave motion. To this end, a new BBM equation has been derived in the presence of a background shear flow, and expressions for the velocity field of the fluid have been deduced from the derivation. Using the description of the particle paths in terms of a two-by-two system of ordinary differential equations and appropriate discretization techniques, close approximations of particle motions were found for both solitary waves and periodic traveling waves. The influence of the background shear flow on the particle motion was considered, and it was found that the polarity of the associated vorticity has a major effect on the shapes of the trajectories.

We would like to point out that in [21], using a fully nonlinear model, it has been established that the behavior of the particle paths in the presence of background vorticity is associated with the existence of stagnation points in the flow. We have experimented with various parameters, but could not find the existence of internal stagnation points in this weakly nonlinear model equation. However, we were able to find situations with closed particle orbits associated with solitary waves, such as observed in field measurements [29].

References

[1] A. Ali, H. Kalisch, Reconstruction of the pressure in long-wave models with constant vorticity, Eur. J. Mech. B, Fluids 37 (2013) 187–194.
[2] M. Bakhoday-Paskyabi, Particle motions beneath irrotational water waves, Ocean Dyn. 65 (8) (2015) 1063–1078.
[3] Beach Erosion Board, A summary of the theory of oscillatory waves, Technical Report No. 2, United States Government Printing Office, 1942.
[4] T.B. Benjamin, The solitary wave on a stream with an arbitrary distribution of vorticity, J. Fluid Mech. 12 (1962) 97–116.
[5] H. Borluk, H. Kalisch, Particle dynamics in the KdV approximation, Wave Motion 49 (2012) 691–709.
[6] M. Bjørnestad, M. Buckley, H. Kalisch, M. Streßer, J. Horstmann, H.G. Frøysa, O.E. Ige, M. Cysewski, R. Carrasco-Alvarez, Lagrangian measurements of orbital velocities in the surf zone, Geophys. Res. Lett. 48 (2021) e2021GL095722.
[7] J.C. Burns, Long waves in running water, Math. Proc. Camb. Philos. Soc. 49 (4) (1953) 695–706.
[8] A. Castro, D. Lannes, Well-posedness and shallow-water stability for a new Hamiltonian formulation of the water waves equations with vorticity, Indiana Univ. Math. J. 64 (2015) 1169–1270.
[9] L. Chen, B. Basu, C.I. Martin, On rotational flows with discontinuous vorticity beneath steady water waves near stagnation, J. Fluid Mech. 912 (2021) A44.
[10] Y.-Y. Chen, H.-C. Hsu, G.-Y. Chen, Lagrangian experiment and solution for irrotational finite-amplitude progressive gravity waves at uniform depth, Fluid Dyn. Res. 42 (2010) 045511.
[11] W. Choi, Strongly nonlinear long gravity waves in uniform shear flows, Phys. Rev. E 68 (2003).
[12] A. Constantin, The trajectories of particles in Stokes waves, Invent. Math. 166 (3) (2006) 523–535.
[13] A. Constantin, J. Escher, Particle trajectories in solitary water waves, Bull. Am. Math. Soc. 44 (2007) 423–431.
[14] A. Constantin, W. Strauss, Pressure beneath a Stokes wave, Commun. Pure Appl. Math. 63 (4) (2010) 533–557.
[15] A. Constantin, G.J. Villari, Particle trajectories in linear water waves, J. Math. Fluid Mech. 10 (2008) 1–18.
[16] D. Crowdy, Explicit solutions for a steady vortex-wave interaction, J. Fluid Mech. 513 (2004) 161–170.
[17] C.W. Curtis, J.D. Carter, H. Kalisch, Particle paths in nonlinear Schrödinger models in the presence of linear shear currents, J. Fluid Mech. 855 (2018) 322–350.
[18] C.W. Curtis, H. Kalisch, Vortex dynamics in nonlinear free surface flows, Phys. Fluids 29 (2017) 032101.
[19] L. Debnath, Nonlinear Water Waves, Academic Press Inc., 1994.
[20] F.J. Gerstner, Theory of Waves, Abhandlungen der Königl, Böhmischen Gesellschaft der Wissenschaften zu Prag, 1802.
[21] X. Guan, Particle trajectories under interactions between solitary waves and a linear shear current, Theor. Appl. Mech. Lett. 10 (2) (2020) 125–131.
[22] D. Henry, On Gerstner's water wave, J. Nonlinear Math. Phys. 15 (2) (2008) 87–95.
[23] H.C. Hsu, Particle trajectories for waves on a linear shear current, Nonlinear Anal., Real World Appl. 14 (2013).
[24] O.E. Ige, Z. Khorsand, Particle trajectories in the BBM approximation, IAENG Int. J. Appl. Math. 50 (3) (2020) 589–600.
[25] C. Kharif, M. Abid, Nonlinear water waves in shallow water in the presence of constant vorticity: a Whitham approach, Eur. J. Mech. B, Fluids 72 (2018) 12–22.
[26] L.F. Kilcher, J.D. Nash, Structure and dynamics of the Columbia river tidal plume front, J. Geophys. Res., Oceans 115 (2010) C05590.
[27] H. Lamb, Hydrodynamics, Dover Publications, New York, 1945.
[28] D.F. Lawden, Elliptic Functions and Applications, Springer, New York, 1989.
[29] W.H. Munk, The solitary wave theory and its application to surf problems, Ann. N.Y. Acad. Sci. 51 (1949) 376–424.
[30] A. Nachbin, R. Ribeiro-Junior, A boundary integral formulation for particle trajectories in Stokes waves, Discrete Contin. Dyn. Syst. 34 (8) (2014) 3135–3153.
[31] R. Ribeiro, P.A. Milewski, A. Nachbin, Flow structure beneath rotational water waves with stagnation points, J. Fluid Mech. 812 (2017) 792–814.
[32] A. Senthilkumar, H. Kalisch, Wave breaking in the KdV equation on a flow with constant vorticity, Eur. J. Mech. B, Fluids 73 (2019) 48–54.
[33] J.J. Stoker, Water Waves. The Mathematical Theory with Applications, Interscience Publ. Inc., New York, 1957.
[34] G.G. Stokes, On the Theory of Oscillatory Waves, Trans. Camb. Phil. Soc., 1847, pp. 441–455. Reprinted in: G.G. Stokes, Mathematical and Physical Papers, vol. I, Cambridge University Press, 1880, pp. 197–229.
[35] J. Shatah, S. Walsh, C. Zeng, Travelling water waves with compactly supported vorticity, Nonlinearity 26 (2013) 1529.
[36] R. Stuhlmeier, Effects of shear flow on KdV balance - applications to tsunami, Commun. Pure Appl. Anal. 11 (2012) 1549–1561.
[37] A.F. Teles da Silva, D.H. Peregrine, Steep, steady surface waves on water of finite depth with constant vorticity, J. Fluid Mech. 195 (1988) 281–302.
[38] R. Thomas, C. Kharif, M. Manna, A nonlinear Schroedinger equation for water waves on finite depth with constant vorticity, Phys. Fluids 24 (2012) 127102.
[39] F. Ursell, Mass transport in gravity waves, Proc. Camb. Philol. Soc. 40 (1953) 145–150.
[40] V. Vasan, K. Oliveras, Pressure beneath a traveling wave with constant vorticity, Discrete Contin. Dyn. Syst. 34 (2014) 3219–3239.
[41] Z. Wang, X. Guan, J.M. Vanden-Broeck, Progressive flexural-gravity waves with constant vorticity, J. Fluid Mech. 905 (2020).
[42] C. Yaosong, L. Guocan, J. Tao, Non-linear water waves on shearing flows, Acta Mech. Sin. 10 (2) (1994) 97–102.

Paper C

Fluid Transport Induced by Internal Waves.

Olufemi Elijah Ige and Henrik Kalisch

Paper D

Particle Trajectories and Wave Breaking in the Gardner Equation.

Olufemi Elijah Ige, Henrik Kalisch, Kaja Elgåen, and Sara Mundal Aase

Graphic design: Communication Division, UiB / Print: Skipnes Kommunikasjon AS

uib.no

ISBN: 9788230850169 (print)
9788230844984 (PDF)